2004-12-07

A Finite Element Simulation of Temperature and Material Flow in Fricton Stir Welding

Mark J. Lasley
Brigham Young University - Provo

A FINITE ELEMENT SIMULATION OF TEMPERATURE AND MATERIAL FLOW IN FRICTION STIR WELDING

by

Mark Jason Lasley

A thesis submitted to the faculty of

Brigham Young University

in partial fulfillment of the requirements for the degree of

Master of Science

School of Technology

Brigham Young University

April 2005

BRIGHAM YOUNG UNIVERSITY

GRADUATE COMMITTEE APPROVAL

of a thesis submitted by

Mark Jason Lasley

This thesis has been read by each member of the following graduate committee and by majority vote has been found satisfactory.

Date	Michael P. Miles, Chair
Date	Tracy W. Nelson
Date	Charles R. Harrell

BRIGHAM YOUNG UNIVERSITY

As chair of the candidate's graduate committee, I have read the thesis of Mark Jason Lasley in its final form and have found that (1) its format, citations, and bibliographical style are consistent and acceptable and fulfill university and department style requirements; (2) its illustrative materials including figures, tables, and charts are in place; and (3) the final manuscript is satisfactory to the graduate committee and is ready for submission to the university library.

_____ _____

Date

Michael P. Miles
Chair, Graduate Committee

Accepted for the Department

_____

Kevin L. Burr
Graduate Coordinator, School of Technology

Accepted for the College

_____

Douglas M. Chabries
Dean, Ira A. Fulton College of Engineering and Technology

ABSTRACT

A FINITE ELEMENT SIMULATION OF TEMPERATURE AND MATERIAL FLOW IN FRICTION STIR WELDING

Mark Jason Lasley

School of Technology

Master of Science

The purpose of this research was to use the Transvalor S.A. product, Forge3, to develop a finite element simulation of the friction stir welding process that improves the predictability of temperature evolution and material flow within the plunge portion of the process. Previous modeling created more heating within the billet than experimental results, probably due to the simplification of the simulation with adiabatic boundary conditions. More realistic tooling temperatures were included in this model as these affect heat evolution which is a determining factor in microcrystalline growth. These results were validated by experimental efforts using a billet and tooling instrumented with thermocouples used to evaluate the temperatures at specific locations over time. Simulation results were compared with previous experiments to validate the predicted material flow.

ACKNOWLEDGEMENTS

I would like to thank those who, through their many gifts of time, teaching, and patience, have helped me to continue my education and complete this thesis. Drs. Michael Miles, my committee chair, Tracy Nelson, and Charles Harrell for their encouragement, advice, and assistance in understanding the procedure needed to create the model as well as the process being modeled. They are the most recent of many teachers including, specifically, Val Hawks, Janet Zylstra, and Cindi Baltzley who have helped me to see beyond the surface information and learn knowledge from the experience as well as how to apply it.

I want to especially thank my parents, Casey and Annetta Lasley, who have always promoted education as the doorway to opportunity. Their encouragement, along with the support of my wife, Amanda, has helped give me the determination to push through the frustrations and onward to the goal. Certainly there were several other people, including Ruth Ann Lowe and Tom Raisor, who offered their encouragement and help throughout this period and I would like to thank them for their assistance.

Table of Contents

1. INTRODUCTION…….. 1
   1.1. Background……1
   1.2. Problem Statement……3
   1.3. Objective of Research……4
   1.4. Purpose of Study……5
   1.5. Methodology……..6
   1.6. Delimitations……..7

2. REVIEW OF LITERATURE……9
   2.1. Introduction……9
   2.2. Developing Friction Stir Welding Models……...11
      2.2.1. Computation Costs and Model Accuracy……... 11
      2.2.2. Meshing Schemes……... 13
      2.2.3. Modeling Techniques……..16
   2.3. Material Flow in Friction Stir Welding……19
   2.4. Summary……..23

3. METHODOLOGY
   3.1. Mesh Development……..25
   3.2. Model Development…….26
      3.2.1. Flow Stress……..33
   3.3. Experimental Design……36

4. RESULTS AND DISCUSSION……...41
   4.1. Experimental Results……... 41
   4.2. Simulation Results……... 43
      4.2.1. Parallel Processing Simulations……..43
      4.2.2. Static Anvil/Dynamic Tool Simulations……45
      4.2.3. Open Table Simulation……... 49
   4.3. Material Flow……...50

5. CONCLUSIONS AND RECOMMENDATIONS……... 53
   5.1. Conclusions……..53
   5.2. Recommendations……54

6. REFERENCES……..57

7. APPENDIX A: Problems and Workarounds…… 61

8. APPENDIX B: Reference (.ref) Files……...67

9. APPENDIX C: Experimental Data……...77

10. APPENDIX D: Simulation Data…….103

List of Tables

Table 1—Composition (%wt) of Materials.....12

List of Figures

Figure 1—Structural failure on a Liberty Ship..... 1

Figure 2—Representation of the effect of adding more processors without improving communication.....5

Figure 3—Basic movement of the Friction Stir Welding tool in relation to the workpiece.....10

Figure 4—Cost of increasing accuracy.....12

Figure 5—Schematic of tool used in the Dickersen model..... 17

Figure 6—Representation of the various "zones" encountered in the FSW process [1] 21

Figure 7—Lagrangian mesh deformation in Forge3.....25

Figure 8—Relative mesh size..... 26

Figure 9—Drawing of the FSW tool.....27

Figure 10—Calculus-type approach to improved tooling temperatures.....31

Figure 11—Results showing the improper temperature calculation.....33

Figure 12—The Hansel-Spittel equation used in Forge3.....34

Figure 13—Tool thermocouple locations..... 36

Figure 14—Relative thermocouple positions in the simulation and experiment.....37

Figure 15—Billet, thermocouple cavity, and thermocouple channel dimensions..... 38

Figure 16—Tool thermocouple locations for experiments 4-6.....38

Figure 17—The FSW setup just prior to the start of an experiment.....39

Figure 18—Graph of the experiments and a comparison average versus Oliphant's averaged data..... 41

Figure 19—Comparison of flexure in the FSW setup..... 42

Figure 20—Screenshot showing dimples and peripheral crumpling..... 44

Figure 21—Slippage between the anvil and billet at the start of the simulation..... 44

Figure 22—Comparison of thermocouple readings as depth increases..... 47

Figure 23—Tool position relative to the anvil..... 47

Figure 24—Comparison of isotherms..... 48

Figure 25—Material flow around the pin and shoulder in the XZ plane..... 51

Figure 26—Material flow around the tool in the XZ plane..... 51

1 INTRODUCTION

1.1 Background

In most structures the weakest point is found where plates or beams are joined together. Along with sudden changes in shape, these points tend to become locations for stress concentrations and increased corrosion which can lead to structural failure. An example can be seen in the Liberty ship in Figure 1. Stronger joints can be made by improving the joining process used to connect metal parts found in the structural skeletons used in buildings, ships, aircraft, and cars. This would reduce failures and increase the level of confidence in their resistance to failure.

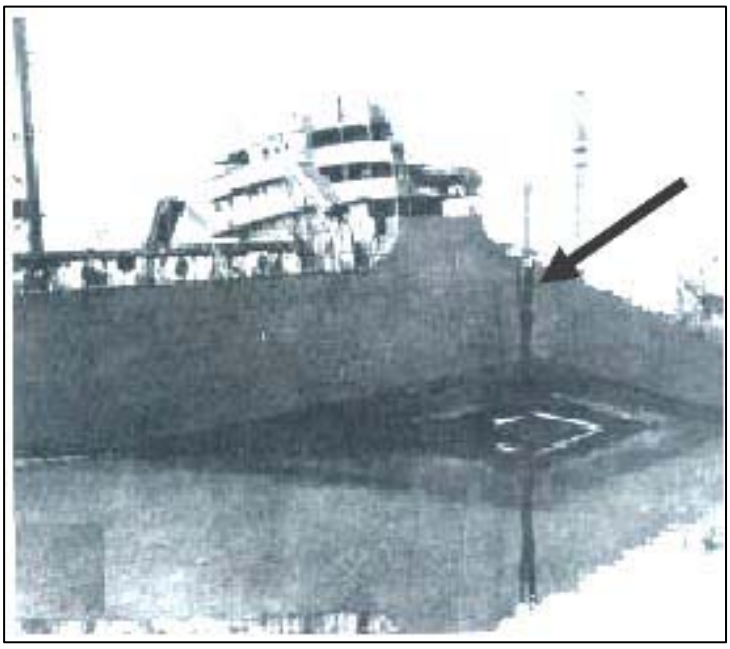

Figure 1: Structural failure on a Liberty ship

Friction stir welding, patented by The Welding Institute in 1991, presents a new technique for material joining and processing. In friction stir welding two or more parts are joined while in the solid state much as in other methods of friction welding that have

been in existence since 1950. Friction stir welding has enjoyed worldwide interest since its inception because of its advantages over traditional joining techniques.

This technology boasts low distortion in long welds, excellent mechanical properties in the weld and heat-affected zone, no fumes or spatters, low shrinkage, as well as being energy efficient. Furthermore, other cost reductions are realized in that the process uses a non-consumable tool. This tool is made of H13 tool steel for aluminum alloy welds. Harder, more durable materials with good red-hot characteristics such as tungsten carbide or polycrystalline cubic boron nitride (PCBN) are used when welding steels and titanium which require a stronger tool than that used for aluminum.

Friction stir welding does not need filler and it is relatively easy to perform. However, it does have some limitations in that every welded piece must be rigidly clamped, welding speeds tend to be low to avoid porosity, and there is a keyhole from where the pin was at in each end of the weld line. This has not slowed its adoption today by companies including Boeing in their work to join aluminum alloys.

The basic tool geometry used in friction stir welding involves a cylindrical, shouldered shape with a concave face. A cylindrical pin is located in the center of this depression and extends beyond the rim. As the tool is revolved and pressed into the material to be welded, the pin helps to plasticize the material deeper inside the plate. As the tool reaches operational depth, the shoulder contacts the surface of the parent material. This increases friction at the top surface and compresses the material that has been stirred by the pin, reconsolidating the material and eliminating voids and porosity. This action does not actually melt the metal and so it creates a solid phase weld that can tolerate some improper weld surface preparation.

1.2 Problem Statement

The friction stir welding process is under review in order to better understand what happens as the material is plasticized and flowed from one part of the weld to another. This contributes to the post-weld microstructure which in turn determines the weld strength. Although friction stir welding has some very interesting advantages, it has proven difficult to study. Several methods for testing and validation have been developed along with a myriad of software packages using different criteria found in friction stir welding. Testing to understand the heat evolution, material flow, and weld development is essential in learning how the microstructures are formed and oriented within the weld. These microstructures and their positions determine the strengths and/or weaknesses of the joint.

The problem in friction stir welding, as with many emerging technologies, is that this testing is expensive in terms of time, materials, and personnel. Much of the body of knowledge on the subject comes from running several experiments for each change in a parameter and then doing several metallurgical sections to study the results. This requires large amounts of time and money which slows the development of applications for this new process.

What is needed is a faster, cheaper, more reliable way to test new theories regarding friction stir welding. This would eliminate unnecessary testing on parameters that do not show improvement or fail to create desirable properties. Finite element modeling is one option which would help determine which parameters should undergo further real-world testing for validation and further analysis.

Previous models have been built with several assumptions as to how the material should be modeled, which meshing schemes are better to use, how the temperature evolves, how heat escapes from the welding area, and how this affects material flow. The material response within the weld, as well as the post-weld microstructure that develops, depends on how the material is heated, cooled, deformed, and the duration of these effects. This makes it imperative that the an improved model include the change in temperatures, strains, and strain rates experienced in the process as well as being able to do so in a reasonable amount of time.

1.3 Objective of Research

With the emergence of faster processors and the evolution of better software, we have the ability to direct the computer's strength of rapid, linear computation on the task of building a numerical model that requires only a small amount of time and is capable of replicating experimental results fromfriction stir welding. Even with these improvements a simulation still requires extensive amounts of time to run to completion. In order to make parametric studies viable, the power of parallel processing must also be harnessed.

The objective of this research is to develop an finite element simulation with improved capability to predict temperature evolution and material flow during the plunge phase. This improved model will then be coupled with the appropriate parallel processing environment. The parallel processing environment is necessary to continue reducing the time needed to perform each simulation. The parallel processing environment is also an important area to study and include as it provides a way to allow processors to "work as a team" on a problem. This is possible by dividing the simulation

into sections and iteratively processing that part of the simulation while passing/sharing information that would affect the results of the problem segment another processor is working on.

There is, however, an economic principle called the law of diminishing returns. This states that as the number of workers (or processors) increases, the incremental reduction in price (processing time needed) decreases if there is not also an improvement in how they work together. The idea goes even further stating that there is a point at which the additional help does not improve the situation and actually reduces the effectiveness of the team. This leads to an increase in needed computational time (for comparing and passing information to each necessary node) as you add more processors. Figure 2 is a graphical representation of this phenomenon.

By creating this improved numerical model and coupling it to a parallel processing network it is hoped that it will enable researchers to study a process while quickly making modifications and checking their results without tying up huge amounts of resources. This promises the opportunity of realizing great improvements in manufacturing and production without the attendant costs of materials and workspace for extensive, yet unprofitable studies down blind alleys.

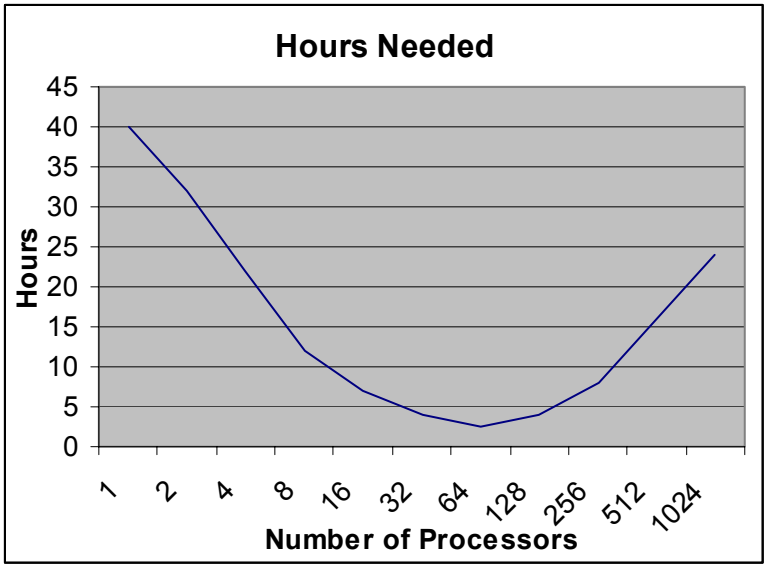

Figure 2: Representation of the effect of adding more processors without improving communication.

1.4 Purpose of Study

The purpose of this research is to improve the understanding of heat evolution and material flow in the friction stir welding process, specifically during the plunge phase. This will be accomplished by developing an improved finite element simulation of the plunge phase of the friction stir welding process that predicts material flow and temperature evolution within the welding zone more accurately. These results will be validated by experimental results where the work piece and tooling will be instrumented with thermocouples to evaluate the temperatures at specific locations over time. Comparison with previous experiments will examine the material flow.

This research builds on experience gained in previous numerical modeling efforts of friction stir welding, specifically in Aluminum 7075-T6. This is a complex and dynamic system that changes as the parent material is brought into contact with the friction stir welding tool in the welding zone, heated, and displaced in relation to the changing conditions of the tool during the initial plunge and subsequent traverse. This computational tool and knowledge could lead to improved understanding of the welding conditions and processes encountered in friction stir welding. This could even include the potential of learning about development of localized property variations within the weld zone to improve the as-welded characteristics of different metals and joints.

1.5 Methodology

This research builds on previous work done using an older version of Forge3 (Oliphant, 2004). The older premises are transferred into the new model (welding parameters, etc.) while removing the adiabatic assumption between tool and billet. This

is replaced with a thermal transfer at the interface between the anvil and billet as well as the billet and tool. The new models use different methods for modeling the temperature evolution in the tooling and how it affects the billet response.

The first model uses the assumptions made in Oliphant's research. Subsequent simulations use an open format table to give the model several "waypoints" from which it can extrapolate the proper temperature at a point in time. In each model, multiple "sensors" are placed within the modeled billet to record strain, strain rate, and temperature evolution. The computational models were run on computers in the Fulton Supercomputing Facility at Brigham Young University. Experimental data was used to compare and validate model results.

1.6 Delimitations

The research will focus only on the plunge phase of the FSW process involving an Aluminum 7075-T6 billet and a FSW tool made of H13 tool steel. Design and testing will be done using only the Forge3 package as it has been previously used in other research and allows for a Lagrangian calculation. Friction and heat transfer selections are discussed in Chapter 3. Only the initial plunge will be studied as further modifications are needed for the current version to model translation of the tool. This study will not take into account any flexure of the machinery or tooling and will only use the smooth-pinned tool geometry. Parallel processing will be explored using resources available in the Ira A. Fulton Supercomputing Facility.

2 REVIEW OF LITERATURE

2.1 Introduction

The friction stir welding process was first developed and patented in late 1991 in the United Kingdom by The Welding Institute (TWI). In this process the weld is made in the solid state much as found in other methods of friction welding that have been in existence since 1950. Friction stir welding has enjoyed worldwide interest since its inception because of its advantages over traditional joining techniques. Kallee and Nicholas' (2004) research cites the advantages of friction stir welding as having low distortion in long welds, excellent mechanical properties in the weld and heat-affected zone, no fumes or spatter, low shrinkage, and energy efficiency.

Further cost reductions are realized as it uses a non-consumable tool, does not need filler, and is relatively easy to perform in the technical sense since there is no welding certification needed. It does have some limitations in that every piece must be rigidly clamped, welding speeds are low, and there is a keyhole at each end of the weld line. Other limitations include: one part must have near-symmetry in one axis and the increasing cost of equipment as part size increases (Dunn, 2002).

In spite of this difficulty, the simplification of joining aluminum alloys has led to the initial commercial adoption of this technique by some Scandinavian companies and by Boeing, (Johnsen, 1999) as well as currently being used in making high-speed trains in

Japan, in military applications, cruise ship decks, electric housings and automotive components used by BMW, Land Rover, Ford, Mazda and various other companies.

Friction stir welding uses a tool that can be made of any material capable of withstanding both the heat buildup and frictional forces encountered in the process. In the case of aluminum alloys, the joining tool is often made of H13 tool steel while other materials such as tungsten carbide or PCBN are a better choice for harder metals. This tool is pressed into the rigidly held workpiece and then translated along the welding line as seen in Figure 3.

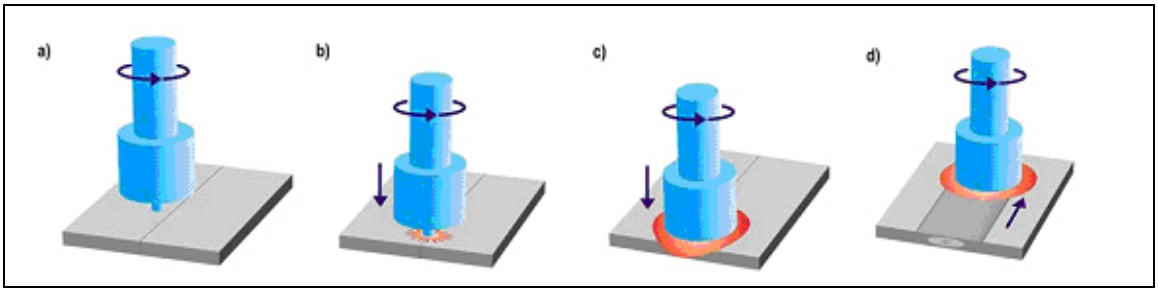

Figure 3: Basic movement of the Friction Stir Welding tool in relation to the workpiece.

The tool takes the general form of a cylindrical, shouldered shape with a slightly concave recess leading to a protruding, rounded pin located in the center. As the tool is forced into the workpiece, this pin works to plasticize the deeper materials at the edges of the plates and also serves as a "forging die" to help consolidate the material that will be joined in the weld. Threads are sometimes found on this pin to increase material mixing.

The shoulder increases friction at the top of the workpiece and transfers material across the plate boundaries. It also works to consolidate the weld material as the tool travels along the workpiece. While this method of joining creates a large amount of heat, it still keeps the material below the melting temperature and thus creates a solid phase weld which can tolerate some improper weld surface preparation (Dunn, 2002).

2.2 Developing Friction Stir Welding Models

Creating an effective model of friction stir welding sounds like a simple, straight-forward task. However, what may appear simple in a superficial glance can become labyrinthine in any attempt at execution. There is a complex interplay from several different factors that change dynamically throughout this process. These changes affect the temperature evolution and material flow within the weld. These effects are also dependent on position, temperature, strain, and strain rate. These determine the stress at any given point and thus determine what type of microstructure and grain orientation will develop. How well these can be determined will affect the final model and its degree of accuracy versus experimental data. Past research has explored many different parameters and assumptions to try and understand what happens in the material during friction stir welding.

2.2.1 Computational Costs and Model Accuracy

Several avenues have been explored to simplify the task of building models by making various assumptions to reduce the complexity of the model. This is due to the increasing computational needs for a highly accurate model as well as limited time and resources. As the desired degree of accuracy increases, there must concurrently be an increase in the computational cost often at a geometric rate as seen in Figure 4.

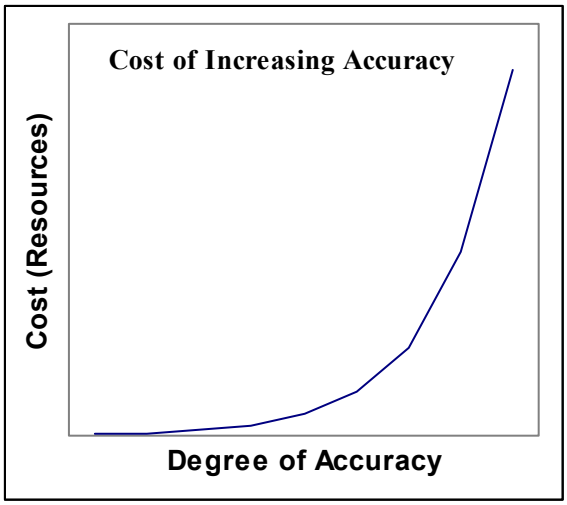

Figure 4: Cost of increasing accuracy

The tool and workpiece geometry, material properties, and processing parameters (RPM, head angle, feedrate, etc.) will vary according to the materials involved and must be included in the model. Previous work by Oliphant has been done to validate the Forge3 software as a viable means of developing a coherent friction stir welding model. In order to observe improvements in this research over Oliphant's modeling efforts, the processing parameters used will duplicate those used by Oliphant. These are given as RPM = 600, head angle = 0°, plunge rate = 1.1867 mm/sec, workpiece material = Al 7075-T6, tool material = H13 steel, and initial temperature = 20°C. Each material has different physical characteristics imparted by its constituent elements. Hoye et al (2003) make special mention of the %wt composition for the tool and workpiece materials which are given in Table 1. This can be used to find the appropriate material definition from the material database included with the Forge3 software package.

Table 1: Composition (%wt) of Materials

	Al	C	Cr	Cu	Fe	Mg	Mn	Mo	P	S	Si	V	Zn	Zr
Al 7075-T6	89.84	--	0.20	1.63	0.10	2.41	0.02	--	--	--	0.06	--	5.73	0.01
H13 (steel)	--	0.38	5.52	--	90.08	--	0.35	1.61	0.01	0.18	1.00	0.87	--	--

Computational costs are an important consideration. In view of the exponential growth in cost for each increment of improved accuracy, it is quickly understood that a

balance must be struck. The Fulton Supercomputing Facility at Brigham Young University provides one of the fastest computers available to this research. By installing and launching the Forge3 computational module on Marylou (one of the supercomputers), it is possible to divide a simulation and run each component over several processors at once to reduce the time needed to complete the model.

How the material is meshed will also affect the computational time. The finer a mesh is, the more nodes there are to compute. Askari et al (2001) have made material meshes that had different volumes allowing for smaller mesh units closer to the tool/workpiece interface. This is important because most of the action takes place in this zone and the objective is to obtain more accurate results where temperature and strain rate gradients are high. Several other researchers have taken the same approach including Bendzsak et al (2000), North et al (2000), and Oliphant (2004), etc.

2.2.2 Meshing Schemes

As part of the development of any numerical model, the type of meshing scheme must be understood in light of the process. Friction stir welding presents a unique situation where there is a large amount of material distortion in various directions around the friction stir welding tool in the X, Y, and Z planes. This "churning" or "chaotic mixing" blends material from the parent components to form the weld nugget.

In either method, materials are modeled as a mesh or network of elements and nodes. The rigidity of the material is dependent on the variable definitions in the material files used by the program. There are two major techniques for applying this information in numerical models. The first is the Eulerian technique which allows the material to

"move" through the mesh while evaluating computations at each of the nodes. A drawback is that computations can be affected by numerical dispersion induced by the material mesh. Steps can be taken to correct this problem such as mesh refinement. Some researchers have opted for Eulerian techniques (Askari et al, 2001; Colegrove, 2000) seeing the idea of material movement through a grid as preferable to a grid attached to the material as in the Lagrangian technique.

This second method is used by the Forge3 computational program which has been validated by Oliphant as a tool with the capability of modeling the friction stir welding process. In the Lagrangian technique the material is represented in much the same way as in the Eulerian method. The major difference is that the mesh velocity and the material velocity are the same. This can prove to be an Achilles' heel in some high-distortion operations such as friction stir welding. The high deformation can cause the mesh to degenerate and overlap itself. This results in "tangling" and node inversion which can lead the computational module to crash. This happens when the computational module is fed improper and/or inconsistent values for the mesh (Askari et al, 2001).

Forge3 counters this shortcoming innovatively by allowing the Lagrangian mesh to be rezoned after a number of computations. This is a user-defined number which must be chosen judiciously. The number of computations must be frequent enough to avoid entanglement but not so numerous that it unnecessarily increases computational time needed to do the extra remeshing. The deformed mesh and material are disassociated and the mesh is reset before entanglement can occur. This effectively reorganizes the meshing arrangement in relation to the material and allows the computational module to continue working on events with large deformations (Oliphant, 2004).

The effort by Askari et al (2001) used the CTH code which is based on the Eulerian (fixed in space) modeling approach and uses the finite-difference (finite-volume) space scheme rather than the more common finite-element. Askari frowns on the Lagrangian (fixed to the material) meshing due to the large deformations involved in friction stir welding which would lead to entangling and improper results. This problem is addressed by Transvalor's Forge3 which limits calculations by the lesser of either the percent deformation or the time step.

The CTH code has the advantage of treating the material as a solid rather than a liquid as several other models do (Askari et al, 2001; Bendzsak et al, 2000). The CTH code works by approximating the shape with multiple rectangular elements "filled" with the appropriate material. This advantage eliminates the need for a finite-element geometry to represent the shape but with the distinct disadvantage that it requires more computational resources to reach a level of accuracy equal to a finite-element with fewer elements. Results from this model were satisfactory while the material was cold, but most of the heat came from plastic work. In the steady state of friction stir welding the softened material would not continue to slide but rather deform.

Work must be done to correctly understand and model material performance under the dynamic changes found in friction stir welding. This relates to the effects of heat, strain, and strain rate but may not be limited to these factors. Continuing research is seeking to improve understanding in this regard and could be used in later models.

2.2.3 Modeling Heat Inputs

Accurate modeling of the friction stir welding process is essential to correctly represent heat generation. Modeling heat evolution in the tool and workpiece is an important step in understanding how it affects material flow and microstructure modification within and surrounding the weld. As the tool makes contact and moves through the workpiece, the heating and shearing effects change the original microstructure of the parent material. Understanding how the particles move and what conditions promote what types of microstructures can help in predicting the proper arrangement to make high-grade welds (Ulysse, 2002). Improved knowledge of microstructure development and control in friction stir welded materials may yield other possibilities such as superior "as-welded" materials and localized alloying to improve mechanical properties.

Friction stir welding focuses on the creation of better joints between two or more pieces. The best expected weld strength is a significant criterion for choosing what types of metals to join as well as choosing the appropriate process. Understanding the thermo-mechanical progression in the friction stir welding process will help to predict the best mix of conditions to create a superior weld. Previous modeling work focuses mainly on heat transfer throughout the workpiece. Research assumptions have looked into understanding the heat evolution through analysis using the Rosenthal equation (Song & Kovacevic, 2003). Dong et al (2001) pointed out that the Rosenthal equation determines values assuming an idealized contact and pressure between the tool and the workpiece.

It is important to review the other bodies associated in the friction stir welding process that could modify the temperature gradients and therefore affect the outcome of

the welds. The tooling as well as the backing plate can greatly affect the amount of energy that stays within the weld and changes the process efficiency. The backing plate is not taken into consideration in most other research as it is felt that it is not a large source of heat loss (Ulysse, 2002).

The tool acts as a medium by which heat generated at the frictional interface can leave the work zone. Testing has shown this loss to be about ten percent of the total heat generated. Tooling designs have been examined with the intent of keeping more heat in the immediate vicinity of the weld. This work has shown that grooved tools may help decrease heat loss through the tool (Dickersen et al, *Heat Flow*, 2003).

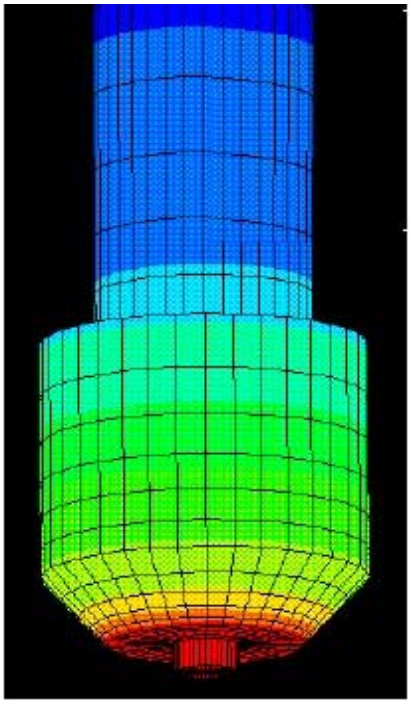

Figure 5: Schematic of tool used in the Dickersen model

Other tooling factors to consider include the actual shape of the major tool body and the pin shape and size. Dickersen (2003) used a tool resembling a drill chuck with a smooth pin as seen in Figure 5. This simplification (the smooth pin) is used in some models while material flow models often include a threaded pin. Several different thread schemes have been pursued to modify material flow or heat transfer. The rule of thumb has been that a right-handed thread is used for counter-clockwise rotating tools and a left-handed thread is used for clockwise rotating tools. This arrangement presents the threads in a position to push material down towards the bottom of the weld.

The method of including the tool's effects in the model depends again on the degree of accuracy desired versus the computational costs that are deemed acceptable. Software capabilities will determine how these can be applied. Oliphant simplified the tooling effects as a simple boundary condition. In order to improve the model's accuracy the heating effects between the workpiece and the tool will need to be included in the model to demonstrate how it changes the results. Further gains may be made by incorporating the effects of the tool holder and backing plate by defining them with thermal boundary conditions as well (Oliphant, 2004). The effects of heat transfer through the backing plate and through the tool and ambient air should help to improve accuracy further while at the same time a finer mesh will allow for more accurate modeling to be run during research simulations.

Ulysse's (2002) model took into account the effects of tool feed rates and RPM settings in thick plate aluminum and how to better model the friction stir welding process in three dimensions. Parametric studies were used in finding a combination of tool settings that promoted a good weld and avoided tool breakage from heat and shear stresses. A line of thermocouples was used to measure temperatures in the workpiece and develop isotherms. This work showed that increasing the feed rate tended to increase shear in the tool pin while increasing the RPMs reduced this force. Parametric tests have shown that there are nominal settings to maximize welding effectiveness while avoiding stress build ups that would cause the tool to fracture during a welding operation. A good model will allow multiple simulations in the same amount of time and will help reduce the total amount of parametric testing needed.

The point in time in which the model examines friction stir welding has also been a major difference between different models. Askari et al (2001) are a prime example of modeling the steady state version and defining a constant temperature throughout the model.

2.3 Material Flow in Friction Stir Welding

Accurate modeling of the friction stir welding process is essential to understanding heat generation and particle motion. Heating and shearing effects change the original parent material microstructure. How this microstructure is created can lead to improvements in the friction stir welding process. Understanding how the particles move and what conditions promote what types of microstructures can help in predicting the proper arrangement to make high-grade welds.

The issue with material flow is that in friction stir welded materials the stress of a point at any given time is dependent on temperature, strain, and strain rate. As heat increases, the stress at that point will decrease *ceteris parabis*. The heating action in friction stir welding is similar to other forms of rotary friction welding. Heat is generated by frictional heating and plastic deformation when the rotating tool contacts and begins to penetrate the component. Material then moves according to a value related to the frictional coefficient.

Heurtier et al (2002) focus their research on the development and use of a thermo-mechanical model of friction stir welding to predict the material flow (strain and temperature maps) during friction stir welding and compare it to experimental measurements. The Heurtier model relied on splitting the problem into two zones. The

first was localized in the flow arm and is mostly affected by the shoulder rotation to a depth of about 2 to 3 millimeters while the second zone was in the weld nugget. This depth approximation is supported by several research efforts (Bendszak et al, 2000; Dunn, 2002; Ulysse, 2002).

These results were analyzed by integration of the model equations to find the strains, strain rates, and temperature estimates for each respective zone. It is important to understand the evolving temperatures, strains, and strain rates of materials so that we can understand the microstructures that are formed. These microstructures determine many of the material's physical properties as well as electrochemical properties.

The predicted temperatures in the model by Heurtier et al were higher than the experimental data although they feel that the magnitude is within an acceptable bound. It is assumed that this is caused by adiabatic self-heating similar to the effects seen by Oliphant (2004) in his research. Changing the initial tooling temperature from 200°C to 400°C made only a 30°C change in the resulting temperatures. Heurtier et al (2002) concluded that this should be due to the drop of flow stress at elevated temperatures.

In research done by Bendzsak et al (2000), material directly under the shoulder appeared to flow in a counter-clockwise movement from the advancing side to the retreating side. This is assumed to be moving at a maximum of 70% of the tool speed which differs from the 40% of tool speed suggested by Dunn (2002). The assumption of 70% of maximum tool speed needs to be clarified further to set up the appropriate rheology for the model. This will affect the values derived from the flow stress equation.

As cutting planes were made deeper into the workpiece, it was found that the rotational effects tapered off and a transition zone of 600 micrometers thickness existed

approximately 1.5 mm below the surface which coincides well with findings by Dunn and Dong et al. After this transition zone, the major factor seemed to be a forging action of the material around the pin which is supported by conclusions from Dong et al (2001).

Dong et al also suggest that one of the implications of their research is that the geometry of the stir pin can be directly related to the variation in heating and plastic deformation. These in turn affect the stress-strain conditions found within the material and thus the resulting microstructures.

Colgrove (2000) also splits his model into two major sections to allow for material flow. The model has a boundary between the "Thermal/Flow Zone," a region of localized friction stir welding effects, and the "Global Thermal Model" which contains everything else. Each region has different parameters used in the calculations at each node. This design makes use of what is essentially a step function between the pseudo-liquid material in the weld and the solids that surround it. If the number of steps between the defined realms of the pseudo-liquid and the solid were increased, the gradient of effects would follow a smoother path and the results would become more realistic until the model accurately predicts real-world conditions. However, available computational resources were limited and this process was not explored.

Colegrove has, however, noted that having the pin heated produced better results for material flow at the top half of the weld, while not heating the pin produced better data for the bottom half of the weld. Results by Dong et al (2001) support this finding. They strongly suggest that friction induced heating is dominant in the upper region of the weld zone and that plastic work induced heating is significant and dominant in the lower region of the weld zone. As a result, it is essential to consider both heating mechanisms,

i.e. friction heating and plastic work, in modeling the heat flow phenomena in the friction stir welding processes.

Song and Kovecevic (2003) agree with these findings, giving it more support through their experiments. They state that the top portion of friction stir welded materials is mostly affected by heat while the bottom portion around the pin is plasticly deformed similar to a forged extrusion process. The extrusion dies are the pin itself and the harder material that has not yet reached the point of plastic deformability. The material is pressed past the pin on its retreating side and consolidated behind the pin by the shoulder and the cooler weld material behind the welding zone that has cooled below the point of being plasticly deformed. A graphic representation can be seen in Figure 6.

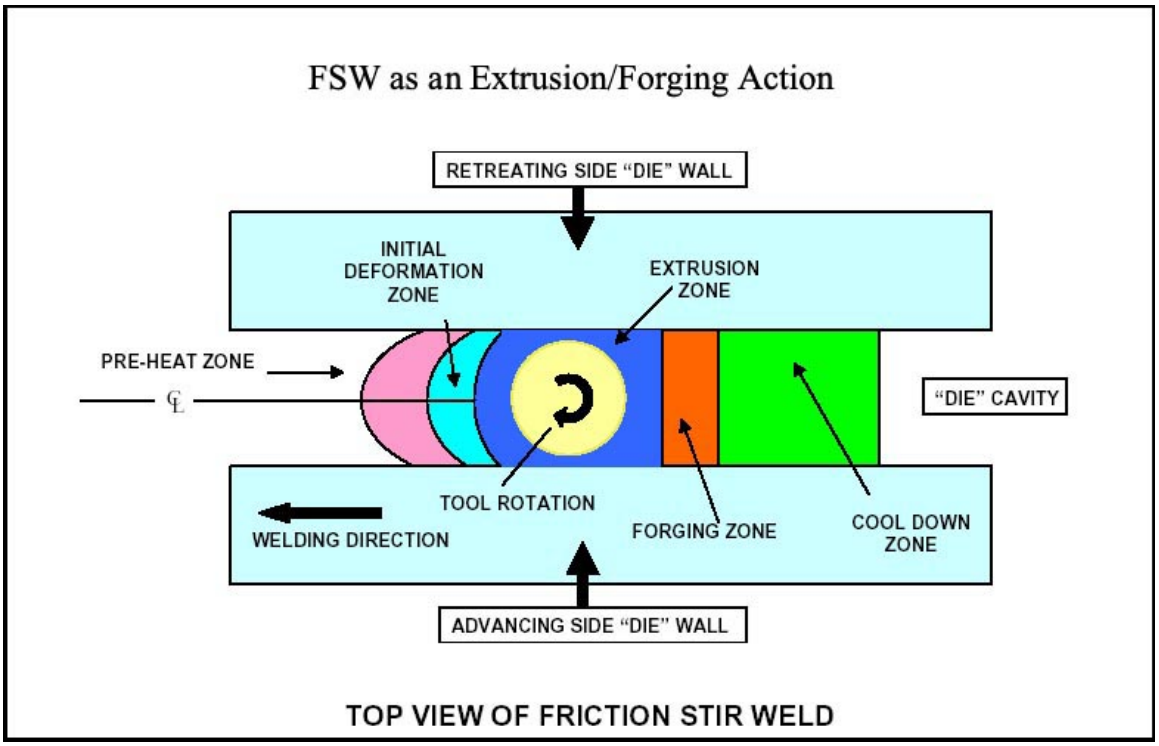

Figure 6: Representation of the various "zones" encountered in the FSW process [1].

2.4 Summary

Friction stir welding is a promising development in the realm of material joining processes. Its benefits are many and even exceed other welding process abilities. Friction stir welding operates on a simple principle that can be applied to many current procedures. Its growing use in joining materials in several industries encourages further research and understanding to produce the knowledge needed to fully benefit from this innovation.

Previous research has looked at trying to mimic experimental results and "get inside" the welding process to understand how it heats up, how the material flows, and what mechanisms are at work within the welding zone. Improved resources such as faster processors and parallel computing environments can be used to refine the degree of resolution attainable within a reasonable span of time. By developing models which yield the same results for temperature and material motion at given increments it is reasonable to assume that the model could then be used to perform parametric studies on a wide range of materials and processing parameters. The advantage would be savings in material, personnel, and machine burden costs. Experiments would be able to focus on exploring other options in material choices and processing parameters to validate favorable results obtained by the model.

3 METHODOLOGY

3.1 Mesh Development

Previous research has shown that Forge3 is a better choice over the Sandia National Labs' Alegra to use in modeling friction stir welding (Oliphant 2004). This research will continue to use the Transvalor S.A. product in an effort to improve previous modeling efforts and maintain a consistent development procedure.

Meshing size and scheme is an important decision as was discussed in Chapter 2. Forge3 is capable of using the Lagrangian technique and applying it to a high deformation problem. It accomplishes this simply by allowing the mesh to move a certain number of increments, as defined by the user, and then simply resetting the numeric mesh to prevent mesh entanglement. This method can be understood by looking at Figure 7, below.

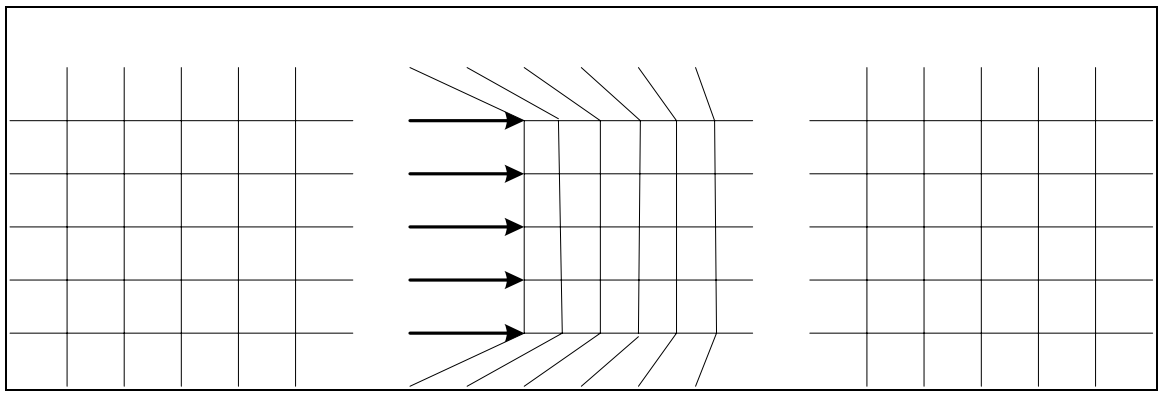

Figure 7: In Forge3 the Lagrangian mesh is allowed to deform while calculations are performed (A & B). The mesh is reset after a user-defined number of computations (C), thus allowing it to work on high-deformation problems without degenerating.

Taking this advantage into account, the model was developed and meshed in such a fashion as to reduce the number of computational nodes. These meshes are built up of many tetrahedral elements of various sizes. Smaller tetrahedrons are found closer to the pin and get larger as they move away from the area of interest. The mesh in the immediate vicinity of the tool is very small to allow for a higher resolution of material heating and motion. As the distance from the center of the billet increases, the size of the mesh increases since little or no motion will be expected at these distances. Figure 8 shows the relative size of the mesh, the smallest mesh being the area where the tool makes contact.

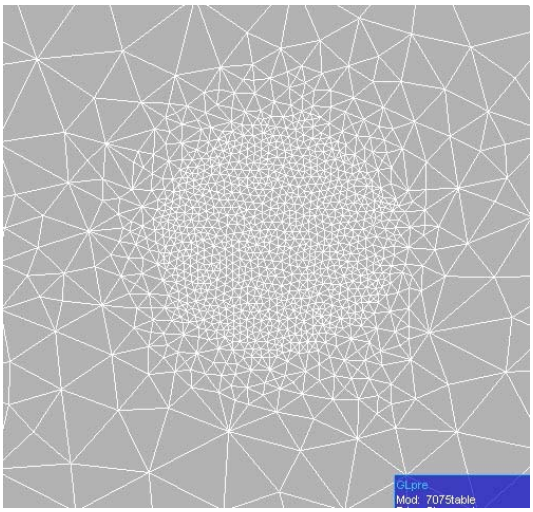

Figure 8: Relative mesh size.

3.2 Model Development

Previous validation of Forge3 Version 6.2 as an adequate tool for building a numerical model of the FSW process has been shown by Oliphant's work on the subject in 2003. This work simply looked at the fact that a rotating tool could be introduced to the workpiece and semi-realistic results would follow. Assumptions had been made to reduce computational time and simplify the model. These included an adiabatic heat transfer between the tooling and the workpiece, essentially trapping almost all the generated heat in the billet leading to greatly inflated heat measurements in the model.

The new model is focused on material flow and therefore must take into account the heat transfer with the air and tooling on the machine. The assumption for heat

transfer with the air is limited to 10% which is the default for the software. The tool is more complex as it is intentionally cooled by a radiator type system inside the tool collar which holds the water temperature at a maximum temperature of 20°C ±1 during the process. This heat removal occurs at the tool-tool holder interface and the effect would only be that the tool would begin at a cooler-than-room temperature value and heat should be evacuated at some higher rate from the tool. Experimental results from such a tool with thermocouples inside are used to define the evolution of temperature over time at the pin and shoulder of the modeled tool. The temperatures in the modeled billet start at 20°C (room temperature) but increase according to the thermal computational module and its inputs defined from the tool in previous experimental results. The results in the billet will be compared with experimental results in Chapter 4.

Work on the model was done with the assumption of a simple FSW tool as seen in Figure 9. This is based on the tool used in validation experiments prior to and during the simulation. The tool is made of H13 tool steel while the workpiece is made of Al 7075-T6.

Mechanical and thermal data are available in the Forge3 database for both the tooling material and for the 7075 aluminum. These are nominal values that are typically used for

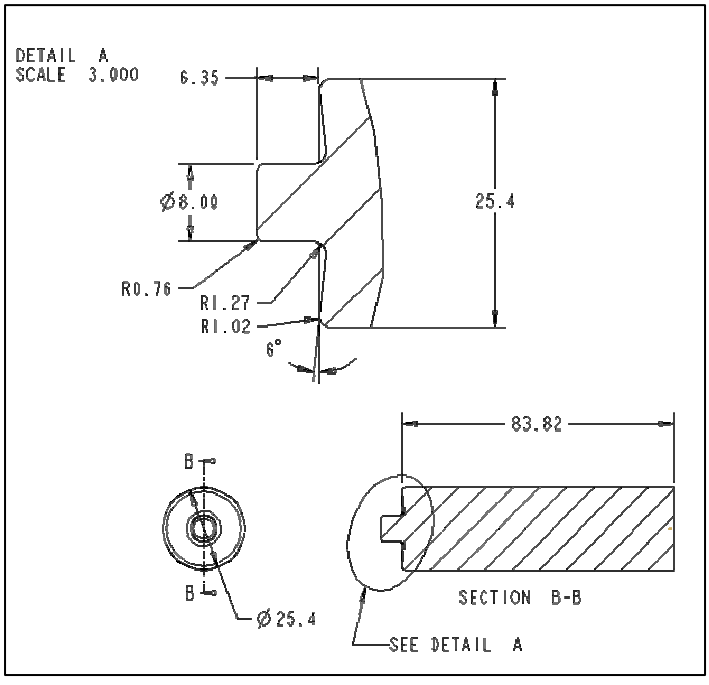

Figure 9: Drawing of the FSW tool.

modeling forging processes. These values can reasonably be used for modeling friction stir welding because forging is a high-strain-rate, high-temperature process friction stir welding.

Due to the high computational needs to run these models the Fulton Supercomputing Facility was sought in order to decrease the time needed to finish a simulation. Several problems developed and workarounds had to be created either in-house or with the aid of Transvalor. The first problem was the need to get a simulation to run across several processors at one time. Following the idea that "many hands make light work," the supercomputers had several processors that could break the simulation into pieces and work out a solution quicker than a single processor. While working with Transvalor and the supercomputer administrators, it became apparent that this was no simple task and an attempt at finishing a single-processor run would occupy the next few months. When the bugs were found and eliminated, it took 42 days of processing to run 5.44 seconds of simulation, or more than a week of computer processing time to calculate a single second of the model time. Part of the time cost is attributed to sharing the processors with other users.

During this time the first modeling attempt was made in an effort to correctly migrate previous work done in Oliphant's research using Forge3 version 6.2 to the updated version 6.3/7.0 beta. The version 6.3 software defines the machine anvil and the FSW tool as "rigid dies" which are capable of motion but do not record thermo-mechanical changes. The tools can be defined at the beginning of the simulation to be at a certain temperature. At this point Oliphant's research defined the tools to be at room temperature (20°C) and having an adiabatic thermal exchange (which negates any

defined temperature or effect this would have on the model). The model was compiled and run to completion at the Fulton Supercomputing Facility with the same results seen in Oliphant's model and the transfer to the newer version was deemed a success.

Progress was made as the support team at Transvalor found a workaround which enabled a model to be run across several processors on one of the supercomputers using version 6.3. The first drawback was that the supercomputer where the computations were being done had only six processors available (of which we were limited to four). The second drawback was that there was no way to dedicate the processors to the model. Solving this problem was paramount to improving the ability to do parametric studies. Coordination with the CAEDM administrator allowed the use of a sixteen-processor supercomputer for a time and later isolated a six-processor box for continuous use on this project.

The third drawback was that during compilation and testing of the models, it was discovered that version 6.3/7.0 beta had several bugs that were distorting the simulation results. These included a situation where the rotating tool caused serious material penetration that was unrealistic. Another problem occured when the tool started to penetrate the billet normally and the surface would take on a distorted appearance. These problems happened while defining the tool and anvil as deformable dies in order to allow for a completely thermo-mechanical computation. Transvalor was notified about these bugs and changes were made after consulting with them.

Taking into account what had been learned from Transvalor as well as receiving an updated version of the software, the next modifications were made to the model and run with these changes in effect to address the software shortcomings. More problems

appeared as work progressed. Appendix A includes examples of these problems, the workarounds that were devised or proposed to overcome them, and the results of these efforts.

This second model retained the same basic tenets of the previous simulation but removed the adiabatic thermal exchange to begin introducing more realistic tooling effects into the model. In this case the tool-billet interface is assumed to be in intimate contact and defined as a "hot-strong" thermal exchange from the included Forge3 files. The first model which simply tried to migrate the simulation from 6.2 to 6.3/7.0 beta showed greatly inflated estimates for the billet temperatures due to the "trapped" heat in the billet. The increased heat would accelerate temperature buildup and change how the material would flow within the model. Results from the modification of the thermal exchange showed interesting divergence from data collected from the previous adiabatic model. These results are discussed in Chapter 4 in relation to each model.

The third model was an attempt to model the FSW tool as a meshed object which allows the user to view how the tool would heat up and act as a type of heat sink. The difference between tool and billet affects the heat transfer from the billet. A larger difference in temperature would allow for more cooling through the tool. This would increase the realism in the model by dynamically changing the amount of heat leaving the billet via the tooling as the difference in temperature changes between bodies.

The processing of this model again ran into problems. Only version 7.0 or higher allows the user to define the tool as another deformable die which would allow for a fully thermo-mechanical computation including the temperature evolution within it. Currently, this version does not have the capability to allow parallel processing and this function is

not expected to be available until the first quarter of 2005 at the soonest. Further research using the thermo-mechanical computation (version 7.0) would have to be done using a single processor with the enormous time cost associated with it. Preliminary attempts showed, however, that there were still computational issues with the beta version forcing another long wait while Transvalor attempted to solve the problem.

At this time another solution based on a calculus-like approach became tenable. Further research could be pursued without waiting for a new version from Transvalor. The basic idea for this approach would be to build the model in a piece-wise manner.

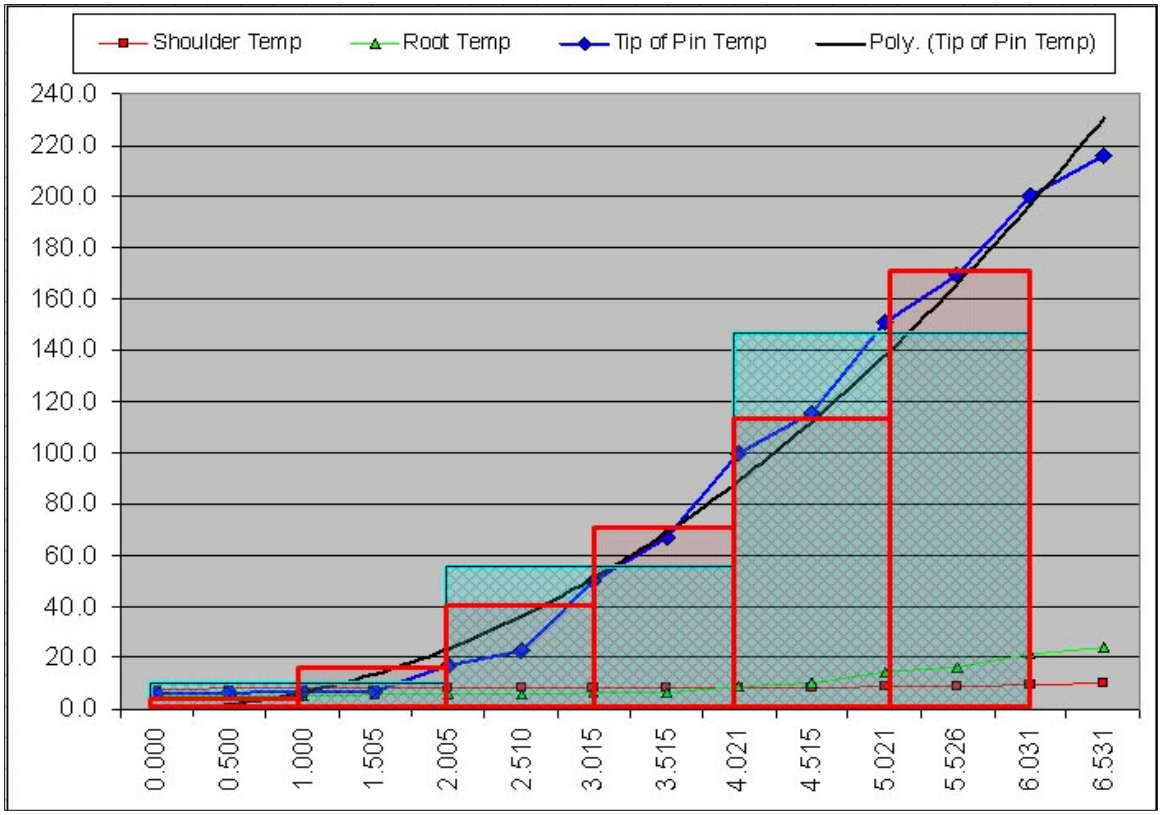

Figure 10: Calculus-type approach to improved tooling temperatures.

This would mean running the model for a given length of time and defining the tool as a rigid die with a specified temperature. As in calculus, as the time between increments

approaches zero the results will more closely match those expected from a continuous function representing experimental observations. This approach can be seen in the change in accuracy by changing from the blue to the red rectangles in Figure 10.

This approach was further refined by defining the temperatures for the tool at certain points in time according to experimental data taken from Oliphant's research data. By applying this in a table format it is possible to allow the model to extrapolate what temperature the tool should be at the relative point in time for the simulation. This is represented by the dark blue line running roughly parallel to the black trend line seen in Figure 10.

Another refinement added the thermal effect associated with the billet-anvil interface to the models. Since the billet is made of aluminum and the anvil upon which it rests is steel most of the heat will be dissipated quickly through the mass of the billet while heating the anvil a small amount. This temperature change in the anvil is assumed to be generally linear. In this model the temperature change in the anvil is defined in the lower rigid die by a table similar to what is used to define the changing temperature in the tool. The beginning temperature is assumed to be room temperature or 20°C and ends at 50°C.

Preliminary results showed that this is yet another area that must be improved as the changing anvil temperature scenario causes the temperature calculations to be completely inaccurate. Very quickly after beginning, the dynamic anvil temperature causes the thermocouple reading to plummet as can be seen in the partial results seen in Figure 11. These results came from a test involving two versions of the same model; the "tool model" was changing the tool temperature while holding the anvil temperature at a

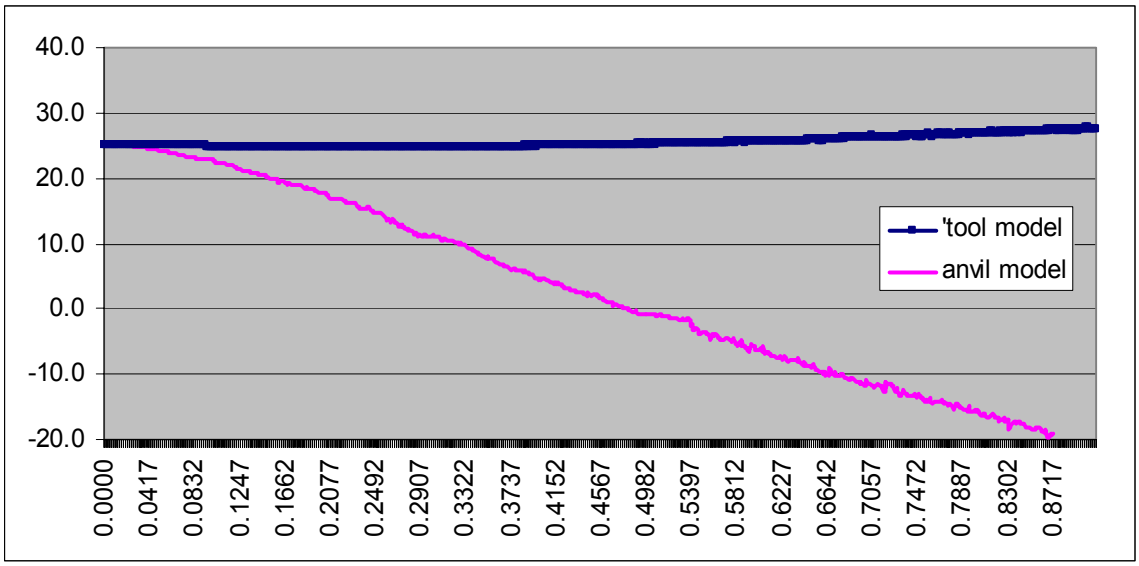

Figure 11: Results from two models showing the improper temperature calculation.

certain level while the "anvil model" varies both the tool and the anvil temperatures. This has proven to be a problem with the software and Transvalor is currently looking into the issue with the developers to discover the source. Due to this issue, the continuously changing temperature on the anvil was eliminated and three models were built to explore the effect of anvil temperature on the model using a static temperature for the anvil equal to 25°C, 50°C, and 75°C, respectively.

3.2.1 Flow Stress

All the previous simulations were run using the "hot" rheology as used in Oliphant's research to preserve continuity. There was some question as to how the results might change if the flow stress data could be improved to include more appropriate values. Flow stress is an important component as it helps to determine the amount of heat from mechanical deformation. It also leads to a better understanding of

the future possibilities of microcrystalline structure formation due to the localized stress and orientation.

Flow stress is dependent on material temperature (T), strain (ε), and strain rate (έ) and is found by using the Hansel-Spittel Rheology Law seen in equation (1). Coefficients m5 through m9 are equal to 0 and this reduces the equation to that seen in equation (2).

Hansel-Spittel rheology law

$$\sigma_f = A e^{m_1 T} \varepsilon^{m_2} \dot{\varepsilon}^{m_3} e^{\frac{m_4}{\varepsilon}} (1+\varepsilon)^{m_5 T} e^{m_7 \varepsilon} \dot{\varepsilon}^{m_8 T} T^{m_9} \quad (1)$$

Thermoecroui :	Thermo-mechanical conditions
Hansel Spittel Nb1,	Hansel-Spittel rheology law
A1 =,	Consistency
m1 =,	Temperature term
m2 =,	Sensitivity to Strain-hardening
m3 =,	Sensitivity to strain rate
m4 =,	Strain softening coefficient
m5=, m6=, m7=, m8=, m9=,	Unused coefficients

$$\sigma_f = A e^{m_1 T} \varepsilon^{m_2} \dot{\varepsilon}^{m_3} e^{\frac{m_4}{\varepsilon}} \quad (2)$$

Figure 12: The Hansel-Spittel equation used in Forge3.

Transvalor uses a database of materials in Forge3 which are defined within two heat classifications with different values for the variables to calculate flow stresses at different temperatures. The "cold" region is defined as temperatures from 20-250°C while 300-500°C is the "hot" region. The domain of temperatures in the friction stir welding process includes both of these ranges and can feasibly be found in very close proximity due to the high temperature gradients which are present.

The domain of T is 20-500°C and the maximum possible strain rate can be calculated using equation (3) during the plunge. The regression coefficients A and m1 through m9 can be understood by Figure 12.

$$\dot{\varepsilon}_{max} = \omega \pi d \qquad (3)$$

where ω is the angular velocity and d is twice the distance of the point in question from the center of the pin.

Considering our operational parameters this gives us a maximum value of 600 RPM * 3.1415 * 25.4mm = 797.94 mm/sec. Evidence from other research has shown that the material in the workpiece only moves at about 40% of the speed of the tooling (Dunn 2002). This would reduce the maximum expected strain rate to 319.18 mm/sec. Actual data to confirm the strain/strain rate/temperature effects on flow stress could not be obtained and it was determined to leave this for future research.

One final simulation was run using the parameters above to examine these results. This was done by creating an "open-format" table and combining the two rheologies into a composite whole to cover the entire "cold-hot" range. The open-table format is created by defining specific temperatures, strains, and strain rates and the resultant flow stress for each combination of parameters in a file separate from the .ref file. An example of this table is included in Appendix B. This table is all that is included in the file. This compound rheology was then available via a callout in the .ref file to the computational module for calculating the correct flow stress according to the values representing any point in the model.

3.3 Experimental Design

The experiment was set up to record data during the first phase of the friction stir welding process—the plunge. The processing parameters set forth for the experiment and simulation are 600 RPM and a plunge rate of 1.1867 mm/sec for six seconds (this six seconds begins once contact is made). The billet is made of Al 7075-T6 and is 19.1 mm thick. Every effort was made to bring both the model and experimental parameters into alignment.

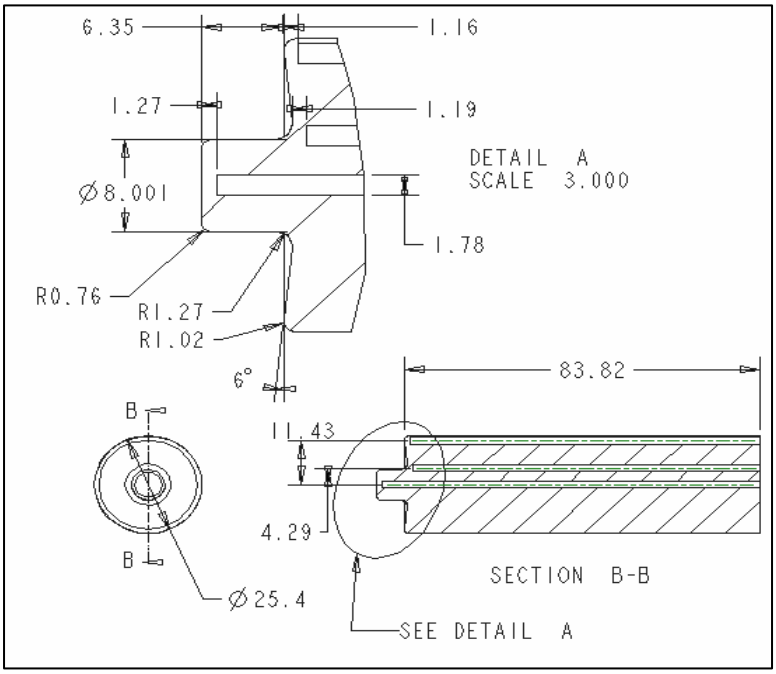

Figure 13: Tool thermocouple locations.

The experiment was run on a Kearney & Trecker Milwalkee horizontal mill located in the Friction Stir Research Laboratory. This setup has been retrofitted with a computer controlled interface as well as a dynamometer. Data collection during the experiment was done via six 1.6mm-diameter type K thermocouples embedded in the billet and another three 1.2 mm-diameter thermocouples in the tool. The thermocouples in the tool are rotating at the same rate as the tool and hard wiring them to the computer would be impossible as the wires would become entangled and break. Instead, a radio frequency collar is located around the tool and receives signals from three special thermocouples

located in the pin, the root, and the shoulder as shown in Figure 13. Only three thermocouples are used as this is the maximum outputs available from the RF collar.

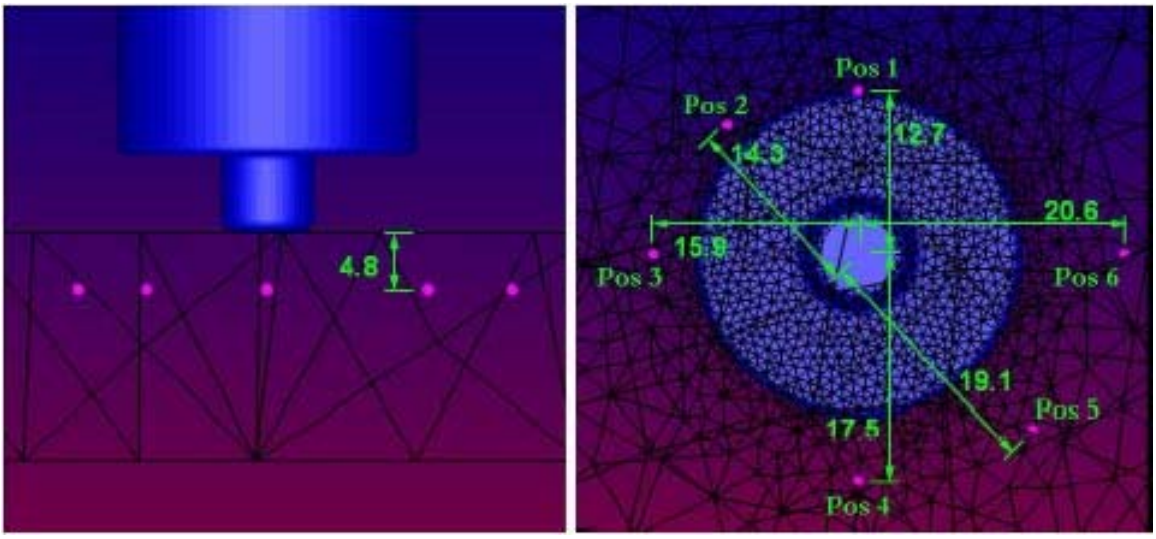

Figure 14: Relative thermocouple positions in the simulation and experiment.

The locations of the thermocouples in the billet are shown above in Figure 14. These positions are identical to those used previously in Oliphant's research to give continuity to the evolution in improved results for the model. Channels were milled into the billet and sacrificial anvil to allow them to sit flat while permitting the thermocouple wires to pass from the point of insertion out to their respective receptacles. The billet dimensions as well as the milled channels for the thermocouple wires can be seen in the Figures 15 and 16.

The experimental runs from Oliphant's research were used in comparison with this new experiment which was coordinated and run with Stan McBride. Six separate runs were conducted and the results tabulated (see Appendix D). The first three experimental runs used thermocouples in the locations shown in Figure 15 while the remaining three runs used the locations shown in figure 16. This was done in an attempt to gain further information between the edge of the tool, specifically as it relates to the temperature

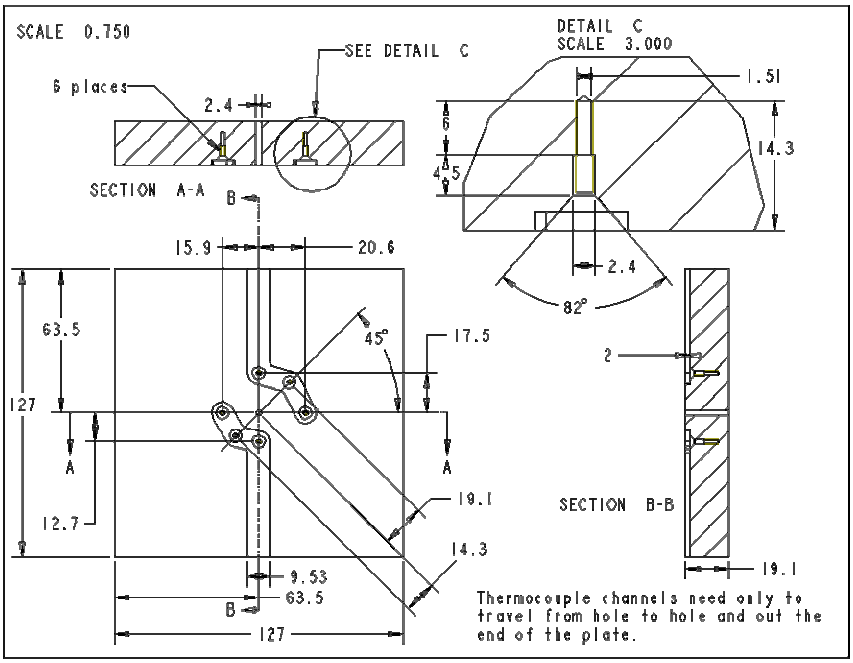

Figure 15: Drawing showing the billet dimensions and thermocouple channels.

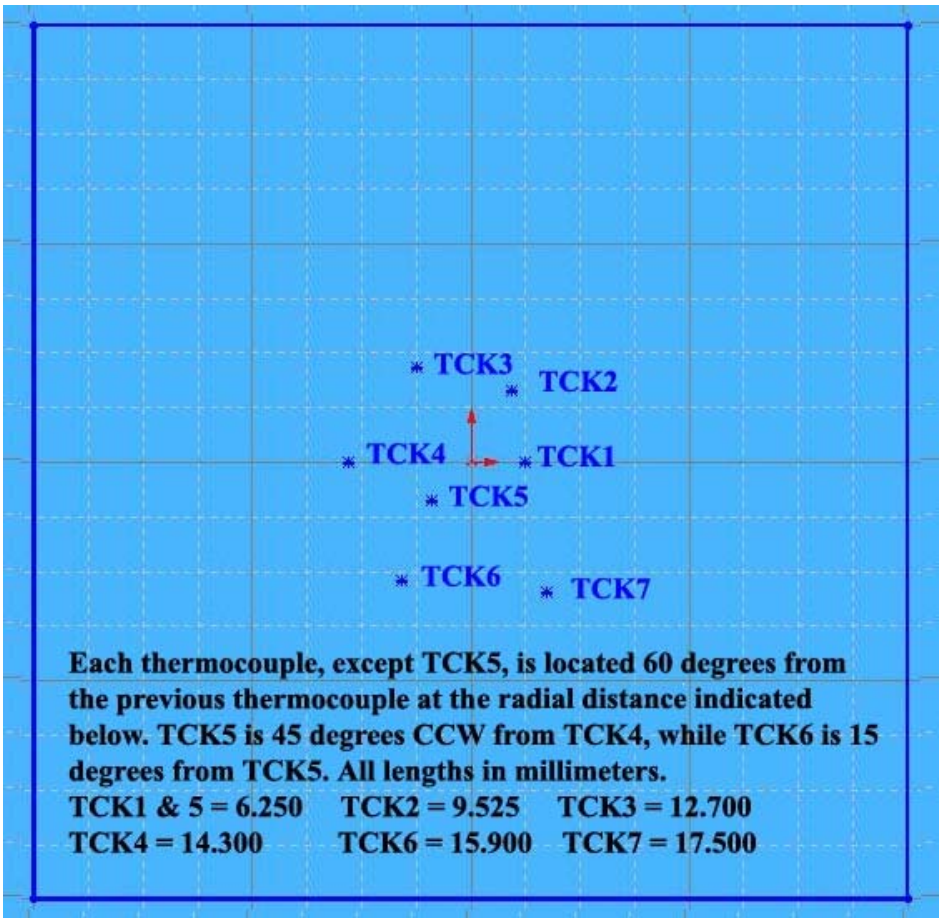

Figure 16: Thermocouple locations in the XY plane for experiments 4, 5, and 6.

gradient around the pin and shoulder. Contact was assumed to occur at the first increment where the Z force became larger than 20 pound-feet. This was designated as the start time, t = 0. Comparison between experimental results and each simulation result will continue in the following chapter.

Figure 17: The FSW setup just prior to the start of an experiment.

4 RESULTS AND DISCUSSION

After completing the different simulations and the experimental work described in the previous chapter the results from each are discussed in this chapter.

4.1 Experimental Results

The data results from the experimental runs done by McBride are included in Appendix C and are compared here with earlier results from Oliphant. Figure 18, below, shows the individual and average results from the new experiment and how they compare to the average values obtained in the previous experiments used by Oliphant.

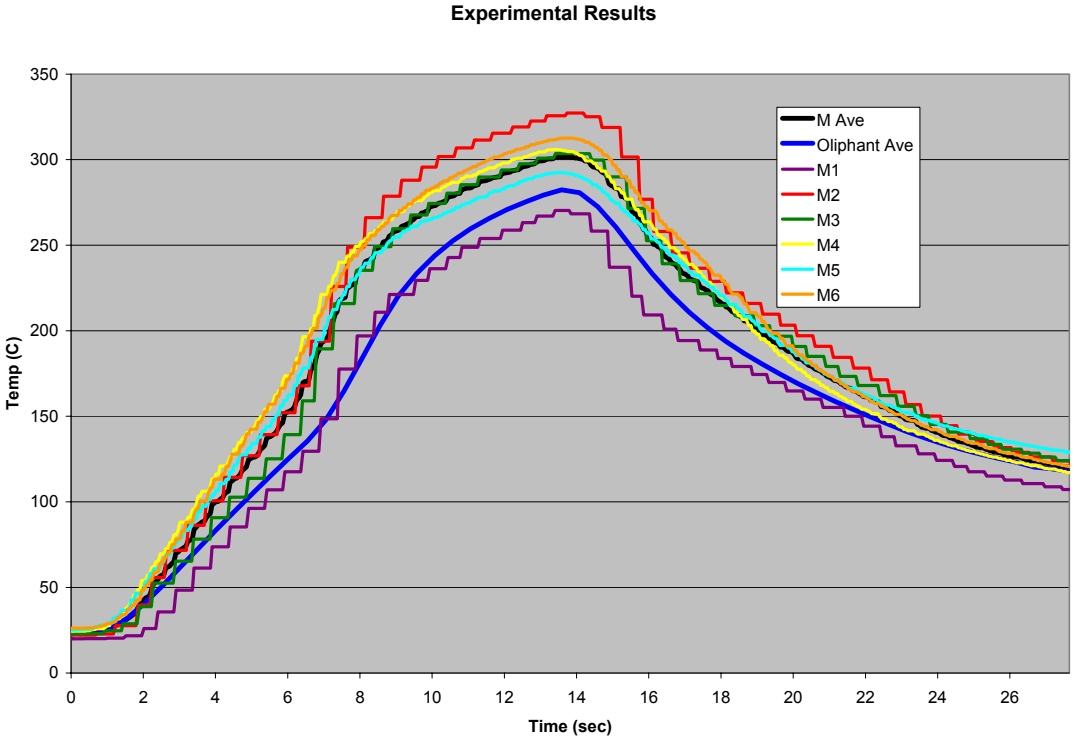

Figure 18: A comparison of the runs and average versus Oliphant's averaged data.

The graph shows that both experiments have the same trends while the first set of experiments (runs 1, 2, and 3) has a larger variance. The second set of experiments (runs 4, 5, and 6) used the layout variation noted in Figure 16 and are more consistent with each other. It is thought that part of this accuracy issue is due to the "learning curve" of setting up the experiment. All runs except the first fall almost entirely within one standard deviation from the average. Oliphant's experimental results also appear to match well with the new experimental results. However, one portion falls below the lower end of the error bars where the maximum deviation is measured at almost 30 degrees. It is felt that overall these results are mutually reinforcing and therefore can be assumed to be valid.

The Kearney & Trecker Milwalkee horizontal milling machine is not perfectly rigid and experiences huge amounts of force. This allows for some flexural differences

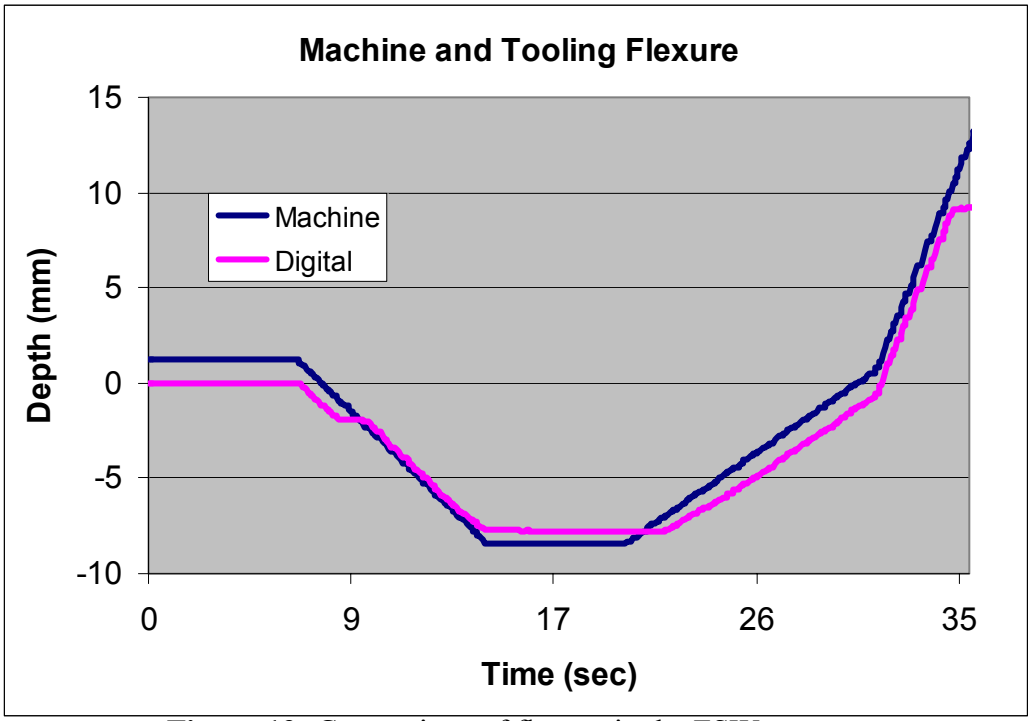

Figure 19: Comparison of flexure in the FSW setup.

between the measured and real machine position is in the Z-axis. This will come into play in the X- and Y-axes during future experimentation of the traverse. During each experiment, a digital depth indicator was set up to give a comparison reading versus the depth output by the machine. These measurements are compared in the Figure 19. All results are compared against the digital readout to reduce any effect machine flexure could have on the results.

4.2 Simulation Results

4.2.1 Parallel Processing Simulations

As noted in previous chapters, processing time is a large consideration in building and executing a simulation. There are different solutions to this problem including running simulations over a parallel processing node or network. The difficulties of this process are noted in Chapter 3. Transvalor tried to coordinate their efforts in producing a viable option which eventually necessitated transferring all work from the IBM supercomputers to the HP-Unix supercomputers.

Work progressed in designing and setting up the new simulations but ran into problems with mesh degeneration in myriad forms. The first problem was previously noted by Oliphant where the geometry of the billet collapses at the edges. Along with this peripheral crumpling, the new parallel model also experienced dimpling on both the top and bottom surface of the billet. An example is shown in Figure 20. At times inexplicable slippage occurred between the billet and the anvil as shown in Figure 21. The rotating tool would increase in diameter and become deformed against the billet at times. After an update by Transvalor, this same setup would no longer be compressed

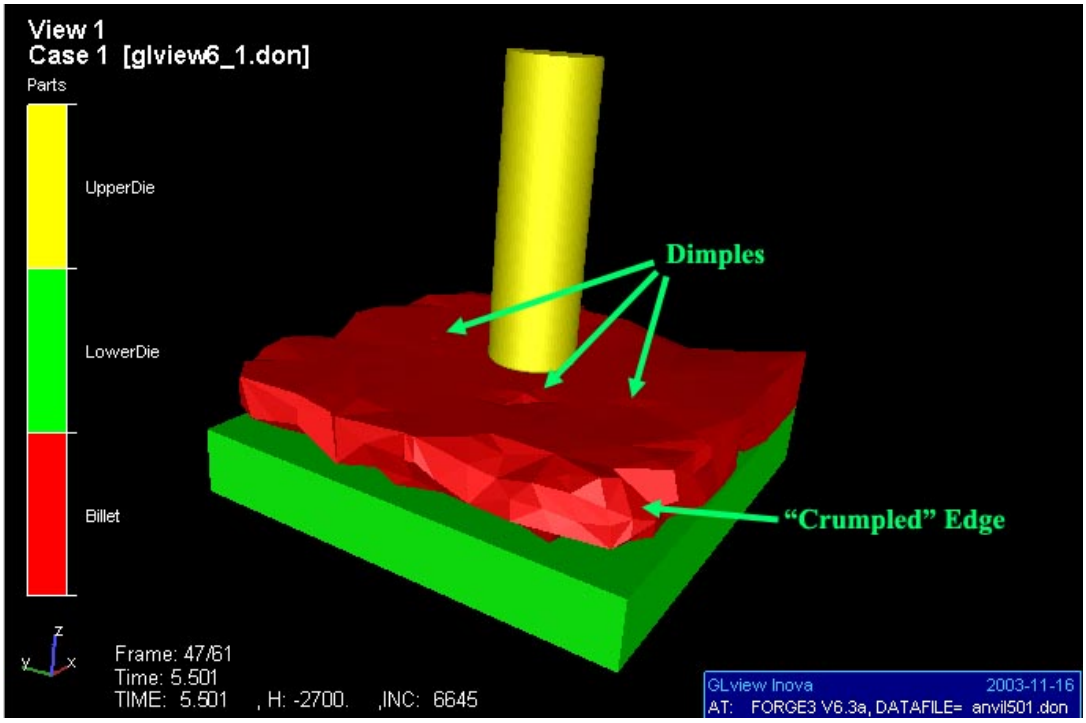

Figure 20: Screenshot showing dimples and peripheral crumpling.

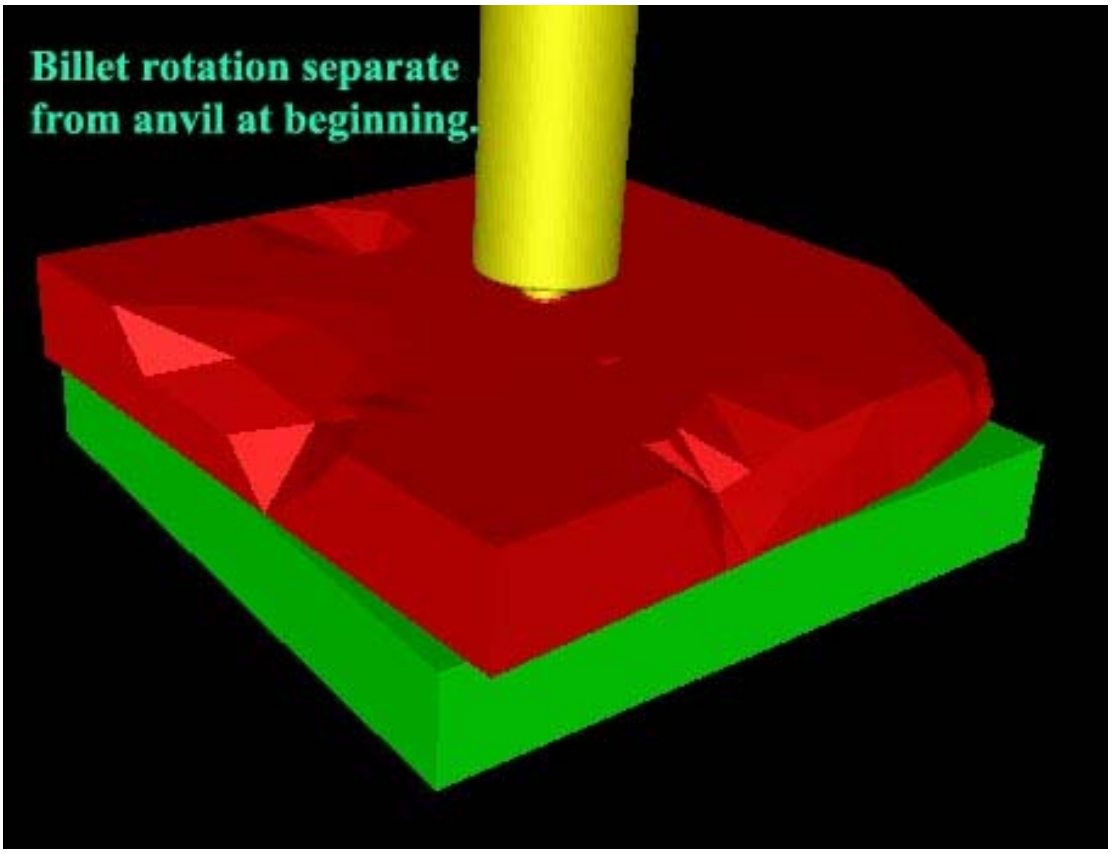

Figure 21: Slippage between the anvil and billet at the start of the simulation.

but actually became elongated and stretched out like taffy. In yet other situations, as the tool began to penetrate into the billet, the top surface of the billet took on a very rough and jagged appearance.

As work progressed and no improvements with the parallel setup seemed to be forthcoming, it was decided to abandon any further attempts to correct the problems with the parallel format at this time. This was a major setback due to the enormous time reduction seen in focusing multiple processors on a single simulation. The single processor simulations that follows took 32 days to complete on an isolated six-processor node. In comparison, the parallel versions of these simulations were completed in four days or less. Everything possible should be done to work out the bugs in the parallel version of Forge3 for future research.

4.2.2 Static Anvil/Dynamic Tool Simulations

With the failure of the parallel processing simulations, more help was sought from Transvalor. While waiting for more information from them, it was decided to tackle the problem with a calculus-like approach. This method is described in Chapter 3. Taking thermocouple readings from experimental results performed previously, the temperatures were included in the simulations by using a table of time-dependent temperatures.

Initial results showed great promise by varying the temperature in the tool. Further accuracy was sought by making a similar table for the anvil. This led to an unexpected failure as the temperature fell dramatically after the beginning of the simulation. It was discovered much later that this was caused by an inappropriate read-in by the software. Where the temperatures were entered in as degrees Celsius, the software interpreted them

as degrees Kelvin on the anvil and degrees Celsius on the tool. Due to this software issue it was decided to make three simulations modeling the anvil at a static temperature value of 25, 50, and 75 degrees Celsius, respectively.

The results from these simulations are shown in Figure 22. Alongside these are Oliphant's Forge3 simulation and experimental average. Also shown are the new experimental average and a final simulation which used the "open table" format which is discussed later. Several screenshots are shown in Figure 23 to demonstrate the relative position of the tool and anvil as well as the material's movement into the void between the tool shoulder and the billet face.

The three static anvil/dynamic tool temperature simulations all follow the same temperature trend as shown in Figure 22. As the pin penetrates the billet, the temperature rises very gradually. The pin forces the billet material to be compressed and pushed out of the hole that is being produced. This material flashes up the pin and starts to make contact with the root and shoulder just after t = 5 seconds. At this point the temperature starts to rise dramatically due to the increased friction between tool and billet.

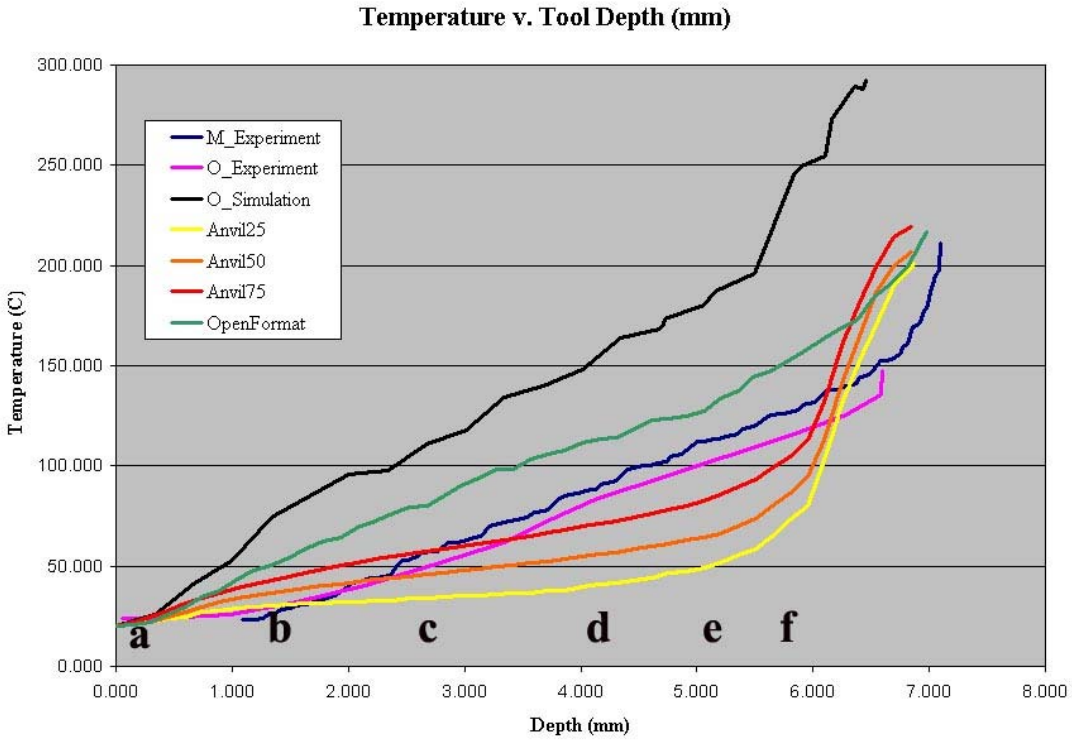

Figure 22: Comparison of thermocouple readings as depth increases.

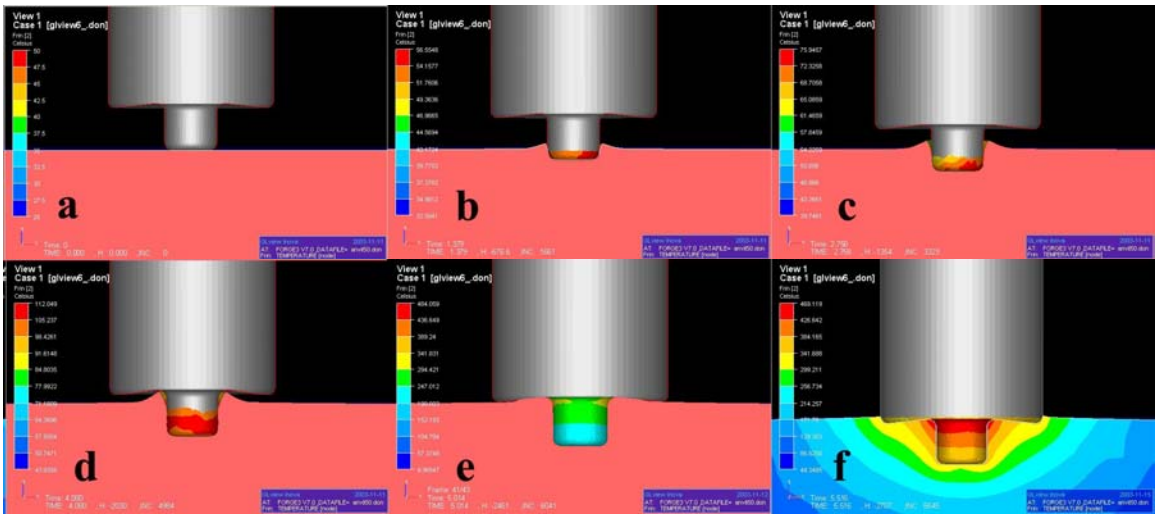

Figure 23: Tool position relative to the anvil. Letters coincide with the approximate depths listed in Figure 22.

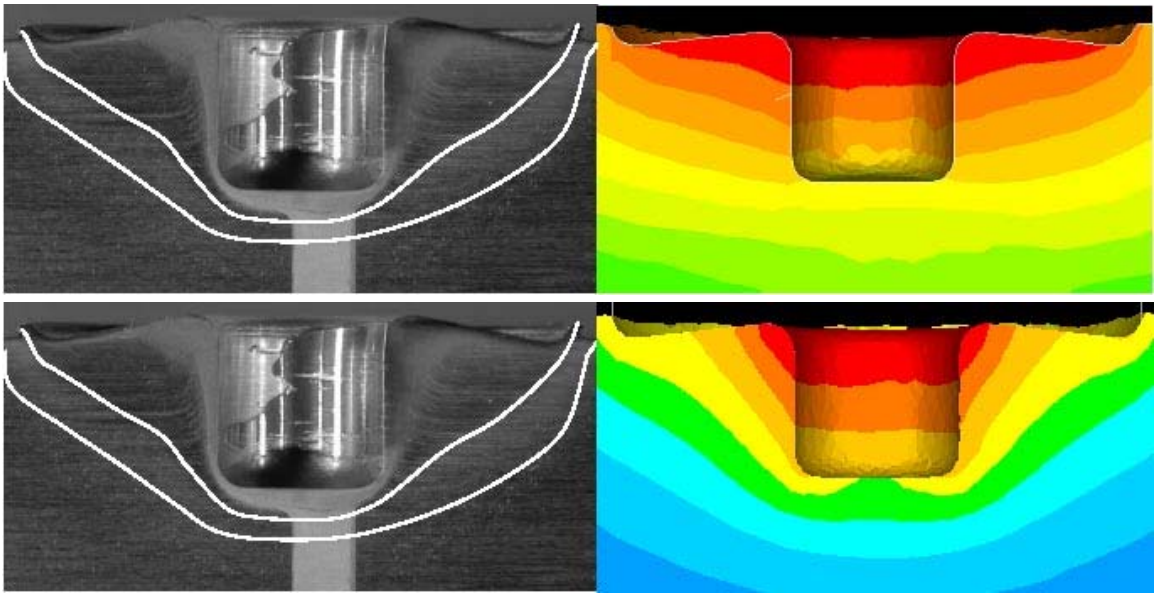

Figure 24: Comparison of isotherms from Oliphant's simulation (top) and Anvil50 (bottom). Notice the improved correlation between the thermomechanical boundaries in the etched metallurgical sample and the improved simulation.

The addition of a non-adiabatic boundary condition permits the model to allow heat to escape via the tool. This effectively frees the energy to move away from the friction area according to the heat flux value appropriate for the changing temperature difference between the anvil and tool. The difference can be seen in Figure 24. The isotherms seen in the top portion show a wide area where the temperature appears to be independent of any effects from the pin. The new simulations show a more trapezoid-like cross section indicating that the pin still contributes to the overall development of the isotherms. The new isotherms also show a much improved correlation with the thermomechanically affected areas in the metallurgical sample.

4.2.3 Open Table Simulation

As the results from the static anvil/dynamic tool simulations appeared to be promising, an attempt to meld the cold and hot rheologies was pursued to improve the calculation of the appropriate flow stress. It was thought that since a large spectrum of temperatures and strains is present in the friction stir process, that it is not correct to use the cold or the hot rheology in exclusion of the other.

The open table format was developed using the Hansen-Spittel Rheology Law used in the software to calculate flow stresses. The software uses either the hot or the cold rheology but has no option for a composite of the two. The values for the cold and hot rheologies were combined to develop a continuous set of values dependent on temperature (20-1000 degrees Celsius), strain, and strain rate (.01-1000). These values were used to cover all values that might be possible during the simulation.

The open table simulation performed well in improving the temperature trend versus the other simulations. The temperature rises in a nearly linear fashion from the very start until the end. Both experimental results show a tendency to rise very slowly for the first millimeter of depth. After this divergence, the open table simulation runs roughly parallel to the experimental results. However, it remains higher than the experimental results by 25 degrees or more over the duration of the simulation. Further results during the traverse would be interesting but were unobtainable due to software limitations at this time.

4.3 Material Flow

Material flow is of great interest in understanding the creation of welds. Several efforts have been made to help increase the body of knowledge on this aspect. The Forge3 software package includes an option where either a single particle or a group of them can be tracked as they progress through the simulation.

Using this option, the plunge appears as a simple forging action with some rotational effects from the pin and shoulder. As can be seen in Figure 25, the material is compressed until it is forced out from under the pin (green arrow) and moves farther from its origin (blue arrow) in a generally expanding pattern seen in Figure 26. At the same time the material closest to the outer edge of the pin (red arrow) is under torque due to the rotating pin.

In previous research, it has been shown that the maximum travel around the tool lies within the realm of 90 to 180 degrees (Dunn, 2002) from the origin. This is dependent on the proximity of the particle to the pin and/or shoulder. In the model, the effect of the shoulder is not fully realized due to another shortcoming. Previous attempts to model the traverse in friction stir welding resulted in the simulation "destroying" any point of contact that would experience very high shear. It is speculated that this is also the case with points that would undergo high amounts of shear in the model being "deleted". When these points exceed some value, the software considers them no longer valid and this results in the cessation of further recording. These points are indicated by a yellow arrow. If the software continued showing the changing position of these points, it is assumed that they would travel very quickly in a rotating pattern following the motion of the shoulder.

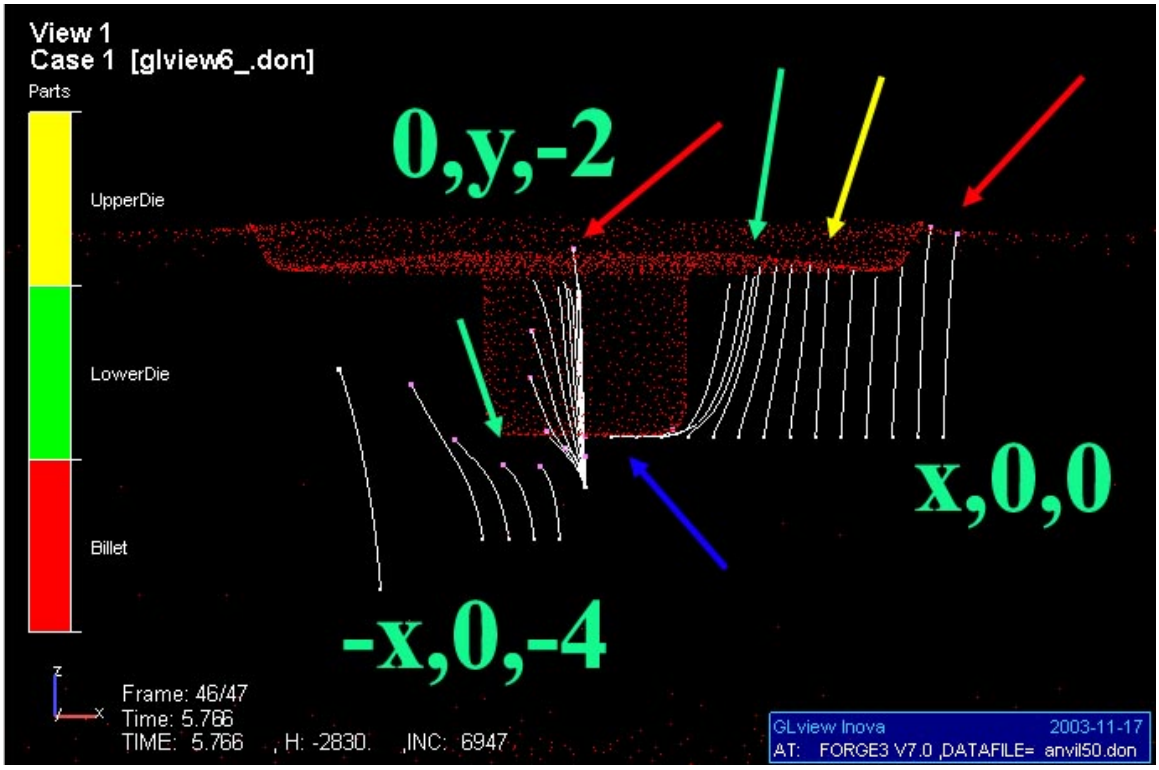

Figure 25: Material flow around the pin and shoulder in the XZ plane.

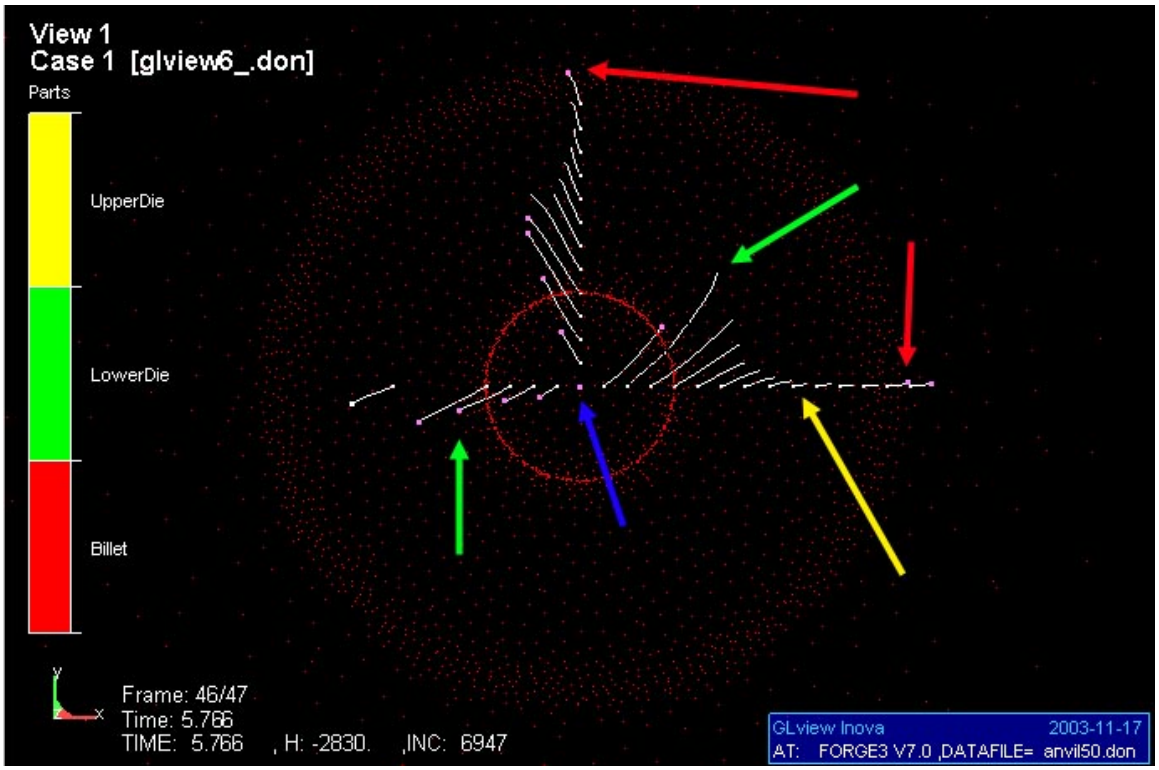

Figure 26: Material flow around the tool in the XZ plane.

In spite of these shortcomings, exploration into the depth of shoulder induced rotational shear was explored. By looking at the data and comparing with prior experimental results (Askari et al, Dunn, etc), the model confirms that the maximum depth of the physical influence of the shoulder on material flow is three millimeters deeper than the tool-billet interface. In spite of these shortfalls, it is assumed that further use of this tool should prove constructive in future research of material flow when the software can model the traverse as well.

5 CONCLUSIONS AND RECOMMENDATIONS

5.1 Conclusions

Forge3 has several advantages over other software packages including the use of a Lagrangian meshing scheme on a high-strain event. However, several limitations are brought to light when the software is applied to the process of Friction Stir Welding. By the end of this research, several issues impeded progress and affected the scope of this project. In view of these obstacles, limitations were realized and workarounds were sought out. Some limiting aspects included the following:

- Divergent results between single and parallel processing versions of the same model may be linked to the billet geometry distortions developed only in the parallel version of the model.
- Inability to model both the tools and billet in a fully coupled thermo-mechanical simulation due to heat inversion, frictional boundary issues, etc. caused by deficiencies in the software.
- Difference in capabilities between versions. Version 6.3 could not run a FSW model on a single processor while version 7.0 could (due to the number of computational nodes). Also, 6.3 could run in parallel environments while 7.0 will not be able to do so until further development is completed in early 2005.

Even with the presence of these shortcomings, improvements in modeling accuracy were seen by eliminating the adiabatic boundary condition and introducing evolving

temperatures at the tool-billet interface. Each variation of the anvil/tool models followed an S-curve which overestimated temperature for the first few seconds and then underestimated the temperature by various margins depending on the value used for the anvil. The best correlation with experimental data is Anvil75 which splits the time it overestimated temperatures evenly with the time it underestimated the temperatures. In all three of these models the temperature then rose quickly as the shoulder made full contact with the billet. The final model temperatures end together in the same temperature realm approximately 50 degrees higher than the experimental results.

The open format model did well in predicting the continued rise in temperature seen in the experimental results. It is an improvement over prior simulation work as it reduces the difference from the experimental results by more than 50 percent. It is assumed that most of these gains were made by modeling the stress flow data from both the hot and cold rheologies as well as eliminating the adiabatic condition.

The models also showed great promise in predicting material flow patterns. There appeared to be agreement with prior findings that the shoulder only affects the top two to three millimeters of material while the pin has greater influence over the remainder of the weld. In this case, the material flows as would be expected of a simple forging action but with the addition of the effects of the rotating tool. Again, further progress should yield better data to corroborate with experimental results.

5.2 Recommendations

While limitations currently exist in the Forge3 package, the potential uses of this software can be realized by continued development and refinement and application to any

model or simulation. The following are recommendations of possible venues of continued research as well as steps to overcome shortcomings expererienced while creating these simulations:

- Explore application of the numerical model for the simulation of friction stir spot welding of components in the automotive, aerospace, and shipbuilding industries.
- Improvements in the software may allow modeling of the traverse portion of friction stir welding and lead to improved understanding of the material flow during the rest of the welding process.
- Examine further improvements such as a fully coupled thermo-mechanical model, include improved tooling temperature evolution and heat transfer equations by using methods that will improve resolution of temperatures, etc. during the experiments.
- Investigate how the factors of strain, strain rate, and temperature affect the material flow and test the accuracy of the model with empirical evidence. Use this information to improve future models.
- Make appropriate changes and examine the model accuracy in relation to welds in steel and other materials.
- Explore modeling of joining dissimilar alloys.

These suggestions represent a part of the possible uses of this simulation and software. Other uses and improvements may be discovered and used to make further improvements over what has already been achieved. The use of a fully thermo-mechanical model applied jointly with the open table format version as well as better temperature/strain/strain rate data could yield the best simulation. This factors would cover the greatest lack of data presently available. These improvements would then be

available for application to welding simulations of various styles and using differenet materials. This would be the full realization of this method of using a finite element simulation to predict the final results of material flow in friction stir welding.

REFERENCES

Arbegast, W. (2002). *Using Gleeble Flow Stress Data to Establish Optimum FSW Processing Parameters in Aluminum Alloys.* Retrieved September 2, 2004, from http://ampcenter.sdsmt.edu/Mechanistic%20FSW%20Model.pdf.

Askari, A., S. Silling, B. London, & M. Mahoney. (2001). *Modeling and Analysis of Friction Stir Welding Processes.* The Minerals, Metals and Materials Society, 2001.

Bendzsak, G., T. North, & C. Smith. (2000). *An Experimentally Validated 3D Model for Friction Stir Welding.* Proceedings of the 2nd International Symposium on Friction Stir Welding. Gothenburg, Sweden.

Colegrove, P. (2000). *Three Dimensional Flow and Thermal Modelling of the Friction Stir Welding Process.* Proceedings of the 2nd International Symposium on Friction Stir Welding. Gothenburg, Sweden.

Colligan, K. (1999). Material Flow Behavior during Friction Stir Welding of Aluminum. *Welding Journal-Welding Research Supplement, 78*, 229s-237s.

Dickerson, T., H. Shercliff, & H. Schmidt. (2003). A Weld Marker Technique for Flow Visualization in FSW. *4th International Symposium on Friction Stir Welding.* Park City, UT.

Dickerson, T., Q. Shi, & H. Shercliff. (2003). *Heat flow into friction stir welding tools.* Proceedings of the 4th International Symposium on Friction Stir Welding. Park City, Utah, UT.

Dong, P., F. Lu, J. Hong, & Z. Cao. (2001). Coupled Thermomechanical Analysis of Friction Stir Welding Process Using Simplified Models. *Science and Technology of Welding and Joining, Vol. 6,* No. 5, pp. 281-287.

Dunn, Z. (2002). *Material Flow Patterns in Aluminum Friction Stir Welding*. Master's thesis, Brigham Young University, Provo, UT.

Forge3 Reference Guide, Release 6.3. Transvalor S.A. 2004.

Guerra, M., J. McClure, L. Murr, & A. Nunes. (2001) Metal Flow During Friction Stir Welding. *Friction Stir Welding and Processing*, TMS, 2001.

Heurtier, P., C. Desrayaud, & F. Montheillet. (2002). A Thermomechanical Analysis of the Friction Stir Welding Process. *Materials Science Forum. Volume 396,* 4, p. 1537-1542.

Hoye, T., P. Colegrove, & H. Shercliff. (2003). Thermal and Microstructure Modelling in Thick Plate Aluminum Alloy 7075 Friction Stir Welds. *Friction Stir Welding II, The Minerals, Metals , and Materials Society, 2003.*

Johnsen, M. (1999). "Friction Stir Welding Takes Off at Boeing." *Welding Journal, Feb. 1999:* 35-39.

Kouznetsova, V., W. Brekelmans, & F. Baaljens. (2003). *An Approach to Micro-macro Modeling of Heterogeneous Materials.* Journal of Computational Mechanics, v. 27: 37-48.

London, B., M. Mahoney, W. Bingle, M. Calabrese, & D. Waldron. (2001). *Experimental methods for determining material flow in friction stir welds.* Proceedings of the 3rd International Friction Stir Welding Symposium. Kobe, Japan.

Mahoney, M. Rockwell Scientific Company, USA.

Nicholas, E. (1999). *Friction Processing Technologies.* Retrieved March 17, 2004, from http://www.twi.co.uk/j32k/protected/band_8/spednsep97.html.

North, T., G. Bendzsak, & C. Smith. (2000). Material Properties Relevant to 3-D FSW Modeling. *2nd International Symposium on Friction Stir Welding*, Sweden, 2000.

Oliphant, A. (2004). *Numerical Modeling of Friction Stir Welding: A Comparison of Alegra and Forge3*. Unpublished thesis, Brigham Young University, Provo, UT.

Reynolds, A. (2000). Visualisation of material flow in autogenous friction stir welds, *Science and Technology of Welding and Joining, 78*, 120-124.

Russel, M., & H. Shercliff. (1999). *Analytical Modelling of Microstructure Development in Friction Stir Welding.* Proc. 1st Int. Symposium On Friction Stir Welding, Thousand Oaks, California, 1999.

Russel, M., H. Shercliff & P. Threadgill. (2001). Development and Application of an Analytical Process Model for FSW, *Aluminum 2001 – Proceedings of the TMS 2001 Aluminum Automotive and Joining Sessions*, 225-234.

Song, M., and R. Kovacevic. (2003). *A Coupled Heat-Transfer Model for Workpiece and Tool in Friction Stir Welding.* 4th International Symposium on FSW, Park City, UT, May 14-16, 2003.

Seidel, T., & A. Reynolds. (2003). Two Dimensional Friction Stir Welding Process Model based on Fluid Mechanics. *Science and Technology of Welding and Joining, Vol 8. No. 3,* 175-183.

Ulysse, P. (2002). Three-Dimensional Modeling of the Friction Stir Welding Process. *International Journal of Machine Tools and Manufacture, 42,* 1549-1557.

APPENDIX A

Problems and Workarounds

Several problems with the software were discovered in the course of this research. This appendix is included to help future users to find possible solutions to these problems until Transvalor can correct them in future versions beyond what is presently available.

PROBLEM: *.vtf files have rearranged/incomplete data from the simulation.

REASON: It appears that when a *.vtf file is copied while the simulation is in progress, it stops writing to it. Although the simulation continues to run, it seems that it also starts to choose random increments to save rather than the user-defined recording parameter. A restart may be the culprit in the strangely rearranged data sets.

SOLUTION: Avoid making any copies of files while the simulation is in progress. If it is imperative that early results be checked, it is suggested that a duplicate simulation be started at the same time as the prime example. The duplicate can be checked for accuracy at some point after which the above problem comes into play. This is essentially a check-once approach that allows the prime example to run to completion without interference and yet allows for early detection of a failing simulation that is wasting computing resources.

PROBLEM: Post-processing of the *fg3 files to check α-posteriori sensors (those put into the simulation following its completion) is incomplete if the number of increments is above 9999.

REASON: This seems to be a simple error in the programming that leaves off the final digit if the increment number is greater than 9999 (e.g. 17650 becomes 1765). If this happens to be the case with the last increment, any increment above the abbreviated number (in this case 1765) will not be calculated.

SOLUTION: The only way around this is to either have the sensors in place before you start the simulation (α-priori sensors) or to go through and renumber the increments before post-processing them for sensor data.

PROBLEM: After installing the most recent Microsoft Updates there are several problems with the Forge3 package.

REASON: There appears to be several issues if the latest Microsoft Updates are installed and these must be addressed by Transvalor to keep everything updated correctly.

SOLUTION: Simply avoid putting the updates on the computer used for pre- and post-processing until an updated version of Forge3 is available. THIS IS A MICROSOFT ONLY PROBLEM!

PROBLEM: Strange FORTRAN messages appear when the simulation is run.

REASON: This can be caused by several issues. The stored files from the simulation may have exceeded the defined quota space, the number of processors indicated in the Forge3 launcher does not coincide with the files for that simulation (four

processors rather than six), the simulation was stopped and restarted without purging the most recent *fg3 file, etc.

SOLUTION: Check each step before restarting the simulation. First, make sure that the quota space has not been reached. If this is the case, either remove unneeded files or increase your quota. Check that the number of *may files is equal to the number input in the Forge3 launcher. Check the list of *fg3 files in the /results directory and remove (rm) the highest numbered *fg3 file and restart. This generally will take care of any problems.

PROBLEM: After checking the above problem and taking corrective action, the simulation starts but it seems to freeze.

REASON: As the simulation continues the time it takes to calculate a single increment may and probably will increase due to latency. Restarting will take longer as the computational module searches through all the files stored to make sure it starts at the correct position and has all the data needed to continue. Again, the later in the simulation that this occurs the more time it will take to restart. It is also possible that the network has timed-out due to inactivity.

SOLUTION: Have patience and allow the simulation to have enough time to make sure that it is not just taking a long time to restart. If there is sufficient evidence that the program has simply stopped, make sure that there is not a time-out feature activated on the computer you are using. If you do not know how to check for this, consult with the administrator.

PROBLEM: An error message appears saying that there are "too many computational nodes" in the simulation.

REASON: This happens when there are too many points in the simulation for version 6.x. This will often happen if you try to run a FSW setup on a single processor using this version. It does not happen when you use version 7.x.

SOLUTION: Use version 7.x if you must use a single processor.

PROBLEM: An error message appears saying that there is no parallel processing abilities with the current software.

REASON: This happens if you try to run version 7.x without having the update expected to be ready in the first quarter of 2005.

SOLUTION: Use version 6.3 if you must use parallel processors.

PROBLEM: When using version 7.0 in a FSW setup (parallel or single processor), the mesh on the billet becomes deformed in an erratic pattern.

REASON: There are still issues with the manner in which the computational node interprets various friction and thermal inputs in the FSW environment when the tool and billet are defined as deformable dies.

SOLUTION: Currently a fully coupled thermo-mechanical model cannot be rendered. Try being creative with the tools available, for example, this research took the tooling temperatures garnered from real experiments and defined this as a table of temperature versus time in the preprocessing. This approaches the effect a changing tool would have on the heat evolution in the billet. Also, if you are using a rotating tool,

make sure that your maximum time step only allows two to four degrees of rotation per increment.

PROBLEM: The billet geometry collapses during a parallel processing simulation.

REASON: It appears that this is another issue with the software that must be addressed by Transvalor before the release of an updated version capable of parallel processing.

SOLUTION: Running the simulation over a single processor may take longer but should circumvent this issue.

APPENDIX B

Reference (.ref) Files

The ".ref" or reference files are important because changes can be made here that do not appear if the .tpf file is opened in the preprocessor. The basic format is the same with each file with the variations following the general format given below.

alma.ref – File from Oliphant's research. The basic model is followed in the other .ref files and only changes are noted in the .ref files following the first.

```
! File Type:                    FORGE3 V7.0 Data File
! Creator:              GLPre Version 2, 3, 0, 26-Release
! Author:               Alma_H._Oliphant
! Creation Date:        2003-10-08 15:31:52
! GLPre active language:English
! System language:  English (United States)
! Data File Name:    almasingle.ref
! Data File Location:           C:\Forge3-V6.3a\GLpre\Computations\almasingle.tsv\almasingle\
!!!!!!!!!!!!!!!!!!!!!!!!!!!!!!!!!!!!!!!!!!!!!!!!!!!!!!!!!!!!!!!!!!!!!!!!!!!!!!!!!!!!!!!


!================================== OBJECTS Block
.OBJETS
   ProjectName = almasingle
   SimulationName = almasingle

   Fout = almasingle.out
   Fres = results\almasingle.res
   Faux = results\almasingle.vtf

   NBSD = 1

   objet 1, NAME=Billet
   objet 1, FMAY=billet.may
   objet 1, NomGen=results\billet_
   objet 1, rheol=1

   outil 1, NAME=LowerDie
   outil 2, NAME=UpperDie
.FIN OBJETS
!==================================

!================================== APPROXIMATION Block
```

```
.APPROXIMATION
   Periode_Meca = 1
.FIN APPROXIMATION
!==================================

!================================== UNITS Block
.UNITES
   MM-MPA-MM.KG.S
.FIN UNITES
!==================================

!================================== RHEOLOGY Block
.RHEOLOGIE

!!!!!!!!!!!!!!!!!!!!
MATERIAU 1       ! (object Billet)
!!!!!!!!!!!!!!!!!!!!
   NORTON-H

   Thermoecroui: Hansel Spittel Nb1,
   ! Material name: AlZn5,6Mg2,5Cu1,6 ----- ENG 7075 -----
! Material type: Al-alloys
! Material subtype: Al-Zn-Cu-Mg
! Properties type: hot forming
! Units: MPa,degC
! Validity domain:
! Temperature: 300 - 500
! Strain: 0.01 - 1
! Strain rate: 0 - 200
A1=765.01908,
m1=-0.0049,
m2=-0.00605,
m3=0.10418,
m4=-0.0013,
m5=0,
m6=0,
m7=0,
m8=0,
m9=0,
eps_ss=0

!Thermal coefficients
mvolumique = 2.800000e-06 !Density
cmassique  = 1.230000e+09 !Specific Heat
conductmat = 2.500000e+05 !Conductivity
epsilon    = 5.000000e-02 !Emissivity

!--------------------------------
OUTIL1                !LowerDie

   !Friction between deformable object and rigid die
   bilateral collant                ! Friction Law

   !Thermal Exchange between part and rigid die
   ! Unit = si
   alphat     = 0.000000e+00  ! Transfert coefficient
```

```
   Effus = 1.176362E+04       ! tool effusivity

   Temp = 20.000000
FIN OUTIL
!--------------------------------

!--------------------------------
OUTIL2                !UpperDie

   !Friction between deformable object and rigid die
   Viscoplastique                ! Friction Law
   alpha = 0.3
   p     = 0.15

   !Thermal Exchange between part and rigid die
   ! Unit = si
   alphat     = 0.000000e+00  ! Transfert coefficient
   Effus = 1.176362E+04       ! tool effusivity

   Temp = 20.000000
FIN OUTIL
!--------------------------------

   !Thermal Exchange between deformable object and air
   AlphaText = 1.000000e+001                    ! Global Transfert Coeff.
   TempExt = 20.000000                          ! Ambient Temperature

   ! Initial temperature has been set in mesh file: already exists in mesh file

!!!!!!!!!!!!!!!!!!!!
FIN MATERIAU
!!!!!!!!!!!!!!!!!!!!

  ! *** User Variable Law: Sigma1
  LOIV MECA
   Sigma1
   Par STRESSTENSOR(6) = EXIST
   Var SIG1 = 0.
  FIN LOI

.FIN RHEOLOGIE
!==================================

!================================== TOLERCONV Block
.TOLERCONV
.FIN TOLERCONV
!==================================

!================================== INCREMENT Block
.INCREMENT
   Deformation= 1.000000e-002
.FIN INCREMENT
!==================================

!================================== EXECUTION Block
.EXECUTION
```

```
   Inertia
   dtMin = 8.300000e-004
   dtMax = 1.000000e-003
   dtSto = 1.250000e-001
   Calcul Outillage
   NO Folds_Detection
.FIN EXECUTION
!================================

!================================ THERMAL Block
.THERMIQUE
.FIN THERMIQUE
!================================

!================================ MESH BOXES Block
.BOITE

OBJET1
  BOX 1
   Type=30                    ! SPHERE
   Lagrangian
   Die= 2              !UpperDie
   Size= 2
   !Param Info: NbPar, Xcenter, Ycenter, Zcenter, Rext, Rint
   Parameters:, 5, 0., 0., 0., 17.5, 13.5
   Matrix:, 1, 0, 0, 0,
            0, 1, 0, 0,
            0, 0, 1, 5,
            0, 0, 0, 1
  END BOX
  BOX 2
   Type=30                    ! SPHERE
   Lagrangian
   Die= 2              !UpperDie
   Size= 5
   !Param Info: NbPar, Xcenter, Ycenter, Zcenter, Rext, Rint
   Parameters:, 5, 0., 0., 0., 22.5, 17.5
   Matrix:, 1, 0, 0, 0,
            0, 1, 0, 0,
            0, 0, 1, 5,
            0, 0, 0, 1
  END BOX
  BOX 3
   Type=30                    ! SPHERE
   Lagrangian
   Die= 2              !UpperDie
   Size= 1
   !Param Info: NbPar, Xcenter, Ycenter, Zcenter, Rext, Rint
   Parameters:, 5, 0., 0., 0., 13.5, 0
   Matrix:, 1, 0, 0, 0,
            0, 1, 0, 0,
            0, 0, 1, 5,
            0, 0, 0, 1
  END BOX
  BOX 4
   Type=30                    ! SPHERE
```

```
  Lagrangian
  Die= 2              !UpperDie
  Size= 10
  !Param Info: NbPar, Xcenter, Ycenter, Zcenter, Rext, Rint
  Parameters:, 5, 0., 0., 0., 32.5, 22.5
  Matrix:, 1, 0, 0, 0,
           0, 1, 0, 0,
           0, 0, 1, 5,
           0, 0, 0, 1
 END BOX
 BOX 5
  Type=30                    ! SPHERE
  Lagrangian
  Die= 2              !UpperDie
  Size= 15
  !Param Info: NbPar, Xcenter, Ycenter, Zcenter, Rext, Rint
  Parameters:, 5, 0., 0., 0., 47.5, 32.5
  Matrix:, 1, 0, 0, 0,
           0, 1, 0, 0,
           0, 0, 1, 5,
           0, 0, 0, 1
 END BOX
FIN OBJET

.FIN BOITE
!================================

!================================ SENSORS Block
.CAPTEURS

OBJET1
  Capteur 1          ! (Thermocouple_Positions group)
   x = 12.7
   y = 0
   z = -4.8
   Lagrangien
  Fin Capteur
  Capteur 2          ! (Thermocouple_Positions group)
   x = 0
   y = 14.3
   z = -4.8
   Lagrangien
  Fin Capteur
  Capteur 3          ! (Thermocouple_Positions group)
   x = -15.9
   y = 0
   z = -4.8
   Lagrangien
  Fin Capteur
  Capteur 4          ! (Thermocouple_Positions group)
   x = 0
   y = -17.5
   z = -4.8
   Lagrangien
  Fin Capteur
  Capteur 5          ! (Thermocouple_Positions group)
```

```
    x = 13.506
    y = -13.506
    z = -4.8
    Lagrangien
   Fin Capteur
   Capteur 6          ! (Thermocouple_Positions group)
    x = -14.566
    y = 14.566
    z = -4.8
    Lagrangien
   Fin Capteur
FIN OBJET

.FIN CAPTEURS
!================================

!================================ BOUNDARY CONDITIONS Block
.CONDLIM

.FIN CONDLIM
!================================

!================================ REMESHING Block
.MAUTO

OBJET1
   periode = 3
   lbase = 20
FIN OBJET

.FIN MAUTO
!================================

!================================ KINEMATICS Block
.CINEMAT_OUT
   Outil2             ! UpperDie
    maitre
   Fin Outil
.FIN CINEMAT_OUT
!================================
```

anvil25.ref, anvil50.ref, anvil75.ref –

In each of these files, the lower die temperature is changed to 25, 50, and 75, respectively. Also, each of these includes a time dependent temperature change which immediately follows the lower die temperature call out. This section of the file is shown below.

```
OUTIL1                !LowerDie

   !Friction between deformable object and rigid die
   bilateral collant                ! Friction Law

   !Thermal Exchange between part and rigid die
   ! Unit = si
   alphat     = 1.000000e+04  ! Transfert coefficient
   Effus = 1.176362E+04       ! tool effusivity

   Temp = 25.000000 !<-- THIS IS THE TEMP REFERRED TO FROM ABOVE.
FIN OUTIL
!---------------------------------

!---------------------------------
OUTIL2                !UpperDie

   !Friction between deformable object and rigid die
   Viscoplastique                ! Friction Law
   alpha = 0.3
   p     = 0.15

   !Thermal Exchange between part and rigid die
   ! Unit = si
   alphat     = 2.000000e+04  ! Transfert coefficient
   Effus = 1.176362E+04       ! tool effusivity

   Temp = 7.000000

  ! *** User Variable Law: PointParPoint-Temperature
 LOIF EVOL !<--THE FOLLOWING SECTION DETERMINES THE TIME DEPENDENT TEMP
   PointParPoint
   Par Code_1 = 4    ! Time dependency
   Par NbPts_1 = 16
   Par Xpts_1 (16) = 0, 0.364, 0.864, 1.369, 1.874, 2.374, 2.88, 3.374, 3.88,
   4.385, 4.89, 5.39, 5.89, 6.39, 6.911, 7
   Par Ypts_1 (16) = 6.4, 6.6, 7.1, 16.8, 22.8, 50.1, 66.9, 99.9, 115.4, 150.9,
   169, 200.3, 215.7, 247, 266.5, 274.7
   Var Temperature = Exist
  FIN LOI !<--THIS IS THE END OF THE TIME DEPENDENT TEMP CALLOUT
FIN OUTIL
```

The final change in files comes from the addition of the open-format table. This data was calculated by using the Hansel-Spittel Rheology Law. The table formatting for Forge3 data is as follows:

```
FSTRES
   9          9          10
*Strain(i),i=1,9
   0.01       0.1        1          5          10         50         100        500        1000
*Strain rate(j),j=1,9
```

0.01 0.1 1 5 10 50 100 500 1000

*Temperature(k),k=1,11

20 50 100 150 200 250 300 350 400 450 500

*(((flow stress(i,j,k),i=1,9),j=1,9),k=1,11)

75.0 211.9 310.2 387.3 425.3 527.9 579.3 718.6 788.4
78.2 220.9 323.5 403.8 443.5 550.4 604.0 749.3 822.1
81.6 230.4 337.3 421.1 462.4 573.9 629.8 781.3 857.2
84.0 237.2 347.3 433.6 476.1 591.0 648.5 804.4 882.6
85.1 240.2 351.7 439.1 482.1 598.4 656.7 814.6 893.8
87.6 247.3 362.1 452.1 496.4 616.2 676.2 838.8 920.0
88.7 250.5 366.7 457.8 502.7 624.0 684.7 849.4 932.0
91.3 257.9 377.6 471.4 517.6 642.5 705.0 874.6 959.6
92.5 261.2 382.4 477.4 524.2 650.6 714.0 885.7 971.8
71.3 201.4 294.8 368.0 404.2 501.6 550.5 682.8 749.2
74.3 210.0 307.4 383.8 421.4 523.1 574.0 712.0 781.2
77.5 218.9 320.5 400.2 439.4 545.4 598.5 742.4 814.6
79.8 225.4 330.0 412.0 452.4 561.6 616.2 764.4 849.4
80.8 228.3 334.2 417.2 458.2 568.7 624.0 774.1 849.4
83.2 235.0 244.1 429.6 471.8 585.6 642.5 797.1 874.6
84.3 238.0 348.8 448.0 491.9 610.6 670.0 831.1 911.9
86.8 245.1 358.8 448.0 491.9 610.6 670.0 831.1 911.9
87.9 248.2 363.3 453.6 498.1 618.3 678.5 841.6 923.5
65.5 184.9 270.8 338.1 371.2 460.8 505.6 627.2 688.2
68.3 192.8 282.3 352.5 387.1 480.4 527.2 654.0 717.6
71.2 201.1 294.4 367.5 402.6 501.0 549.7 681.9 748.2
73.3 207.0 303.1 378.4 415.6 515.8 566.0 702.1 770.4
74.2 209.7 307.0 383.2 420.8 522.4 573.2 711.0 780.2
76.4 215.9 316.1 394.6 433.3 537.8 590.2 732.1 803.3
77.4 218.6 320.1 399.6 438.8 544.7 597.7 741.4 813.5
79.7 225.1 329.6 411.5 451.8 560.8 615.4 763.4 837.6
80.7 228.0 333.7 416.7 457.5 567.9 623.2 773.0 848.2
60.2 169.9 248.7 310.5 341.0 423.2 464.4 576.1 632.1
62.7 177.1 259.3 323.8 355.5 441.3 484.2 600.7 659.1
65.4 184.7 270.4 337.6 370.7 460.1 504.9 626.3 687.2
67.3 190.2 278.4 347.6 381.7 473.8 519.9 644.9 707.6
68.2 192.6 281.9 352.0 386.5 479.8 526.5 653.1 716.6
70.2 198.3 290.3 362.4 398.0 494.0 542.1 672.5 737.8
71.1 200.8 294.0 367.0 403.1 500.3 549.0 681.0 747.2
73.2 206.8 302.7 377.9 415.0 515.1 565.2 701.2 769.3
74.1 209.4 306.5 382.7 420.3 521.6 572.4 710.1 779.1
55.3 156.0 228.4 285.2 313.2 388.7 426.6 529.1 580.6
57.6 162.7 238.2 297.4 326.6 405.3 444.8 551.7 605.4
60.1 169.6 248.4 310.1 340.5 422.6 463.8 575.3 631.2
61.9 174.7 255.7 319.3 350.6 435.2 477.5 592.4 650.0
62.6 176.9 259.0 323.3 355.0 440.7 483.6 599.9 658.2
64.5 182.1 266.7 332.9 365.6 453.8 497.9 617.7 677.7
65.3 184.4 270.0 337.1 370.2 459.5 504.2 625.5 686.3
67.3 189.9 278.0 347.1 381.2 473.1 519.2 644.0 706.7
68.1 192.3 281.6 351.5 386.0 479.1 525.8 652.2 715.6
50.8 143.3 209.8 262.0 287.7 357.1 391.8 486.0 533.3
52.9 149.4 218.8 273.2 300.0 372.3 408.5 506.8 556.1
55.2 155.8 228.1 284.8 312.8 388.2 426.0 528.4 579.0
56.8 160.4 234.9 293.3 322.0 399.7 438.6 544.1 597.0
57.5 162.5 237.9 297.0 326.1 404.8 444.2 551.0 604.6
59.2 167.3 244.9 305.8 335.8 416.8 457.3 567.3 622.5
60.0 169.4 248.0 309.7 340.0 422.1 463.1 574.5 630.4

61.8	174.4	255.4	318.8	350.1	434.6	476.9	591.6	649.1
62.6	176.6	258.6	322.9	354.6	440.1	482.9	599.0	657.3
104.9	112.2	109.8	107.4	106.4	104.1	103.1	100.8	99.9
132.0	141.1	138.1	135.1	133.9	130.9	129.7	126.8	125.6
166.0	177.5	173.7	170.0	168.4	164.7	163.1	159.5	158.0
194.8	208.4	203.8	199.5	197.7	193.3	191.5	187.3	185.5
208.8	223.3	218.4	213.8	211.8	207.1	205.2	200.7	198.7
245.1	262.1	256.4	251.0	248.6	243.2	240.8	235.5	233.3
262.6	280.8	274.7	268.9	266.4	260.5	258.1	252.4	250.0
308.2	329.7	322.5	315.7	312.7	305.8	302.9	296.3	293.4
330.3	353.2	345.6	338.2	335.1	327.7	324.6	317.4	314.4
82.6	88.3	86.4	84.6	83.8	81.9	81.1	79.4	78.6
103.9	111.1	108.7	106.4	105.4	103.0	102.1	99.8	98.9
130.6	139.7	136.7	133.8	132.5	129.6	128.4	125.6	124.4
153.3	164.0	160.4	157.0	155.6	152.1	150.7	147.4	146.0
164.3	175.7	171.9	168.3	166.7	163.0	161.5	157.9	156.4
192.9	206.3	201.8	197.5	195.7	191.4	189.5	185.4	183.6
206.7	221.0	216.2	211.6	209.6	205.1	203.1	198.6	196.7
242.6	259.4	253.8	248.4	246.1	240.7	238.4	233.2	230.9
259.9	278.0	272.0	266.2	263.7	257.9	255.5	249.8	247.5
65.0	69.5	68.0	66.6	65.9	64.5	63.9	62.5	61.9
81.7	87.4	85.5	83.7	82.9	81.1	80.3	78.6	77.8
102.8	109.9	107.6	105.3	104.3	102.0	101.0	98.8	97.9
120.7	129.1	126.3	123.6	122.4	119.7	118.6	116.0	114.9
129.3	138.3	135.3	132.4	131.2	128.3	127.1	124.3	123.1
151.8	162.3	158.8	155.5	154.0	150.6	149.2	145.9	144.5
162.6	173.9	170.2	166.6	165.0	161.4	159.8	156.3	154.8
190.9	204.2	199.8	195.5	193.7	189.4	187.5	183.5	181.8
204.6	218.8	214.0	209.5	207.5	203.0	201.0	196.6	194.7
51.1	54.7	53.5	52.4	51.9	50.7	50.3	49.2	48.7
64.3	68.8	67.3	65.9	65.3	63.8	63.2	61.8	61.2
80.9	86.5	84.7	82.9	82.1	80.3	79.5	77.8	77.0
95.0	101.6	99.4	97.3	96.4	94.2	93.3	91.3	90.4
101.8	108.8	106.5	104.2	103.2	101.0	100.0	97.8	96.9
119.5	127.8	125.0	122.3	121.2	118.5	117.4	114.8	113.7
128.0	136.9	133.9	131.1	129.9	127.0	125.8	123.0	121.9
150.3	160.7	157.2	153.9	152.4	149.1	147.7	144.4	143.0
161.0	172.2	168.5	164.9	163.3	159.8	158.2	154.7	153.3
40.3	43.0	42.1	41.2	40.8	39.9	39.6	38.7	38.3
50.6	54.1	53.0	51.8	51.4	50.2	49.8	48.7	48.2
63.7	68.1	66.6	65.2	64.6	63.2	62.6	61.2	60.6
74.8	79.9	78.2	76.6	75.8	74.2	73.5	71.8	76.2
80.1	85.7	83.8	82.0	81.3	79.5	78.7	77.0	76.2
94.0	100.6	98.4	96.3	95.4	93.3	92.4	90.4	89.5
100.7	107.7	105.4	103.2	102.2	100.0	99.0	96.8	95.9
118.3	126.5	123.7	121.1	120.0	117.3	116.2	113.7	112.6
126.7	135.5	132.6	129.8	128.5	125.7	124.5	121.8	120.6

APPENDIX C

Experimental Results

The first six seconds of data from each experimental run as well as the new and old average values are contained in this appendix. The thermocouple which coincides with 12.7mm is TCK1 in runs 1-3, and TCK3 in runs 4-6.

Run 1

TIME	X-LBF	Z-LBF	Y-LBF	PWR	mm	TCK1	TCK2	TCK3	TCK4	TCK5	TCK6
00.000	4.89	481.56	0.81	12.00	1.18	19.99	21.00	20.31	20.23	20.56	20.58
00.063	11.00	440.97	-20.18	12.00	1.33	19.99	21.00	20.31	20.23	20.60	20.58
00.125	11.00	440.97	-20.18	13.00	1.33	19.99	21.00	20.31	20.23	20.60	20.58
00.172	11.00	440.97	-20.99	13.00	1.51	19.99	21.00	20.35	20.23	20.60	20.58
00.234	11.00	440.97	-20.99	13.00	1.51	19.99	21.00	20.35	20.23	20.60	20.58
00.281	15.89	431.41	-27.04	13.00	1.71	19.99	21.00	20.35	20.23	20.60	20.58
00.344	15.89	431.41	-27.04	13.00	1.71	19.99	21.00	20.35	20.23	20.60	20.58
00.391	0.81	425.05	-27.04	16.00	1.71	20.07	21.04	20.35	20.23	20.60	20.58
00.453	0.81	425.05	-27.04	16.00	1.71	20.07	21.04	20.35	20.23	20.60	20.58
00.516	0.81	427.43	-29.47	19.00	1.83	20.07	21.04	20.35	20.23	20.64	20.62
00.563	-8.96	876.36	-36.73	15.00	1.87	20.07	21.04	20.35	20.23	20.60	20.62
00.625	-8.96	876.36	-36.73	15.00	1.87	20.07	21.04	20.35	20.23	20.60	20.62
00.672	-21.59	1443.88	-107.37	23.00	1.90	20.07	21.04	20.35	20.26	20.64	20.66
00.734	-21.59	1443.88	-107.37	23.00	1.90	20.07	21.04	20.35	20.26	20.64	20.66
00.781	-21.59	1443.88	-106.56	23.00	1.92	20.07	21.04	20.38	20.26	20.68	20.70
00.844	-21.59	1443.88	-106.56	23.00	1.92	20.07	21.04	20.38	20.26	20.68	20.70
00.906	-39.51	1615.81	-106.56	24.00	1.92	20.07	21.04	20.38	20.26	20.68	20.70
00.953	-39.51	1615.81	-106.56	24.00	1.92	20.07	21.04	20.38	20.26	20.68	20.70
01.016	-53.36	2050.41	-120.69	17.00	1.92	20.37	21.19	20.42	20.30	20.71	20.69
01.063	-46.03	2375.16	-156.61	17.00	1.92	20.37	21.19	20.46	20.34	20.75	20.77
01.125	-46.03	2375.16	-156.61	21.00	1.92	20.37	21.19	20.46	20.34	20.75	20.77
01.172	-46.03	2375.16	-157.01	21.00	1.93	20.37	21.19	20.57	20.45	20.83	20.85
01.234	-46.03	2375.16	-157.01	21.00	1.93	20.37	21.19	20.57	20.45	20.83	20.85
01.297	-45.21	2774.74	-157.01	28.00	1.93	20.37	21.19	20.57	20.45	20.83	20.85
01.344	-45.21	2774.74	-157.01	28.00	1.93	20.37	21.19	20.57	20.45	20.83	20.85
01.406	-45.21	2774.74	-156.21	28.00	1.95	20.37	21.19	20.73	20.53	20.98	20.96
01.453	-45.21	2774.74	-156.21	28.00	1.95	20.37	21.19	20.73	20.53	20.98	20.96
01.516	-65.98	3916.95	8.07	32.00	1.95	21.75	21.91	20.95	20.80	21.25	21.23
01.563	-67.21	5273.28	8.07	33.00	1.95	21.75	21.91	20.95	20.80	21.25	21.23
01.625	-67.21	5273.28	0.00	33.00	2.00	21.75	21.91	21.26	20.99	21.44	21.34

Run 1

TIME	X-LBF	Z-LBF	Y-LBF	PWR	mm	TCK1	TCK2	TCK3	TCK4	TCK5
01.688	-68.84	5767.57	8.07	37.00	2.06	21.75	21.91	21.83	21.48	21.86
01.734	-68.84	5767.57	8.07	37.00	2.06	21.75	21.91	21.83	21.48	21.86
01.797	-59.47	6092.33	8.07	37.00	2.06	21.75	21.91	21.83	21.48	21.86
01.844	-59.47	6092.33	8.07	37.00	2.06	21.75	21.91	21.83	21.48	21.86
01.906	-59.47	6092.33	17.76	37.00	2.16	21.75	21.91	22.40	22.02	22.28
01.953	-59.47	6092.33	17.76	37.00	2.16	21.75	21.91	22.40	22.02	22.28
02.016	-21.99	6319.97	35.52	34.00	2.29	25.97	24.88	23.09	22.66	23.15
02.063	-19.55	6354.20	35.52	40.00	2.29	25.97	24.88	23.09	22.66	23.15
02.125	-19.55	6354.20	59.33	40.00	2.41	25.97	24.88	24.38	23.88	23.88
02.188	-12.22	6216.50	58.53	46.00	2.58	25.97	24.88	25.52	25.06	24.75
02.234	-12.22	6216.50	58.53	46.00	2.58	25.97	24.88	25.52	25.06	24.75
02.297	12.63	6147.25	58.53	44.00	2.58	25.97	24.88	25.52	25.06	24.75
02.344	12.63	6147.25	58.53	44.00	2.58	25.97	24.88	25.52	25.06	24.75
02.406	49.28	6065.26	60.14	39.00	2.70	35.73	32.31	27.58	26.81	26.39
02.453	49.28	6065.26	60.14	39.00	2.70	35.73	32.31	27.58	26.81	26.39
02.516	49.28	6065.26	60.95	39.00	2.90	35.73	32.31	28.98	28.06	27.52
02.578	77.80	5967.36	60.95	43.00	2.90	35.73	32.31	28.98	28.06	27.52
02.625	77.80	5967.36	52.47	43.00	3.05	35.73	32.31	31.17	30.15	29.34
02.688	115.27	5776.33	33.50	43.00	3.21	35.73	32.31	32.72	31.62	30.63
02.734	115.27	5776.33	33.50	43.00	3.21	35.73	32.31	32.72	31.62	30.63
02.797	138.89	5670.46	23.01	49.00	3.34	35.73	32.31	35.14	34.15	32.71
02.844	138.89	5670.46	23.01	49.00	3.34	35.73	32.31	35.14	34.15	32.71
02.906	151.11	5572.56	23.01	40.00	3.34	48.46	42.12	35.14	34.15	32.71
02.969	151.11	5572.56	23.01	40.00	3.34	48.46	42.12	35.14	34.15	32.71
03.016	151.11	5572.56	6.46	40.00	3.50	48.46	42.12	37.13	35.73	34.37
03.078	129.93	5510.47	6.46	45.00	3.50	48.46	42.12	37.13	35.73	34.37
03.125	129.93	5510.47	-31.89	45.00	3.63	48.46	42.12	39.65	38.14	36.55
03.188	116.90	5517.64	-49.65	51.00	3.78	48.46	42.12	41.37	39.75	38.06
03.234	116.90	5517.64	-49.65	51.00	3.78	48.46	42.12	41.37	39.75	38.06
03.297	116.49	5605.19	-72.65	49.00	3.94	48.46	42.12	43.99	42.23	40.42
03.359	116.49	5605.19	-72.65	49.00	3.94	48.46	42.12	43.99	42.23	40.42
03.406	99.79	5711.06	-72.65	45.00	3.94	61.29	53.01	43.99	42.23	40.42
03.469	99.79	5711.06	-72.65	45.00	3.94	61.29	53.01	43.99	42.23	40.42
03.516	74.95	5824.88	-74.67	47.00	4.05	61.29	53.01	45.71	43.83	41.92
03.578	74.95	5824.88	-84.76	47.00	4.18	61.29	53.01	47.46	45.48	43.49
03.625	74.95	5824.88	-84.76	47.00	4.18	61.29	53.01	47.46	45.48	43.49
03.688	33.40	5925.17	-86.38	46.00	4.30	61.29	53.01	50.33	48.20	46.07
03.750	33.40	5925.17	-86.38	46.00	4.30	61.29	53.01	50.33	48.20	46.07
03.797	-13.44	6093.12	-71.85	45.00	4.49	61.29	53.01	51.96	49.80	47.60
03.859	-13.44	6093.12	-71.85	45.00	4.49	61.29	53.01	51.96	49.80	47.60
03.906	-39.92	6141.68	-71.85	52.00	4.49	73.74	63.52	51.96	49.80	47.60
03.969	-39.92	6141.68	-71.85	52.00	4.63	73.74	63.52	51.96	49.80	47.60
04.016	-73.72	6158.39	-60.54	49.00	4.63	73.74	63.52	54.45	52.22	49.91
04.078	-73.72	6158.39	-41.17	49.00	4.78	73.74	63.52	56.97	54.59	52.10
04.141	-91.24	6164.76	-41.17	50.00	4.78	73.74	63.52	56.97	54.59	52.10
04.188	-91.24	6164.76	-33.50	50.00	4.94	73.74	63.52	58.64	56.15	53.62
04.250	-91.24	6164.76	-33.50	50.00	4.94	73.74	63.52	58.64	56.15	53.62
04.297	-96.53	6180.68	-33.50	47.00	4.94	73.74	63.52	58.64	56.15	53.62
04.359	-96.53	6180.68	-33.50	47.00	4.94	73.74	63.52	58.64	56.15	53.62

Run 1

TIME	X-LBF	Z-LBF	Y-LBF	PWR	mm	TCK1	TCK2	TCK3	TCK4	TCK5	TCK6
04.406	-100.20	6207.74	-12.11	49.00	5.09	85.36	73.31	61.04	58.78	55.88	50.00
04.469	-100.20	6207.74	16.95	49.00	5.27	85.36	73.31	63.00	58.78	55.88	50.00
04.531	-92.05	6229.23	16.95	45.00	5.27	85.36	73.31	63.00	60.34	57.63	51.30
04.578	-92.05	6229.23	24.62	45.00	5.38	85.36	73.31	65.44	62.70	59.85	53.57
04.641	-92.05	6229.23	24.62	45.00	5.38	85.36	73.31	65.44	62.70	59.85	53.57
04.688	-72.09	6253.91	35.12	52.00	5.52	85.36	73.31	67.07	64.22	61.36	54.94
04.750	-72.09	6253.91	35.12	52.00	5.52	85.36	73.31	67.07	64.22	61.36	54.94
04.797	-8.96	6296.09	37.94	49.00	5.65	85.36	73.31	69.47	66.54	63.62	56.90
04.859	-8.96	6296.09	37.94	49.00	5.65	85.36	73.31	69.47	66.54	63.62	56.90
04.922	13.44	6318.38	32.69	50.00	5.83	96.20	83.12	71.09	68.09	65.10	58.24
04.969	13.44	6318.38	32.69	50.00	5.83	96.20	83.12	71.09	68.09	65.10	58.24
05.031	46.03	6337.48	32.69	56.00	5.83	96.20	83.12	71.09	68.09	65.10	58.24
05.078	85.54	6337.48	16.55	56.00	5.97	96.20	83.12	72.71	69.90	66.57	59.57
05.141	85.54	6351.01	16.55	49.00	5.97	96.20	83.12	72.71	69.90	66.57	59.57
05.188	85.54	6351.01	10.09	49.00	6.10	96.20	83.12	75.30	72.15	69.01	61.57
05.250	85.54	6351.01	10.09	49.00	6.10	96.20	83.12	75.30	72.15	69.01	61.57
05.313	112.01	6368.53	-7.67	58.00	6.26	96.20	83.12	76.88	73.70	70.45	62.90
05.359	112.01	6368.53	-7.67	58.00	6.26	96.20	83.12	76.88	73.70	70.45	62.90
05.422	130.34	6420.26	-7.67	51.00	6.26	107.05	92.32	76.88	73.70	70.45	62.90
05.469	130.34	6420.26	-7.67	51.00	6.43	107.05	92.32	76.88	73.70	70.45	62.90
05.531	148.26	6460.06	-21.39	54.00	6.43	107.05	92.32	79.17	75.95	72.63	65.12
05.578	148.26	6460.06	-73.46	54.00	6.53	107.05	92.32	81.49	78.24	74.80	67.11
05.641	148.26	6460.06	-73.46	54.00	6.53	107.05	92.32	81.49	78.24	74.80	67.11
05.703	171.07	6753.77	-95.66	68.00	6.70	107.05	92.32	83.04	79.97	76.98	69.07
05.750	171.07	6753.77	-95.66	68.00	6.70	107.05	92.32	83.04	79.97	76.98	69.07
05.813	153.15	7028.38	-103.73	66.00	6.78	107.05	92.32	85.33	82.23	78.64	70.36
05.859	153.15	7028.38	-103.73	66.00	6.78	107.05	92.32	85.33	82.23	78.64	70.36
05.922	136.86	7176.43	-103.73	69.00	6.78	117.63	101.67	85.33	82.23	78.64	70.36
05.969	136.86	7176.43	-103.73	69.00	6.78	117.63	101.67	85.33	82.23	78.64	70.36
06.031	138.08	7339.60	-115.84	76.00	6.89	117.63	101.67	87.22	83.78	80.15	71.72
06.078	138.08	7339.60	-113.82	76.00	7.00	117.63	101.67	89.77	86.21	82.44	73.75
06.141	138.08	7339.60	-113.82	76.00	7.00	117.63	101.67	89.77	86.21	82.44	73.75
06.203	82.28	7638.89	-93.64	74.00	7.16	117.63	101.67	91.51	87.95	84.06	75.41
06.250	82.28	7638.89	-93.64	74.00	7.16	117.63	101.67	91.51	87.95	84.06	75.41
06.313	22.81	7730.42	-70.64	77.00	7.28	117.63	101.67	94.28	90.69	86.58	77.63
06.359	22.81	7730.42	-70.64	77.00	7.28	117.63	101.67	94.28	90.69	86.58	77.63
06.422	-33.81	7860.96	-70.64	80.00	7.28	129.51	112.40	94.28	90.69	86.58	77.63
06.469	-33.81	7860.96	-70.64	80.00	7.41	129.51	112.40	94.28	90.69	86.58	77.63
06.531	-85.94	8063.14	-65.39	101.00	7.41	129.51	112.40	97.28	94.02	89.31	79.99
06.594	-85.94	8063.14	-94.45	101.00	7.52	129.51	112.40	99.36	96.20	91.68	81.72
06.641	-85.94	8063.14	-94.45	101.00	7.52	129.51	112.40	99.36	96.20	91.68	81.72
06.703	-137.26	8804.18	-138.85	111.00	7.57	129.51	112.40	102.04	98.61	93.90	83.53
06.750	-137.26	8804.18	-138.85	111.00	7.57	129.51	112.40	102.04	98.61	93.90	83.53
06.813	-118.93	9374.09	-188.90	110.00	7.61	129.51	112.40	106.17	102.66	97.75	86.63
06.859	-118.93	9374.09	-188.90	110.00	7.61	129.51	112.40	106.17	102.66	97.75	86.63
06.922	-84.31	10030.77	-205.45	108.00	7.65	148.56	128.09	109.41	105.71	100.76	89.33
06.984	-84.31	10030.77	-205.45	108.00	7.65	148.56	128.09	109.41	105.71	100.76	89.33
07.031	-84.31	10030.77	-205.45	108.00	7.65	148.56	128.09	109.41	105.71	100.76	89.33

Run 2

TIME	X-LBF	Z-LBF	Y-LBF	PWR	mm	TCK1	TCK2	TCK3	TCK4	TCK5	TCK6
00.000	8.15	23.88	0.81	17.00	1.04	22.16	23.05	22.40	22.28	22.66	22.67
00.063	8.15	23.88	0.81	12.00	1.04	22.16	23.05	22.40	22.28	22.66	22.67
00.109	8.15	23.88	-12.92	12.00	1.12	22.16	23.05	22.37	22.31	22.66	22.67
00.172	8.15	23.88	-12.92	12.00	1.12	22.16	23.05	22.37	22.31	22.66	22.67
00.219	14.66	357.39	-76.69	17.00	1.14	22.12	23.05	22.40	22.31	22.66	22.63
00.281	14.66	357.39	-76.69	17.00	1.14	22.12	23.05	22.40	22.31	22.66	22.63
00.328	20.37	834.97	-76.69	21.00	1.14	22.12	23.05	22.40	22.31	22.66	22.63
00.391	20.37	834.97	-76.69	21.00	1.16	22.12	23.05	22.40	22.31	22.66	22.63
00.453	95.31	1420.80	-154.19	23.00	1.16	22.12	23.05	22.40	22.31	22.66	22.67
00.500	120.97	1609.44	-154.19	20.00	1.17	22.12	23.05	22.44	22.31	22.66	22.67
00.563	120.97	1609.44	-154.19	20.00	1.17	22.12	23.05	22.44	22.31	22.66	22.67
00.625	103.46	2024.14	-125.13	18.00	1.17	22.12	23.05	22.55	22.35	22.69	22.67
00.672	103.46	2024.14	-125.13	18.00	1.17	22.12	23.05	22.55	22.35	22.69	22.67
00.734	64.36	2313.08	-125.13	22.00	1.17	22.84	23.54	22.55	22.35	22.69	22.67
00.781	64.36	2313.08	-125.13	22.00	1.17	22.84	23.54	22.55	22.35	22.69	22.67
00.844	64.36	2313.08	-76.69	22.00	1.17	22.84	23.54	22.71	22.35	22.69	22.71
00.891	-61.91	2765.19	-76.69	28.00	1.17	22.84	23.54	22.71	22.35	22.69	22.71
00.953	-61.91	2765.19	-79.52	28.00	1.18	22.84	23.54	23.16	22.47	22.73	22.75
01.000	-83.09	3312.02	3.23	41.00	1.20	22.84	23.54	23.70	22.54	22.81	22.78
01.063	-83.09	3312.02	3.23	41.00	1.20	22.84	23.54	23.70	22.54	22.81	22.78
01.125	-93.68	4037.14	-54.09	34.00	1.25	22.84	23.54	24.65	22.73	22.96	22.94
01.172	-93.68	4037.14	-54.09	34.00	1.25	22.84	23.54	24.65	22.73	22.96	22.94
01.234	-72.91	5075.08	-54.09	37.00	1.25	27.59	27.84	24.65	22.73	22.96	22.94
01.297	-72.91	5075.08	-37.94	37.00	1.35	27.59	27.84	25.60	22.85	23.11	23.09
01.359	-73.32	5364.81	-37.94	37.00	1.35	27.59	27.84	25.60	22.85	23.11	23.09
01.406	-73.32	5364.81	-49.24	39.00	1.47	27.59	27.84	27.54	23.42	23.42	23.36
01.469	-73.32	5364.81	-49.24	39.00	1.47	27.59	27.84	27.54	23.42	23.42	23.36
01.516	-78.61	5551.07	-46.82	34.00	1.64	27.59	27.84	29.88	24.10	23.91	23.74
01.578	-78.61	5551.07	-46.82	34.00	1.64	27.59	27.84	29.88	24.10	23.91	23.74
01.625	-103.46	5762.00	-46.82	42.00	1.64	27.59	27.84	29.88	24.10	23.91	23.74
01.688	-103.46	5762.00	-46.82	42.00	1.64	27.59	27.84	29.88	24.10	23.91	23.74
01.734	-103.46	5762.00	-33.10	42.00	1.78	27.59	27.84	32.72	25.02	24.63	24.31
01.797	-93.68	5823.29	-33.10	42.00	1.78	27.59	27.84	32.72	25.02	24.63	24.31
01.859	-93.68	5823.29	-6.05	45.00	1.97	39.66	39.98	36.07	26.08	25.43	24.99
01.906	-90.02	5881.39	-6.05	41.00	1.97	39.66	39.98	36.07	26.08	25.43	24.99
01.969	-90.02	5881.39	-6.05	41.00	1.97	39.66	39.98	36.07	26.08	25.43	24.99
02.016	-92.05	5883.78	6.05	40.00	2.10	39.66	39.98	38.18	26.92	26.42	25.90
02.078	-92.05	5883.78	6.05	40.00	2.10	39.66	39.98	38.18	26.92	26.42	25.90
02.141	-92.05	5883.78	22.60	40.00	2.21	39.66	39.98	41.44	28.47	27.14	26.51
02.188	-92.05	5883.78	22.60	40.00	2.21	39.66	39.98	41.44	28.47	27.14	26.51
02.250	-75.76	5882.19	31.48	38.00	2.36	55.77	55.00	43.58	29.49	27.94	27.20
02.297	-48.88	5867.07	31.48	38.00	2.36	55.77	55.00	43.58	29.49	27.94	27.20
02.359	-48.88	5867.07	44.80	41.00	2.52	55.77	55.00	45.82	30.52	28.73	27.88
02.406	-4.48	5850.35	46.82	39.00	2.65	55.77	55.00	49.47	32.18	30.17	29.05
02.469	-4.48	5850.35	46.82	39.00	2.65	55.77	55.00	49.47	32.18	30.17	29.05
02.516	29.33	5847.96	46.82	46.00	2.65	55.77	55.00	49.47	32.18	30.17	29.05
02.578	29.33	5847.96	46.82	46.00	2.65	55.77	55.00	49.47	32.18	30.17	29.05
02.641	61.10	5834.43	45.21	45.00	2.80	71.66	70.20	51.63	33.27	31.08	29.81
02.688	61.10	5834.43	45.21	45.00	2.80	71.66	70.20	51.63	33.27	31.08	29.81
02.750	61.10	5834.43	37.54	45.00	2.92	71.66	70.20	54.89	35.05	32.52	31.21

Run 2

TIME	X-LBF	Z-LBF	Y-LBF	PWR	mm	TCK1	TCK2	TCK3	TCK4	TCK5	TCK6
02.797	89.61	5832.04	37.54	45.00	2.92	71.66	70.20	54.89	35.05	32.52	31.21
02.859	89.61	5832.04	16.95	48.00	3.10	71.66	70.20	57.08	36.48	33.50	32.08
02.906	114.45	5852.74	7.27	46.00	3.23	71.66	70.20	60.27	38.32	35.01	33.44
02.969	114.45	5852.74	7.27	46.00	3.23	71.66	70.20	60.27	38.32	35.01	33.44
03.031	125.86	5869.45	-12.51	44.00	3.35	71.66	70.20	62.41	39.56	36.02	34.34
03.078	125.86	5869.45	-12.51	44.00	3.35	71.66	70.20	62.41	39.56	36.02	34.34
03.141	125.86	5869.45	-12.51	44.00	3.35	71.66	70.20	62.41	39.56	36.02	34.34
03.188	125.86	5869.45	-12.51	44.00	3.35	71.66	70.20	62.41	39.56	36.02	34.34
03.250	139.30	5883.78	-26.64	38.00	3.51	86.28	84.18	65.92	41.43	37.79	35.81
03.313	138.49	5889.35	-46.01	52.00	3.66	86.28	84.18	68.06	41.43	37.79	35.81
03.359	138.49	5889.35	-46.01	52.00	3.66	86.28	84.18	68.06	42.67	38.84	36.79
03.422	120.16	5872.64	-70.64	49.00	3.81	86.28	84.18	71.16	44.87	40.46	38.22
03.469	120.16	5872.64	-70.64	49.00	3.81	86.28	84.18	71.16	44.87	40.46	38.22
03.531	94.09	5825.68	-75.48	41.00	3.96	86.28	84.18	73.27	46.14	41.54	39.38
03.578	94.09	5825.68	-75.48	41.00	3.96	86.28	84.18	73.27	46.14	41.54	39.38
03.641	94.09	5825.68	-75.48	41.00	3.96	86.28	84.18	73.27	46.14	41.54	39.38
03.688	94.09	5825.68	-75.48	41.00	3.96	86.28	84.18	73.27	46.14	41.54	39.38
03.750	74.13	5811.35	-79.11	55.00	4.13	100.53	97.95	76.36	48.08	43.23	40.92
03.813	39.10	5812.94	-78.71	44.00	4.24	100.53	97.95	78.39	49.42	44.57	41.97
03.859	39.10	5812.94	-78.71	44.00	4.24	100.53	97.95	78.39	49.42	44.57	41.97
03.922	-5.70	5840.00	-71.44	50.00	4.40	100.53	97.95	81.82	51.39	46.25	43.50
03.969	-5.70	5840.00	-71.44	50.00	4.40	100.53	97.95	81.82	51.39	46.25	43.50
04.031	-59.87	5907.66	-71.44	59.00	4.40	100.53	97.95	81.82	51.39	46.25	43.50
04.078	-59.87	5907.66	-71.44	59.00	4.40	100.53	97.95	81.82	51.39	46.25	43.50
04.141	-59.87	5907.66	-57.72	59.00	4.58	100.53	97.95	83.85	52.69	47.40	44.55
04.203	-59.87	5907.66	-57.72	59.00	4.58	100.53	97.95	83.85	52.69	47.40	44.55
04.250	-78.61	5936.32	-47.22	50.00	4.71	114.32	111.35	86.88	54.92	49.12	46.15
04.313	-116.08	5958.60	-19.37	47.00	4.90	114.32	111.35	89.84	56.92	49.12	46.15
04.359	-116.08	5958.60	-19.37	47.00	4.90	114.32	111.35	89.84	56.92	50.83	47.94
04.422	-112.83	5964.97	-19.37	51.00	4.90	114.32	111.35	89.84	56.92	50.83	47.94
04.484	-112.83	5964.97	-19.37	51.00	4.90	114.32	111.35	89.84	56.92	50.83	47.94
04.531	-112.83	5964.97	-6.46	51.00	5.04	114.32	111.35	92.80	58.92	52.54	49.58
04.594	-112.83	5964.97	-6.46	51.00	5.04	114.32	111.35	92.80	58.92	52.54	49.58
04.641	-96.53	5968.95	12.92	50.00	5.18	114.32	111.35	94.76	60.25	53.91	50.66
04.703	-96.53	5968.95	12.92	50.00	5.18	114.32	111.35	94.76	60.25	53.91	50.66
04.750	-70.06	5972.93	34.71	52.00	5.36	126.94	123.56	97.99	62.21	55.66	52.29
04.813	-45.21	5984.87	34.71	57.00	5.36	126.94	123.56	97.99	62.21	55.66	52.29
04.859	-45.21	5984.87	34.71	57.00	5.36	126.94	123.56	97.99	62.21	55.66	52.29
04.922	-45.21	5984.87	39.56	57.00	5.51	126.94	123.56	100.84	64.39	57.40	53.93
04.984	-45.21	5984.87	39.56	57.00	5.51	126.94	123.56	100.84	64.39	57.40	53.93
05.031	-3.26	5985.67	41.98	53.00	5.65	126.94	123.56	102.74	65.72	58.58	55.04
05.094	-3.26	5985.67	41.98	53.00	5.65	126.94	123.56	102.74	65.72	58.58	55.04
05.141	42.77	6034.22	23.81	57.00	5.77	126.94	123.56	105.57	67.72	60.32	56.86
05.203	42.77	6034.22	23.81	57.00	5.77	126.94	123.56	105.57	67.72	60.32	56.86
05.250	109.16	6572.29	0.40	79.00	5.89	139.31	135.61	107.39	69.04	61.69	57.97
05.313	137.26	6737.06	0.40	73.00	5.89	139.31	135.61	107.39	69.04	61.69	57.97
05.375	137.26	6737.06	0.40	73.00	5.89	139.31	135.61	107.39	69.04	61.69	57.97
05.422	137.26	6737.06	-24.62	73.00	6.02	139.31	135.61	110.67	71.00	63.43	59.64

Run 2

TIME	X-LBF	Z-LBF	Y-LBF	PWR	mm	TCK1	TCK2	TCK3	TCK4	TCK5	TCK6
05.484	137.26	6737.06	-24.62	73.00	6.02	139.31	135.61	110.67	71.00	63.43	59.64
05.531	175.14	6893.86	-44.40	70.00	6.14	139.31	135.61	112.73	72.29	64.61	60.75
05.594	175.14	6893.86	-44.40	70.00	6.14	139.31	135.61	112.73	72.29	64.61	60.75
05.641	191.44	7067.38	-95.66	76.00	6.27	139.31	135.61	115.98	74.65	66.42	62.45
05.703	196.73	7482.08	-95.66	76.00	6.27	139.31	135.61	115.98	74.65	66.42	62.45
05.766	196.73	7482.08	-95.66	77.00	6.27	152.13	148.56	115.98	74.65	66.42	62.45
05.813	211.39	7664.36	-120.69	77.00	6.42	152.13	148.56	119.40	76.79	68.31	64.18
05.875	211.39	7664.36	-120.69	75.00	6.42	152.13	148.56	119.40	76.79	68.31	64.18
05.922	211.39	7664.36	-130.78	75.00	6.54	152.13	148.56	121.84	78.23	69.52	65.59
05.984	211.39	7664.36	-130.78	75.00	6.54	152.13	148.56	121.84	78.23	69.52	65.59
06.031	219.54	7867.33	-154.19	85.00	6.64	152.13	148.56	125.79	80.48	71.70	67.40
06.094	219.54	7867.33	-154.19	85.00	6.64	152.13	148.56	125.79	80.48	71.70	67.40
06.156	226.46	8119.65	-194.55	92.00	6.73	152.13	148.56	129.18	82.11	73.07	68.69
06.203	257.01	8992.83	-194.55	92.00	6.73	152.13	148.56	129.18	82.11	73.07	68.69
06.266	257.01	8992.83	-194.55	98.00	6.73	167.78	164.12	129.18	82.11	73.07	68.69
06.313	257.01	8992.83	-257.92	98.00	6.82	167.78	164.12	134.47	85.10	75.24	70.68
06.375	257.01	8992.83	-257.92	98.00	6.82	167.78	164.12	134.47	85.10	75.24	70.68
06.438	283.49	9602.54	-388.70	105.00	6.87	167.78	164.12	141.11	88.16	77.64	72.78
06.484	283.49	9602.54	-388.70	105.00	6.87	167.78	164.12	141.11	88.16	77.64	72.78
06.547	299.37	10947.72	-388.70	113.00	6.87	167.78	164.12	141.11	88.16	77.64	72.78
06.594	299.37	10947.72	-388.70	113.00	6.87	167.78	164.12	141.11	88.16	77.64	72.78
06.656	303.04	11647.37	-418.57	112.00	6.94	193.90	193.37	149.06	91.82	80.26	75.37
06.703	303.04	11647.37	-429.06	112.00	6.99	193.90	193.37	154.86	94.45	82.55	76.99
06.766	303.04	11647.37	-429.06	112.00	6.99	193.90	193.37	154.86	94.45	82.55	76.99
06.828	303.45	12387.62	-404.04	111.00	7.03	193.90	193.37	164.92	98.94	85.83	79.68
06.875	303.45	12387.62	-404.04	111.00	7.03	193.90	193.37	164.92	98.94	85.83	79.68
06.938	303.85	13962.84	-404.04	111.00	7.03	193.90	193.37	164.92	98.94	85.83	79.68
06.984	303.85	13962.84	-404.04	111.00	7.03	193.90	193.37	164.92	98.94	85.83	79.68
07.047	316.07	14796.22	-376.18	110.00	7.07	193.90	193.37	173.67	103.58	89.45	82.64

Run 3

TIME	X-LBF	Z-LBF	Y-LBF	mm	TCK1	TCK2	TCK3	TCK4	TCK5	TCK6
00.000	-59.06	457.68	-2.42	1.07	22.95	23.72	23.15	23.14	23.33	23.38
00.047	-59.06	457.68	-43.59	1.11	22.95	23.72	23.19	23.14	23.37	23.35
00.110	-59.06	457.68	-43.59	1.11	22.95	23.72	23.19	23.14	23.37	23.35
00.157	-122.19	997.35	-134.41	1.13	22.95	23.72	23.23	23.14	23.37	23.38
00.219	-122.19	997.35	-134.41	1.13	22.95	23.72	23.23	23.14	23.37	23.38
00.266	-138.49	1470.95	92.43	1.15	22.95	23.72	23.23	23.17	23.37	23.38
00.328	-138.49	1470.95	92.43	1.15	22.95	23.72	23.23	23.17	23.37	23.38
00.391	-206.51	1677.10	92.43	1.15	23.06	23.76	23.23	23.17	23.37	23.38
00.438	-206.51	1677.10	163.87	1.15	23.06	23.76	23.27	23.17	23.41	23.38
00.500	-206.51	1677.10	163.87	1.15	23.06	23.76	23.27	23.17	23.41	23.38
00.547	-272.08	2076.68	256.31	1.15	23.06	23.76	23.31	23.17	23.44	23.46
00.610	-272.08	2076.68	256.31	1.15	23.06	23.76	23.31	23.17	23.44	23.46
00.657	-319.33	2766.78	256.31	1.15	23.06	23.76	23.31	23.17	23.44	23.46
00.719	-319.33	2766.78	256.31	1.15	23.06	23.76	23.31	23.17	23.44	23.46
00.766	-277.79	3275.40	258.32	1.17	23.06	23.76	23.38	23.25	23.44	23.54
00.828	-277.79	3275.40	258.32	1.17	23.06	23.76	23.38	23.25	23.44	23.54
00.891	-277.79	3275.40	219.58	1.18	23.06	23.76	23.61	23.40	23.56	23.69
00.938	-158.44	3897.05	219.58	1.18	24.66	24.48	23.61	23.40	23.56	23.69
01.000	-158.44	3897.05	145.31	1.23	24.66	24.48	23.84	23.55	23.64	23.84
01.047	-88.39	4582.38	57.72	1.26	24.66	24.48	24.22	23.86	23.86	24.11
01.110	-88.39	4582.38	57.72	1.26	24.66	24.48	24.22	23.86	23.86	24.11
01.157	-72.91	5282.03	54.09	1.31	24.66	24.48	24.56	24.13	24.02	24.34
01.219	-72.91	5282.03	54.09	1.31	24.66	24.48	24.56	24.13	24.02	24.34
01.282	72.50	6361.36	54.09	1.31	24.66	24.48	24.56	24.13	24.02	24.34
01.328	72.50	6361.36	54.09	1.31	24.66	24.48	24.56	24.13	24.02	24.34
01.391	72.50	6361.36	30.68	1.39	24.66	24.48	25.25	24.62	24.36	24.79
01.438	92.46	6517.37	30.68	1.39	28.76	26.92	25.25	24.62	24.36	24.79
01.500	92.46	6517.37	7.67	1.57	28.76	26.92	25.82	25.04	24.70	25.17
01.547	83.09	6499.06	-7.27	1.71	28.76	26.92	26.96	26.07	25.31	25.17
01.610	83.09	6499.06	-7.27	1.71	28.76	26.92	26.96	26.07	25.31	25.86
01.672	100.61	6409.92	-7.27	1.71	28.76	26.92	26.96	26.07	25.31	25.86
01.719	100.61	6409.92	-7.27	1.71	28.76	26.92	26.96	26.07	25.31	25.86
01.782	100.61	6409.92	-11.71	1.86	28.76	26.92	28.13	26.82	25.80	26.58
01.828	100.61	6409.92	-11.71	1.86	28.76	26.92	28.13	26.82	25.80	26.58
01.891	102.64	6405.94	-14.53	2.01	38.83	33.46	29.95	28.27	26.75	27.68
01.938	98.16	6428.22	-14.53	2.01	38.83	33.46	29.95	28.27	26.75	27.68
02.000	98.16	6428.22	-18.97	2.14	38.83	33.46	31.27	29.33	27.55	28.55
02.063	91.64	6465.63	-44.00	2.26	38.83	33.46	33.47	31.18	28.88	30.03
02.110	91.64	6465.63	-44.00	2.26	38.83	33.46	33.47	31.18	28.88	30.03
02.172	92.87	6511.80	-51.66	2.40	38.83	33.46	34.97	32.69	30.01	31.05
02.219	92.87	6511.80	-51.66	2.40	38.83	33.46	34.97	32.69	30.01	31.05
02.282	84.72	6503.04	-51.66	2.40	52.53	43.15	34.97	32.69	30.01	31.05
02.328	84.72	6503.04	-51.66	2.40	52.53	43.15	34.97	32.69	30.01	31.05
02.391	84.72	6503.04	-55.30	2.56	52.53	43.15	37.31	34.80	31.60	32.71
02.453	66.39	6487.12	-55.30	2.56	52.53	43.15	37.31	34.80	31.60	32.71
02.500	66.39	6487.12	-59.33	2.70	52.53	43.15	39.11	36.16	32.77	33.88
02.563	48.47	6455.29	-61.76	2.84	52.53	43.15	40.76	37.66	33.94	35.28
02.610	48.47	6455.29	-61.76	2.84	52.53	43.15	40.76	37.66	33.94	35.28

Run 3

TIME	X-LBF	Z-LBF	Y-LBF	mm	TCK1	TCK2	TCK3	TCK4	TCK5	TCK6
02.610	48.47	6455.29	-61.76	2.84	52.53	43.15	40.76	37.66	33.94	35.28
02.672	32.58	6404.34	-54.49	2.96	52.53	43.15	43.16	39.92	35.79	37.08
02.719	32.58	6404.34	-54.49	2.96	52.53	43.15	43.16	39.92	35.79	37.08
02.782	-3.26	6288.13	-46.01	3.15	52.53	43.15	44.80	41.38	37.10	38.32
02.828	-3.26	6288.13	-46.01	3.15	52.53	43.15	44.80	41.38	37.10	38.32
02.891	-32.99	6230.03	-46.01	3.15	65.38	53.47	44.80	41.38	37.10	38.32
02.953	-32.99	6230.03	-43.59	3.26	65.38	53.47	46.44	43.14	38.64	39.60
03.000	-32.99	6230.03	-43.59	3.26	65.38	53.47	46.44	43.14	38.64	39.60
03.063	-45.21	6172.72	-33.10	3.41	65.38	53.47	48.94	45.45	40.67	41.51
03.110	-45.21	6172.72	-33.10	3.41	65.38	53.47	48.94	45.45	40.67	41.51
03.172	-48.06	6127.35	-24.22	3.58	65.38	53.47	50.80	46.98	42.06	42.82
03.219	-48.06	6127.35	-24.22	3.58	65.38	53.47	50.80	46.98	42.06	42.82
03.282	-51.73	6078.00	-8.48	3.70	65.38	53.47	53.29	49.29	44.15	45.02
03.344	-51.73	6078.00	-8.48	3.70	65.38	53.47	53.29	49.29	44.15	45.02
03.391	-60.69	6015.12	0.81	3.87	78.22	63.80	55.00	50.86	45.61	46.33
03.453	-60.69	6015.12	0.81	3.87	78.22	63.80	55.00	50.86	45.61	46.33
03.500	-60.69	6015.12	0.81	3.87	78.22	63.80	55.00	50.86	45.61	46.33
03.563	-43.58	6003.18	8.48	4.04	78.22	63.80	57.52	53.16	48.03	48.42
03.610	-43.58	6003.18	8.48	4.04	78.22	63.80	57.52	53.16	48.03	48.42
03.672	-12.63	5984.87	18.57	4.22	78.22	63.80	60.04	55.79	50.23	50.43
03.735	-12.63	5984.87	18.57	4.22	78.22	63.80	60.04	55.79	50.23	50.43
03.782	-2.44	5978.50	18.57	4.22	78.22	63.80	60.04	55.79	50.23	50.43
03.844	-2.44	5978.50	18.57	4.22	78.22	63.80	60.04	55.79	50.23	50.43
03.891	17.92	5968.95	19.78	4.35	90.78	73.73	61.70	57.39	51.72	51.80
03.953	17.92	5968.95	18.57	4.52	90.78	73.73	64.43	59.72	53.98	53.88
04.016	17.92	5968.95	18.57	4.52	90.78	73.73	64.43	59.72	53.98	53.88
04.063	41.55	5969.75	8.48	4.66	90.78	73.73	66.10	61.31	55.46	55.52
04.125	41.55	5969.75	8.48	4.66	90.78	73.73	66.10	61.31	55.46	55.52
04.172	75.76	5965.77	-2.42	4.80	90.78	73.73	68.57	63.64	57.72	57.59
04.235	75.76	5965.77	-2.42	4.80	90.78	73.73	68.57	63.64	57.72	57.59
04.282	75.76	5965.77	-2.42	4.80	90.78	73.73	68.57	63.64	57.72	57.59
04.344	75.76	5965.77	-2.42	4.80	90.78	73.73	68.57	63.64	57.72	57.59
04.391	83.91	5959.40	-13.72	5.00	102.72	83.66	71.04	66.26	60.24	59.66
04.453	95.72	5953.03	-13.72	5.00	102.72	83.66	71.04	66.26	60.24	59.66
04.516	95.72	5953.03	-35.52	5.13	102.72	83.66	72.67	67.85	61.76	61.03
04.563	106.31	5944.28	-47.22	5.25	102.72	83.66	74.29	69.40	63.27	62.44
04.625	106.31	5944.28	-47.22	5.25	102.72	83.66	74.29	69.40	63.27	62.44
04.672	104.68	5938.70	-54.49	5.37	102.72	83.66	76.98	71.80	65.53	64.55
04.735	104.68	5938.70	-54.49	5.37	102.72	83.66	76.98	71.80	65.53	64.55
04.782	91.64	5936.32	-54.49	5.37	102.72	83.66	76.98	71.80	65.53	64.55
04.844	91.64	5936.32	-54.49	5.37	102.72	83.66	76.98	71.80	65.53	64.55
04.907	94.50	5970.54	-62.97	5.57	113.83	92.97	79.34	74.12	67.85	66.84
04.953	100.20	6308.83	-62.97	5.57	113.83	92.97	79.34	74.12	67.85	66.84
05.016	100.20	6308.83	-77.90	5.73	113.83	92.97	81.74	76.45	70.29	68.90
05.063	81.46	6542.84	-77.90	5.73	113.83	92.97	81.74	76.45	70.29	68.90
05.125	81.46	6542.84	-77.90	5.73	113.83	92.97	81.74	76.45	70.29	68.90
05.172	81.46	6542.84	-75.48	5.85	113.83	92.97	84.10	79.03	72.54	70.93
05.235	81.46	6542.84	-75.48	5.85	113.83	92.97	84.10	79.03	72.54	70.93

Run 3

TIME	X-LBF	Z-LBF	Y-LBF	mm	TCK1	TCK2	TCK3	TCK4	TCK5	TCK6
05.282	51.32	6724.32	-70.64	5.98	113.83	92.97	85.73	80.58	74.02	72.33
05.344	51.32	6724.32	-70.64	5.98	113.83	92.97	85.73	80.58	74.02	72.33
05.407	36.25	6871.58	-58.93	6.11	125.20	102.62	87.65	82.13	75.57	73.77
05.453	17.11	7194.74	-58.93	6.11	125.20	102.62	87.65	82.13	75.57	73.77
05.516	17.11	7194.74	-51.66	6.24	125.20	102.62	90.24	84.53	77.89	75.91
05.563	11.00	7340.40	-51.66	6.24	125.20	102.62	90.24	84.53	77.89	75.91
05.625	11.00	7340.40	-51.66	6.24	125.20	102.62	90.24	84.53	77.89	75.91
05.672	24.44	7480.49	-32.69	6.36	125.20	102.62	92.01	86.23	79.44	77.68
05.735	24.44	7480.49	-32.69	6.36	125.20	102.62	92.01	86.23	79.44	77.68
05.797	24.44	7480.49	-17.36	6.47	125.20	102.62	94.86	89.11	82.17	80.04
05.844	24.44	7480.49	-17.36	6.47	125.20	102.62	94.86	89.11	82.17	80.04
05.907	50.51	7634.91	41.98	6.61	139.30	113.73	98.01	91.96	84.75	82.55
05.953	158.85	8165.02	41.98	6.61	139.30	113.73	98.01	91.96	84.75	82.55
06.016	158.85	8165.02	41.98	6.61	139.30	113.73	98.01	91.96	84.75	82.55
06.063	213.84	8165.02	81.53	6.72	139.30	113.73	101.95	95.14	87.52	85.29
06.125	213.84	8591.66	81.53	6.72	139.30	113.73	101.95	95.14	87.52	85.29
06.172	213.84	8591.66	126.74	6.78	139.30	113.73	104.67	97.70	90.70	88.28
06.235	213.84	8591.66	126.74	6.78	139.30	113.73	104.67	97.70	90.70	88.28
06.297	257.01	9143.26	126.74	6.78	139.30	113.73	104.67	97.70	90.70	88.28
06.344	257.01	9143.26	126.74	6.78	139.30	113.73	104.67	97.70	90.70	88.28
06.407	306.71	10488.45	115.44	6.84	159.08	129.36	109.36	102.34	93.11	90.68
06.453	306.71	10488.45	62.56	6.89	159.08	129.36	115.04	108.00	93.11	90.68
06.516	306.71	10488.45	62.56	6.89	159.08	129.36	115.04	108.00	97.82	95.31
06.563	302.63	11259.74	4.04	6.93	159.08	129.36	121.68	114.76	102.64	100.02
06.625	302.63	11259.74	4.04	6.93	159.08	129.36	121.68	114.76	102.64	100.02
06.688	316.89	12969.47	4.04	6.93	159.08	129.36	121.68	114.76	102.64	100.02
06.735	316.89	12969.47	4.04	6.93	159.08	129.36	121.68	114.76	102.64	100.02
06.797	339.29	13892.00	-56.91	6.96	189.43	153.63	129.44	120.83	107.74	104.93
06.844	339.29	13892.00	-56.91	6.96	189.43	153.63	129.44	120.83	107.74	104.93
06.907	339.29	13892.00	-138.45	6.98	189.43	153.63	133.93	124.82	111.29	108.21
06.953	332.77	14804.97	-138.45	6.98	189.43	153.63	133.93	124.82	111.29	108.21
07.016	332.77	14804.97	-272.86	7.00	189.43	153.63	140.49	130.55	116.56	113.06

Run 4

TIME	X-LBF	Z-LBF	Y-LBF	PWR	mm	TCK1	TCK2	TCK3	TCK4	TCK5	TCK6
00.000	-5.70	268.24	-0.40	11.00	1.07	24.25	24.87	24.44	24.38	24.54	24.51
00.047	-5.70	268.24	-85.17	11.00	1.11	24.25	24.87	24.47	24.42	24.54	24.51
00.110	-27.70	715.57	-85.17	21.00	1.11	24.25	24.87	24.47	24.42	24.54	24.51
00.157	-27.70	715.57	-85.17	21.00	1.11	24.25	24.87	24.47	24.42	24.54	24.51
00.219	-107.12	1551.34	-129.16	20.00	1.13	24.25	24.87	24.44	24.42	24.57	24.51
00.266	-107.12	1551.34	-129.16	20.00	1.13	24.25	24.87	24.44	24.42	24.57	24.51
00.329	-107.12	1551.34	-169.53	20.00	1.15	24.25	24.87	24.51	24.42	24.65	24.55
00.391	-107.12	1551.34	-169.53	20.00	1.15	24.25	24.87	24.51	24.42	24.65	24.55
00.438	-137.67	1736.80	-48.44	15.00	1.15	24.25	24.87	24.78	24.49	24.88	24.51
00.500	-221.58	1943.75	3.23	15.00	1.15	24.25	24.87	24.78	24.49	24.88	24.51
00.547	-221.58	1943.75	3.23	15.00	1.15	24.25	24.87	25.05	24.53	25.18	24.55
00.610	-283.90	2202.44	94.85	19.00	1.13	24.75	26.47	25.43	24.57	25.60	24.59
00.657	-283.90	2202.44	94.85	19.00	1.13	24.75	26.47	25.43	24.57	25.60	24.59
00.719	-422.79	2527.99	449.65	29.00	1.14	24.75	26.47	25.88	24.76	26.13	24.63
00.782	-422.79	2527.99	449.65	29.00	1.14	24.75	26.47	25.88	24.76	26.13	24.63
00.829	-516.88	2883.79	449.65	29.00	1.14	24.75	26.47	25.88	24.76	26.13	24.63
00.891	-516.88	2883.79	449.65	29.00	1.14	24.75	26.47	25.88	24.76	26.13	24.63
00.954	-6.92	4119.13	198.18	29.00	1.18	24.75	26.47	26.76	25.02	27.35	24.70
01.000	-6.92	4119.13	57.32	29.00	1.18	24.75	26.47	27.63	25.40	28.79	24.78
01.063	-6.92	4119.13	57.32	29.00	1.18	24.75	26.47	27.63	25.40	28.79	24.78
01.110	-50.91	4836.29	44.40	34.00	1.22	27.90	33.21	29.56	26.09	31.70	25.05
01.172	-50.91	4836.29	44.40	34.00	1.22	27.90	33.21	29.56	26.09	31.70	25.05
01.219	-54.99	5378.34	35.12	38.00	1.33	27.90	33.21	31.64	26.81	34.38	25.31
01.282	-54.99	5378.34	35.12	38.00	1.33	27.90	33.21	31.64	26.81	34.38	25.31
01.344	-33.40	5678.42	35.12	39.00	1.33	27.90	33.21	31.64	26.81	34.38	25.31
01.391	-29.33	5846.37	29.47	39.00	1.45	27.90	33.21	35.07	28.37	39.46	25.88
01.454	-29.33	5846.37	29.47	42.00	1.45	27.90	33.21	35.07	28.37	39.46	25.88
01.516	-29.33	5846.37	24.62	42.00	1.57	27.90	33.21	37.78	29.65	43.32	26.41
01.563	-29.33	5846.37	24.62	42.00	1.57	27.90	33.21	37.78	29.65	43.32	26.41
01.625	-12.22	5867.86	23.41	41.00	1.72	38.84	51.59	40.67	31.17	47.35	27.06
01.672	-12.22	5867.86	23.41	41.00	1.72	38.84	51.59	40.67	31.17	47.35	27.06
01.735	12.22	5889.35	23.81	46.00	1.84	38.84	51.59	45.42	34.11	54.27	28.31
01.782	12.22	5889.35	23.81	46.00	1.84	38.84	51.59	45.42	34.11	54.27	28.31
01.844	36.66	5910.85	19.78	43.00	2.02	38.84	51.59	48.63	36.03	58.34	29.22
01.907	45.62	5946.66	19.78	39.00	2.12	38.84	51.59	48.63	36.03	58.34	29.22
01.954	45.62	5946.66	10.09	39.00	2.12	38.84	51.59	54.02	39.08	64.26	31.00
02.016	79.83	5993.63	10.09	40.00	2.12	56.47	76.33	54.02	39.08	64.26	31.00
02.063	79.83	5993.63	10.09	40.00	2.12	56.47	76.33	54.02	39.08	64.26	31.00
02.125	79.83	5993.63	2.42	40.00	2.27	56.47	76.33	57.17	41.06	68.14	32.17
02.172	79.83	5993.63	2.42	40.00	2.27	56.47	76.33	57.17	41.06	68.14	32.17
02.235	98.16	6000.79	-8.07	43.00	2.43	56.47	76.33	61.91	44.13	73.75	33.98
02.297	98.16	6000.79	-8.07	43.00	2.43	56.47	76.33	61.91	44.13	73.75	33.98
02.344	105.09	5989.65	-16.15	44.00	2.59	56.47	76.33	65.05	46.26	77.40	35.26
02.407	96.94	5969.75	-16.15	47.00	2.59	56.47	76.33	65.05	46.26	77.40	35.26
02.469	96.94	5969.75	-37.13	47.00	2.71	56.47	76.33	69.67	49.76	83.38	37.22
02.516	94.90	5937.11	-37.13	39.00	2.71	74.25	99.36	69.67	49.76	83.38	37.22
02.579	94.90	5937.11	-37.13	39.00	2.71	74.25	99.36	69.67	49.76	83.38	37.22
02.625	89.61	5889.35	-48.03	42.00	2.83	74.25	99.36	72.69	51.85	86.92	38.54

Run 4

TIME	X-LBF	Z-LBF	Y-LBF	PWR	mm	TCK1	TCK2	TCK3	TCK4	TCK5	TCK6
02.688	89.61	5889.35	-48.03	42.00	2.83	74.25	99.36	72.69	51.85	86.92	38.54
02.735	89.61	5889.35	-53.68	42.00	3.00	74.25	99.36	76.23	53.93	90.36	39.92
02.797	89.61	5889.35	-53.68	42.00	3.00	74.25	99.36	76.23	53.93	90.36	39.92
02.844	69.24	5861.50	-60.54	43.00	3.16	74.25	99.36	80.70	57.08	95.54	42.21
02.907	50.10	5828.86	-60.54	45.00	3.16	74.25	99.36	80.70	57.08	95.54	42.21
02.969	50.10	5828.86	-63.37	45.00	3.28	74.25	99.36	83.72	59.11	98.96	43.59
03.016	34.62	5803.39	-58.12	44.00	3.43	95.27	120.34	88.16	62.63	104.05	45.76
03.079	34.62	5803.39	-58.12	44.00	3.43	95.27	120.34	88.16	62.63	104.05	45.76
03.125	-5.70	5752.45	-58.12	49.00	3.43	95.27	120.34	88.16	62.63	104.05	45.76
03.188	-5.70	5752.45	-58.12	49.00	3.43	95.27	120.34	88.16	62.63	104.05	45.76
03.235	-5.70	5752.45	-52.88	49.00	3.62	95.27	120.34	91.11	64.74	107.88	47.18
03.297	-5.70	5752.45	-52.88	49.00	3.62	95.27	120.34	91.11	64.74	107.88	47.18
03.360	-29.33	5723.79	-48.84	45.00	3.75	95.27	120.34	95.52	67.80	112.85	49.38
03.407	-46.43	5681.61	-48.84	45.00	3.75	95.27	120.34	95.52	67.80	112.85	49.38
03.469	-46.43	5681.61	-38.35	45.00	3.89	95.27	120.34	98.97	69.90	116.10	50.79
03.516	-48.06	5650.56	-15.74	48.00	4.06	115.30	140.96	103.35	73.00	121.02	53.28
03.579	-48.06	5650.56	-15.74	48.00	4.06	115.30	140.96	103.35	73.00	121.02	53.28
03.625	-54.17	5612.36	-9.69	49.00	4.19	115.30	140.96	106.22	75.11	124.21	54.73
03.688	-54.17	5612.36	-9.69	49.00	4.19	115.30	140.96	106.22	75.11	124.21	54.73
03.750	-64.76	5564.60	-9.69	48.00	4.19	115.30	140.96	106.22	75.11	124.21	54.73
03.797	-64.76	5564.60	-9.69	48.00	4.19	115.30	140.96	106.22	75.11	124.21	54.73
03.860	-56.21	5548.68	0.81	49.00	4.32	115.30	140.96	109.09	77.50	127.34	56.21
03.907	-56.21	5548.68	8.07	49.00	4.44	115.30	140.96	113.42	80.57	132.59	58.43
03.969	-56.21	5548.68	8.07	49.00	4.44	115.30	140.96	113.42	80.57	132.59	58.43
04.016	-35.03	5544.70	13.32	45.00	4.62	132.23	161.44	116.27	82.60	135.69	59.91
04.079	-35.03	5544.70	13.32	45.00	4.62	132.23	161.44	116.27	82.60	135.69	59.91
04.125	-14.26	5537.54	17.76	50.00	4.76	132.23	161.44	120.99	85.70	140.28	62.13
04.188	-14.26	5537.54	17.76	50.00	4.76	132.23	161.44	120.99	85.70	140.28	62.13
04.250	17.11	5527.19	17.76	49.00	4.76	132.23	161.44	120.99	85.70	140.28	62.13
04.297	17.11	5527.19	17.76	49.00	4.88	132.23	161.44	120.99	85.70	140.28	62.13
04.360	42.77	5531.97	13.72	48.00	4.88	132.23	161.44	123.77	87.69	143.35	63.83
04.407	42.77	5531.97	11.71	48.00	5.04	132.23	161.44	126.56	89.65	146.28	66.09
04.469	42.77	5531.97	11.71	48.00	5.04	132.23	161.44	126.56	89.65	146.28	66.09
04.516	65.58	5535.15	4.44	52.00	5.16	132.23	161.44	130.75	92.94	150.74	67.53
04.579	65.58	5535.15	4.44	52.00	5.16	132.23	161.44	130.75	92.94	150.74	67.53
04.641	78.61	5540.72	-17.36	52.00	5.34	149.39	181.08	134.76	95.94	155.74	69.74
04.688	78.61	5540.72	-17.36	52.00	5.34	149.39	181.08	134.76	95.94	155.74	69.74
04.750	82.28	5552.66	-26.24	55.00	5.45	149.39	181.08	137.41	97.87	158.65	71.22
04.797	82.28	5552.66	-26.24	55.00	5.45	149.39	181.08	137.41	97.87	158.65	71.22
04.860	112.01	5578.93	-39.56	56.00	5.60	149.39	181.08	140.56	99.80	161.56	72.66
04.907	140.52	5753.24	-39.56	57.00	5.60	149.39	181.08	140.56	99.80	161.56	72.66
04.969	140.52	5753.24	-39.56	57.00	5.60	149.39	181.08	140.56	99.80	161.56	72.66
05.032	140.52	5753.24	-71.04	57.00	5.74	149.39	181.08	143.25	101.77	164.28	74.09
05.079	140.52	5753.24	-71.04	57.00	5.74	149.39	181.08	143.25	101.77	164.28	74.09
05.141	134.41	6050.14	-79.11	71.00	5.84	166.63	202.90	147.21	104.60	168.50	76.53
05.188	134.41	6050.14	-79.11	71.00	5.84	166.63	202.90	147.21	104.60	168.50	76.53
05.250	125.45	6246.74	-77.09	69.00	5.94	166.63	202.90	149.84	106.91	171.37	77.97
05.313	124.64	6402.75	-77.09	69.00	5.94	166.63	202.90	149.84	106.91	171.37	77.97

Run 4

TIME	X-LBF	Z-LBF	Y-LBF	PWR	mm	TCK1	TCK2	TCK3	TCK4	TCK5	TCK6
05.360	124.64	6402.75	-70.64	69.00	6.05	166.63	202.90	154.12	109.96	176.67	80.18
05.422	98.98	6764.12	-70.64	69.00	6.05	166.63	202.90	154.12	109.96	176.67	80.18
05.469	98.98	6764.12	-70.64	69.00	6.05	166.63	202.90	154.12	109.96	176.67	80.18
05.532	63.13	6986.99	-58.12	69.00	6.18	166.63	202.90	157.13	112.09	180.01	81.69
05.579	63.13	6986.99	-58.12	69.00	6.18	166.63	202.90	157.13	112.09	180.01	81.69
05.641	63.13	6986.99	-43.19	81.00	6.28	183.49	225.09	162.11	115.46	185.27	84.06
05.688	63.13	6986.99	-43.19	81.00	6.28	183.49	225.09	162.11	115.46	185.27	84.06
05.750	21.18	7213.05	-21.80	77.00	6.36	183.49	225.09	165.06	117.93	189.19	85.68
05.813	-9.37	7471.73	-21.80	77.00	6.36	183.49	225.09	165.06	117.93	189.19	85.68
05.860	-9.37	7471.73	24.22	87.00	6.45	183.49	225.09	170.08	121.76	195.38	88.53
05.922	-46.84	8145.92	50.05	92.00	6.53	183.49	225.09	173.65	125.22	195.38	88.53
05.969	-46.84	8145.92	50.05	92.00	6.53	183.49	225.09	173.65	125.22	200.67	90.37
06.032	-47.25	8617.93	50.05	94.00	6.53	202.58	244.50	173.65	125.22	200.67	90.37
06.094	-47.25	8617.93	50.05	94.00	6.53	202.58	244.50	173.65	125.22	200.67	90.37
06.141	-47.25	8617.93	74.27	94.00	6.59	202.58	244.50	177.76	128.42	205.82	92.30
06.204	-47.25	8617.93	74.27	94.00	6.59	202.58	244.50	177.76	128.42	205.82	92.30
06.250	-36.25	9187.84	75.88	101.00	6.63	202.58	244.50	184.02	134.05	215.85	95.56
06.313	-24.44	9841.33	75.88	101.00	6.63	202.58	244.50	184.02	134.05	215.85	95.56
06.360	-24.44	9841.33	44.80	102.00	6.68	202.58	244.50	189.32	138.14	222.00	97.93
06.422	-13.44	10549.74	15.74	104.00	6.73	202.58	244.50	196.54	144.75	231.53	97.93
06.485	-13.44	10549.74	15.74	104.00	6.73	202.58	244.50	196.54	144.75	231.53	101.94
06.532	32.99	12098.69	15.74	112.00	6.73	229.19	259.78	196.54	144.75	231.53	101.94
06.594	32.99	12098.69	15.74	112.00	6.73	229.19	259.78	196.54	144.75	231.53	101.94
06.641	66.80	12929.67	-27.04	111.00	6.76	229.19	259.78	201.42	149.51	236.85	104.80
06.704	66.80	12929.67	-27.04	111.00	6.76	229.19	259.78	201.42	149.51	236.85	104.80
06.750	66.80	12929.67	-69.42	111.00	6.79	229.19	259.78	208.97	157.61	244.69	109.87
06.813	110.79	13770.22	-69.42	111.00	6.79	229.19	259.78	208.97	157.61	244.69	109.87
06.875	110.79	13770.22	-119.88	117.00	6.84	229.19	259.78	214.45	162.55	249.61	113.12
06.922	140.11	14652.94	-245.81	109.00	6.89	229.19	259.78	221.25	169.83	256.06	118.21
06.985	140.11	14652.94	-245.81	109.00	6.89	229.19	259.78	221.25	169.83	256.06	118.21
07.032	189.81	15553.18	-245.81	111.00	6.89	246.23	275.85	221.25	169.83	256.06	118.21

Run 5

TIME	X-LBF	Z-LBF	Y-LBF	PWR	mm	TCK1	TCK2	TCK3	TCK4	TCK5	TCK6
00.000	-71.69	172.72	-41.17	13.00	1.12	24.90	25.48	25.14	25.08	25.12	25.10
00.063	-71.69	172.72	-41.17	13.00	1.12	24.90	25.48	25.14	25.08	25.12	25.10
00.125	-173.11	1025.20	-41.17	20.00	1.12	24.90	25.48	25.14	25.08	25.12	25.10
00.172	-173.11	1025.20	-64.18	20.00	1.14	24.90	25.48	25.17	25.08	25.16	25.14
00.235	-123.01	1261.61	-64.18	28.00	1.14	24.90	25.48	25.17	25.08	25.16	25.14
00.281	-21.59	1318.92	-109.79	19.00	1.13	24.90	25.48	25.33	25.12	25.50	25.10
00.344	-21.59	1318.92	-109.79	19.00	1.13	24.90	25.48	25.33	25.12	25.50	25.10
00.391	90.42	1468.56	-132.79	23.00	1.12	24.90	25.48	25.59	25.19	26.03	25.10
00.453	90.42	1468.56	-132.79	23.00	1.12	24.90	25.48	25.59	25.19	26.03	25.10
00.516	215.87	1645.26	-132.79	24.00	1.12	26.27	27.04	25.59	25.19	26.03	25.10
00.563	215.87	1645.26	-132.79	24.00	1.13	26.27	27.04	25.59	25.19	26.03	25.10
00.625	215.87	1645.26	-234.11	24.00	1.13	26.27	27.04	26.24	25.50	27.40	25.21
00.672	353.55	1891.22	-464.18	20.00	1.11	26.27	27.04	27.19	25.88	29.11	25.21
00.735	353.55	1891.22	-464.18	20.00	1.11	26.27	27.04	27.19	25.88	29.11	25.40
00.781	548.65	2672.85	-561.45	28.00	1.14	26.27	27.04	27.87	26.26	30.43	25.52
00.844	548.65	2672.85	-561.45	28.00	1.14	26.27	27.04	27.87	26.26	30.43	25.52
00.906	127.90	3136.11	-561.45	30.00	1.14	26.27	27.04	27.87	26.26	30.43	25.52
00.953	127.90	3136.11	-561.45	30.00	1.14	26.27	27.04	27.87	26.26	30.43	25.52
01.016	73.32	3667.81	-269.22	30.00	1.20	31.65	31.89	29.08	27.05	32.89	25.86
01.063	73.32	3667.81	-269.22	30.00	1.26	31.65	31.89	29.08	27.05	32.89	25.86
01.125	162.11	4266.38	-87.59	37.00	1.26	31.65	31.89	30.07	27.70	36.13	26.32
01.172	162.11	4266.38	-56.10	37.00	1.32	31.65	31.89	32.00	28.95	38.91	26.70
01.235	162.11	4266.38	-56.10	37.00	1.32	31.65	31.89	32.00	28.95	38.91	26.70
01.297	118.12	5078.26	-51.26	33.00	1.40	31.65	31.89	33.51	29.97	42.88	27.19
01.344	118.12	5078.26	-51.26	33.00	1.40	31.65	31.89	33.51	29.97	42.88	27.19
01.406	109.97	5305.91	-55.70	38.00	1.53	31.65	31.89	36.67	31.90	48.97	28.21
01.453	109.97	5305.91	-55.70	38.00	1.53	31.65	31.89	36.67	31.90	48.97	28.21
01.516	109.57	5439.63	-55.70	38.00	1.53	43.78	41.55	36.67	31.90	48.97	28.21
01.563	109.57	5439.63	-55.70	38.00	1.66	43.78	41.55	36.67	31.90	48.97	28.21
01.625	72.50	5590.07	-65.39	41.00	1.66	43.78	41.55	38.96	33.41	53.35	29.01
01.672	72.50	5590.07	-75.48	41.00	1.83	43.78	41.55	42.64	36.35	60.32	30.45
01.735	72.50	5590.07	-75.48	41.00	1.83	43.78	41.55	42.64	36.35	60.32	30.45
01.797	59.87	5641.01	-77.09	35.00	1.98	43.78	41.55	46.60	39.24	67.31	32.15
01.844	59.87	5641.01	-77.09	35.00	1.98	43.78	41.55	46.60	39.24	67.31	32.15
01.906	39.10	5678.42	-77.09	38.00	1.98	63.25	57.71	46.60	39.24	67.31	32.15
01.953	39.10	5678.42	-77.09	38.00	1.98	63.25	57.71	46.60	39.24	67.31	32.15
02.016	-8.55	5707.08	-72.25	43.00	2.14	63.25	57.71	49.32	41.34	71.81	33.36
02.063	-8.55	5707.08	-66.20	43.00	2.26	63.25	57.71	53.40	41.34	71.81	33.36
02.125	-8.55	5707.08	-66.20	43.00	2.26	63.25	57.71	53.40	44.41	79.26	35.35
02.188	-49.28	5696.73	-60.54	43.00	2.42	63.25	57.71	58.00	47.54	85.76	35.35
02.235	-49.28	5696.73	-60.54	43.00	2.42	63.25	57.71	58.00	47.54	85.76	37.69
02.297	-63.95	5665.69	-50.45	46.00	2.57	63.25	57.71	60.78	50.08	89.93	39.11
02.344	-63.95	5665.69	-50.45	46.00	2.57	63.25	57.71	60.78	50.08	89.93	39.11
02.406	-74.54	5623.50	-50.45	37.00	2.57	82.51	74.04	60.78	50.08	89.93	39.11
02.453	-74.54	5623.50	-50.45	37.00	2.57	82.51	74.04	60.78	50.08	89.93	39.11
02.516	-74.54	5623.50	-24.62	37.00	2.76	82.51	74.04	64.88	53.24	96.19	41.40
02.563	-93.27	5533.56	-24.62	37.00	2.76	82.51	74.04	64.88	53.24	96.19	41.40
02.625	-93.27	5533.56	-16.55	39.00	2.94	82.51	74.04	69.02	56.54	102.28	43.72

Run 5

TIME	X-LBF	Z-LBF	Y-LBF	PWR	mm	TCK1	TCK2	TCK3	TCK4	TCK5	TCK6
02.688	-97.35	5492.17	-16.55	41.00	2.94	82.51	74.04	69.02	56.54	102.28	43.72
02.735	-97.35	5492.17	-16.55	41.00	2.94	82.51	74.04	69.02	56.54	102.28	43.72
02.797	-79.83	5453.16	6.46	47.00	3.09	82.51	74.04	73.19	59.80	108.98	46.07
02.844	-79.83	5453.16	6.46	47.00	3.09	82.51	74.04	73.19	59.80	108.98	46.07
02.906	-79.83	5453.16	19.78	47.00	3.23	82.51	74.04	76.40	61.94	112.97	47.68
02.953	-79.83	5453.16	19.78	47.00	3.23	82.51	74.04	76.40	61.94	112.97	47.68
03.016	-59.87	5408.59	21.80	47.00	3.35	101.57	90.76	79.13	64.12	116.90	49.54
03.078	-28.92	5353.67	21.80	47.00	3.35	101.57	90.76	79.13	64.12	116.90	49.54
03.125	-28.92	5353.67	26.24	49.00	3.54	101.57	90.76	83.26	67.78	122.80	52.03
03.188	-1.63	5335.36	26.24	45.00	3.54	101.57	90.76	83.26	67.78	122.80	52.03
03.235	-1.63	5335.36	26.24	45.00	3.54	101.57	90.76	83.26	67.78	122.80	52.03
03.297	30.96	5313.87	24.62	48.00	3.69	101.57	90.76	85.99	69.92	126.64	53.67
03.344	30.96	5313.87	24.62	48.00	3.69	101.57	90.76	85.99	69.92	126.64	53.67
03.406	30.96	5313.87	20.99	48.00	3.83	101.57	90.76	90.09	73.17	132.41	56.15
03.469	30.96	5313.87	20.99	48.00	3.83	101.57	90.76	90.09	73.17	132.41	56.15
03.516	65.58	5286.81	8.07	49.00	4.01	121.56	107.24	94.20	76.41	138.70	58.63
03.578	73.72	5279.64	8.07	49.00	4.01	121.56	107.24	94.20	76.41	138.70	58.63
03.625	73.72	5279.64	-18.16	48.00	4.13	121.56	107.24	97.35	78.59	142.42	60.34
03.688	94.90	5270.09	-18.16	49.00	4.13	121.56	107.24	97.35	78.59	142.42	60.34
03.735	94.90	5270.09	-18.16	49.00	4.13	121.56	107.24	97.35	78.59	142.42	60.34
03.797	109.97	5270.09	-27.85	49.00	4.31	121.56	107.24	101.36	82.09	148.17	63.11
03.860	109.97	5270.09	-27.85	49.00	4.31	121.56	107.24	101.36	82.09	148.17	63.11
03.906	109.97	5249.40	-42.78	45.00	4.43	121.56	107.24	104.00	84.27	151.98	64.77
03.969	109.97	5249.40	-42.78	45.00	4.43	121.56	107.24	104.00	84.27	151.98	64.77
04.016	96.94	5246.21	-52.47	50.00	4.55	139.38	122.74	106.64	86.38	155.72	66.43
04.078	87.98	5248.60	-52.47	50.00	4.55	139.38	122.74	106.64	86.38	155.72	66.43
04.125	87.98	5248.60	-64.98	48.00	4.71	139.38	122.74	110.56	89.56	161.77	68.98
04.188	70.46	5253.38	-64.98	50.00	4.71	139.38	122.74	110.56	89.56	161.77	68.98
04.235	70.46	5253.38	-64.98	50.00	4.71	139.38	122.74	110.56	89.56	161.77	68.98
04.297	70.46	5253.38	-77.90	50.00	4.88	139.38	122.74	113.18	91.59	167.05	71.49
04.360	70.46	5253.38	-77.90	50.00	4.88	139.38	122.74	113.18	91.59	167.05	71.49
04.406	44.80	5258.15	-80.32	54.00	5.05	139.38	122.74	117.48	94.63	170.62	73.15
04.469	44.80	5258.15	-80.32	54.00	5.05	139.38	122.74	117.48	94.63	170.62	73.15
04.516	9.37	5271.68	-77.90	54.00	5.18	159.09	138.22	121.31	98.00	175.99	75.92
04.578	-16.70	5278.85	-77.90	54.00	5.18	159.09	138.22	121.31	98.00	175.99	75.92
04.625	-16.70	5278.85	-61.76	50.00	5.29	159.09	138.22	123.83	100.08	179.57	77.58
04.688	-27.29	5289.99	-52.47	50.00	5.47	159.09	138.22	127.56	100.08	179.57	77.58
04.750	-27.29	5289.99	-52.47	50.00	5.47	159.09	138.22	127.56	103.09	184.94	80.01
04.797	-48.47	5297.95	-52.47	49.00	5.47	159.09	138.22	127.56	103.09	184.94	80.01
04.860	-48.47	5297.95	-52.47	49.00	5.47	159.09	138.22	127.56	103.09	184.94	80.01
04.906	-52.54	5481.02	-39.56	61.00	5.65	177.00	153.14	131.25	106.10	190.48	82.48
04.969	-52.54	5481.02	-39.56	61.00	5.65	177.00	153.14	131.25	106.10	190.48	82.48
05.016	-52.54	5481.02	-21.39	61.00	5.75	177.00	153.14	134.13	108.04	193.82	84.11
05.078	-48.06	5710.26	-21.39	61.00	5.75	177.00	153.14	134.13	108.04	193.82	84.11
05.141	-48.06	5710.26	-21.39	65.00	5.75	177.00	153.14	134.13	108.04	193.82	84.11
05.188	-30.14	5880.60	-12.51	68.00	5.88	177.00	153.14	137.76	111.02	198.92	86.58
05.250	-30.14	5880.60	-12.51	68.00	5.88	177.00	153.14	137.76	111.02	198.92	86.58
05.297	-10.18	6034.22	-7.27	71.00	6.05	177.00	153.14	141.48	114.57	204.87	89.28

Run 5

TIME	X-LBF	Z-LBF	Y-LBF	PWR	mm	TCK1	TCK2	TCK3	TCK4	TCK5	TCK6
05.360	-10.18	6034.22	-7.27	71.00	6.05	177.00	153.14	141.48	114.57	204.87	89.28
05.406	8.55	6191.82	-12.51	73.00	6.18	195.86	167.53	144.10	116.82	209.70	91.02
05.469	8.55	6191.82	-12.51	73.00	6.18	195.86	167.53	144.10	116.82	209.70	91.02
05.531	60.69	6589.80	-12.51	78.00	6.18	195.86	167.53	144.10	116.82	209.70	91.02
05.578	60.69	6589.80	-12.11	78.00	6.28	195.86	167.53	148.14	120.46	209.70	91.02
05.641	60.69	6589.80	-12.11	78.00	6.28	195.86	167.53	148.14	120.46	217.70	93.72
05.688	133.60	6812.67	-14.13	79.00	6.36	195.86	167.53	151.00	122.98	221.21	95.61
05.750	133.60	6812.67	-14.13	79.00	6.36	195.86	167.53	151.00	122.98	221.21	95.61
05.797	140.52	7060.22	-18.57	78.00	6.46	195.86	167.53	156.00	126.97	227.09	98.58
05.860	140.52	7060.22	-18.57	78.00	6.46	195.86	167.53	156.00	126.97	227.09	98.58
05.906	138.89	7382.59	-37.13	86.00	6.54	195.86	167.53	159.25	130.36	232.08	100.65
05.969	138.89	7382.59	-37.13	86.00	6.54	195.86	167.53	159.25	130.36	232.08	100.65
06.031	142.56	7766.24	-107.77	93.00	6.61	219.31	189.46	162.58	133.42	236.45	103.22
06.078	142.56	7766.24	-107.77	93.00	6.61	219.31	189.46	162.58	133.42	236.45	103.22
06.141	142.56	7766.24	-107.77	93.00	6.61	219.31	189.46	162.58	133.42	236.45	103.22
06.188	155.19	8790.65	-144.10	94.00	6.67	219.31	189.46	168.06	138.39	243.76	103.22
06.250	155.19	8790.65	-144.10	94.00	6.67	219.31	189.46	168.06	138.39	243.76	106.76
06.297	143.37	9423.44	-190.51	99.00	6.73	219.31	189.46	174.09	143.70	250.91	110.60
06.360	143.37	9423.44	-190.51	99.00	6.73	219.31	189.46	174.09	143.70	250.91	110.60
06.422	150.71	10103.20	-283.35	103.00	6.77	242.18	211.40	178.16	147.51	255.09	113.32
06.469	150.71	10103.20	-283.35	103.00	6.77	242.18	211.40	178.16	147.51	255.09	113.32
06.531	150.71	10103.20	-283.35	103.00	6.77	242.18	211.40	178.16	147.51	255.09	113.32
06.578	150.71	10103.20	-283.35	103.00	6.77	242.18	211.40	178.16	147.51	255.09	113.32
06.641	168.22	11624.29	-317.25	105.00	6.81	242.18	211.40	184.53	153.54	261.23	117.74
06.688	165.78	12436.18	-317.25	106.00	6.85	242.18	211.40	184.53	153.54	261.23	117.74
06.750	165.78	12436.18	-360.44	106.00	6.85	242.18	211.40	190.72	160.65	267.75	122.55
06.797	161.30	13259.21	-395.96	108.00	6.88	242.18	211.40	194.98	165.13	272.51	126.42
06.860	161.30	13259.21	-395.96	108.00	6.88	242.18	211.40	194.98	165.13	272.51	126.42
06.922	147.85	14016.96	-395.96	110.00	6.88	256.68	230.31	194.98	165.13	272.51	126.42
06.969	147.85	14016.96	-395.96	110.00	6.88	256.68	230.31	194.98	165.13	272.51	126.42
07.031	147.85	14016.96	-397.58	110.00	6.90	256.68	230.31	202.12	172.07	281.06	131.71

Run 6

TIME	X-LBF	Z-LBF	Y-LBF	PWR	mm	TCK1	TCK2	TCK3	TCK4	TCK5	TCK6
00.000	48.88	35.82	-4.44	15.00	1.05	25.87	26.45	26.14	26.08	26.09	26.03
00.046	48.88	35.82	-4.44	15.00	1.05	25.87	26.45	26.14	26.08	26.09	26.03
00.109	48.88	35.82	-4.44	15.00	1.05	25.87	26.45	26.14	26.08	26.09	26.03
00.171	126.67	384.45	-31.08	17.00	1.11	25.87	26.45	26.14	26.01	26.09	26.03
00.218	126.67	384.45	-31.08	17.00	1.11	25.87	26.45	26.14	26.01	26.09	26.03
00.281	261.49	887.50	-274.87	22.00	1.14	25.87	26.45	26.14	26.12	26.13	25.99
00.328	261.49	887.50	-274.87	22.00	1.14	25.87	26.45	26.14	26.12	26.13	25.99
00.390	349.07	1211.46	-393.14	19.00	1.14	25.87	26.45	26.22	26.08	26.36	26.07
00.437	349.07	1211.46	-393.14	19.00	1.14	25.87	26.45	26.22	26.08	26.36	26.07
00.500	401.20	1568.85	-429.87	24.00	1.11	26.14	29.75	26.37	26.08	26.81	26.03
00.562	345.81	1798.88	-429.87	24.00	1.11	26.14	29.75	26.37	26.08	26.81	26.03
00.609	345.81	1798.88	-429.87	21.00	1.11	26.14	29.75	26.37	26.08	26.81	26.03
00.671	345.81	1798.88	-416.14	21.00	1.14	26.14	29.75	26.79	26.31	27.91	26.07
00.734	345.81	1798.88	-416.14	21.00	1.14	26.14	29.75	26.79	26.31	27.91	26.07
00.796	252.13	2105.33	-307.57	24.00	1.14	26.14	29.75	27.24	26.46	28.90	26.10
00.843	252.13	2105.33	-307.57	24.00	1.14	26.14	29.75	27.24	26.46	28.90	26.10
00.906	35.84	2511.27	216.75	30.00	1.14	26.14	29.75	28.15	26.80	30.64	26.18
00.953	-397.94	2990.45	216.75	28.00	1.14	28.98	38.91	28.15	26.80	30.64	26.18
01.015	-397.94	2990.45	342.68	28.00	1.21	28.98	38.91	28.99	27.15	32.34	26.29
01.062	-96.13	4076.14	342.68	28.00	1.21	28.98	38.91	28.99	27.15	32.34	26.29
01.125	-96.13	4076.14	342.68	28.00	1.21	28.98	38.91	28.99	27.15	32.34	26.29
01.171	-96.13	4076.14	-40.77	28.00	1.25	28.98	38.91	29.93	27.71	35.32	26.52
01.234	-96.13	4076.14	-40.77	28.00	1.25	28.98	38.91	29.93	27.71	35.32	26.52
01.296	-11.00	4697.00	-96.06	42.00	1.33	28.98	38.91	32.39	28.93	39.42	26.83
01.343	-11.00	4697.00	-96.06	42.00	1.33	28.98	38.91	32.39	28.93	39.42	26.83
01.406	-29.73	5160.25	-80.73	37.00	1.45	28.98	38.91	34.09	29.80	42.86	27.13
01.453	-49.28	5436.45	-80.73	37.00	1.45	36.68	60.40	34.09	29.80	42.86	27.13
01.515	-49.28	5436.45	-80.73	42.00	1.45	36.68	60.40	34.09	29.80	42.86	27.13
01.562	-49.28	5436.45	-72.65	42.00	1.56	36.68	60.40	37.18	31.54	48.87	27.70
01.625	-49.28	5436.45	-72.65	42.00	1.56	36.68	60.40	37.18	31.54	48.87	27.70
01.687	-60.28	5672.06	-63.37	39.00	1.69	36.68	60.40	39.54	32.90	53.11	28.23
01.734	-60.28	5672.06	-63.37	39.00	1.69	36.68	60.40	39.54	32.90	53.11	28.23
01.796	-72.50	5729.36	-46.01	37.00	1.79	36.68	60.40	42.61	34.67	58.23	28.84
01.843	-72.50	5729.36	-46.01	37.00	1.79	36.68	60.40	42.61	34.67	58.23	28.84
01.906	-87.16	5765.18	-46.01	37.00	1.79	36.68	60.40	42.61	34.67	58.23	28.84
01.953	-87.16	5765.18	-24.62	37.00	1.99	36.68	60.40	48.33	38.28	66.81	30.31
02.015	-85.13	5805.78	-24.62	42.00	1.99	51.11	88.68	48.33	38.28	66.81	30.31
02.078	-72.91	5801.80	-15.34	42.00	2.12	51.11	88.68	51.30	40.23	70.98	31.15
02.125	-72.91	5801.80	-15.34	42.00	2.12	51.11	88.68	51.30	40.23	70.98	31.15
02.187	-72.91	5801.80	-1.21	42.00	2.28	51.11	88.68	54.31	42.14	75.11	32.28
02.234	-72.91	5801.80	-1.21	42.00	2.28	51.11	88.68	54.31	42.14	75.11	32.28
02.296	-68.02	5781.10	19.37	37.00	2.45	51.11	88.68	58.94	45.14	81.08	33.86
02.343	-68.02	5781.10	19.37	37.00	2.45	51.11	88.68	58.94	45.14	81.08	33.86
02.406	-63.54	5739.71	19.37	44.00	2.45	51.11	88.68	58.94	45.14	81.08	33.86
02.468	-63.54	5739.71	25.83	44.00	2.60	51.11	88.68	64.12	48.60	87.55	35.56
02.515	-63.54	5739.71	25.83	44.00	2.60	51.11	88.68	64.12	48.60	87.55	35.56
02.578	-20.77	5633.05	32.29	47.00	2.73	69.07	113.57	67.26	50.69	91.35	36.73
02.625	-20.77	5633.05	32.29	47.00	2.73	69.07	113.57	67.26	50.69	91.35	36.73

Run 6

TIME	X-LBF	Z-LBF	Y-LBF	PWR	mm	TCK1	TCK2	TCK3	TCK4	TCK5	TCK6
02.687	8.15	5582.11	31.89	38.00	2.91	69.07	113.57	70.40	52.73	95.17	37.89
02.734	8.15	5582.11	31.89	38.00	2.91	69.07	113.57	70.40	52.73	95.17	37.89
02.796	27.70	5523.21	18.57	46.00	3.05	69.07	113.57	75.08	55.96	100.77	39.73
02.859	74.54	5435.65	18.57	46.00	3.05	69.07	113.57	75.08	55.96	100.77	39.73
02.906	74.54	5435.65	6.86	40.00	3.17	69.07	113.57	78.18	58.04	104.49	41.27
02.968	103.46	5403.81	6.86	40.00	3.17	87.74	137.68	78.18	58.04	104.49	41.27
03.015	103.46	5403.81	6.86	40.00	3.17	87.74	137.68	78.18	58.04	104.49	41.27
03.078	111.20	5369.59	1.21	49.00	3.35	87.74	137.68	82.91	61.14	109.97	43.25
03.125	111.20	5369.59	1.21	49.00	3.35	87.74	137.68	82.91	61.14	109.97	43.25
03.187	111.20	5369.59	-19.78	49.00	3.54	87.74	137.68	88.08	64.77	115.98	45.27
03.250	111.20	5369.59	-19.78	49.00	3.54	87.74	137.68	88.08	64.77	115.98	45.27
03.296	108.75	5347.30	-19.78	43.00	3.54	87.74	137.68	88.08	64.77	115.98	45.27
03.359	107.53	5331.38	-19.78	43.00	3.54	87.74	137.68	88.08	64.77	115.98	45.27
03.406	107.53	5331.38	-33.50	47.00	3.75	87.74	137.68	92.77	67.98	121.31	47.32
03.468	114.05	5315.46	-38.75	47.00	3.88	87.74	137.68	95.89	70.16	124.81	48.70
03.515	114.05	5315.46	-38.75	47.00	3.88	87.74	137.68	95.89	70.16	124.81	48.70
03.578	109.97	5307.50	-58.53	48.00	4.03	106.02	159.62	100.52	73.29	129.94	50.82
03.640	109.97	5307.50	-58.53	48.00	4.03	106.02	159.62	100.52	73.29	129.94	50.82
03.687	90.42	5299.54	-58.53	49.00	4.03	106.02	159.62	100.52	73.29	129.94	50.82
03.750	90.42	5299.54	-58.53	49.00	4.03	106.02	159.62	100.52	73.29	129.94	50.82
03.796	66.39	5286.01	-67.00	48.00	4.22	106.02	159.62	105.10	76.47	135.00	53.16
03.859	66.39	5286.01	-69.02	48.00	4.34	106.02	159.62	108.15	78.61	138.91	54.61
03.906	54.99	5267.70	-69.02	52.00	4.34	106.02	159.62	108.15	78.61	138.91	54.61
03.968	32.99	5248.60	-61.76	48.00	4.55	125.38	181.18	113.19	82.00	138.91	54.61
04.031	32.99	5248.60	-61.76	48.00	4.55	125.38	181.18	113.19	82.00	143.80	56.76
04.078	-32.18	5246.21	-61.76	46.00	4.55	125.38	181.18	113.19	82.00	143.80	56.76
04.140	-32.18	5246.21	-61.76	46.00	4.55	125.38	181.18	113.19	82.00	143.80	56.76
04.187	-32.18	5246.21	-53.68	46.00	4.67	125.38	181.18	116.15	84.10	146.93	58.21
04.250	-32.18	5246.21	-53.68	46.00	4.67	125.38	181.18	116.15	84.10	146.93	58.21
04.296	-56.21	5256.56	-48.44	47.00	4.80	125.38	181.18	120.65	87.17	151.73	60.35
04.359	-68.02	5267.70	-48.44	47.00	4.80	125.38	181.18	120.65	87.17	151.73	60.35
04.421	-68.02	5267.70	-30.27	48.00	4.97	125.38	181.18	125.05	90.20	156.43	62.50
04.468	-74.54	5276.46	-15.74	50.00	5.10	125.38	181.18	127.91	92.16	156.43	62.50
04.531	-74.54	5276.46	-15.74	50.00	5.10	125.38	181.18	127.91	92.16	159.52	64.20
04.578	-83.50	5286.01	-15.74	49.00	5.10	145.49	201.96	127.91	92.16	159.52	64.20
04.640	-83.50	5286.01	-15.74	49.00	5.10	145.49	201.96	127.91	92.16	159.52	64.20
04.687	-91.64	5291.58	-8.07	55.00	5.25	145.49	201.96	132.63	95.49	164.62	66.38
04.750	-91.64	5291.58	-8.07	55.00	5.25	145.49	201.96	132.63	95.49	164.62	66.38
04.812	-62.32	5291.58	6.05	53.00	5.39	145.49	201.96	135.47	97.50	167.72	67.82
04.859	-62.32	5291.58	19.37	53.00	5.57	145.49	201.96	139.68	100.43	172.25	69.96
04.921	-62.32	5291.58	19.37	53.00	5.57	145.49	201.96	139.68	100.43	172.25	69.96
04.968	-43.99	5294.77	2.02	49.00	5.69	145.49	201.96	142.45	102.40	175.28	71.40
05.031	-43.99	5294.77	2.02	49.00	5.69	145.49	201.96	142.45	102.40	175.28	71.40
05.078	1.63	5628.28	2.02	57.00	5.69	163.74	221.71	142.45	102.40	175.28	71.40
05.140	1.63	5628.28	2.02	57.00	5.69	163.74	221.71	142.45	102.40	175.28	71.40
05.187	49.28	5850.35	-10.49	76.00	5.80	163.74	221.71	146.63	105.26	179.66	73.57
05.250	49.28	5850.35	-10.49	76.00	5.80	163.74	221.71	146.63	105.26	179.66	73.57
05.312	90.02	6044.57	-10.49	66.00	5.97	163.74	221.71	149.49	107.24	182.73	75.20

Run 6

TIME	X-LBF	Z-LBF	Y-LBF	PWR	mm	TCK1	TCK2	TCK3	TCK4	TCK5	TCK6
05.359	90.02	6044.57	-18.97	66.00	6.02	163.74	221.71	152.74	109.47	186.58	76.63
05.421	90.02	6044.57	-18.97	66.00	6.02	163.74	221.71	152.74	109.47	186.58	76.63
05.468	120.97	6222.86	-49.65	75.00	6.14	163.74	221.71	157.13	112.65	191.99	78.81
05.531	120.97	6222.86	-49.65	75.00	6.14	163.74	221.71	157.13	112.65	191.99	78.81
05.578	165.37	6682.93	-49.65	80.00	6.14	180.94	244.90	157.13	112.65	191.99	78.81
05.640	165.37	6682.93	-49.65	80.00	6.14	180.94	244.90	157.13	112.65	191.99	78.81
05.703	165.37	6682.93	-62.56	80.00	6.29	180.94	244.90	161.72	115.98	197.75	81.03
05.750	165.37	6682.93	-62.56	80.00	6.29	180.94	244.90	161.72	115.98	197.75	81.03
05.812	191.84	6934.46	-78.71	76.00	6.40	180.94	244.90	166.47	119.61	203.93	83.35
05.859	193.07	7574.41	-78.71	85.00	6.40	180.94	244.90	166.47	119.61	203.93	83.35
05.921	193.07	7574.41	-78.71	85.00	6.40	180.94	244.90	166.47	119.61	203.93	83.35
05.968	193.07	7574.41	-93.24	85.00	6.49	180.94	244.90	171.50	123.52	210.83	85.79
06.031	193.07	7574.41	-93.24	85.00	6.49	180.94	244.90	171.50	123.52	210.83	85.79
06.093	186.55	7987.52	-109.79	88.00	6.55	208.54	267.08	174.99	126.91	216.61	87.78
06.140	186.55	7987.52	-109.79	88.00	6.55	208.54	267.08	174.99	126.91	216.61	87.78
06.203	183.70	8492.16	-159.43	96.00	6.61	208.54	267.08	181.10	131.55	225.09	90.52
06.250	183.70	8492.16	-159.43	96.00	6.61	208.54	267.08	181.10	131.55	225.09	90.52
06.312	179.22	9071.63	-159.43	94.00	6.61	208.54	267.08	181.10	131.55	225.09	90.52
06.359	179.22	9071.63	-190.11	94.00	6.66	208.54	267.08	186.94	136.89	233.88	93.52
06.421	152.74	10442.28	-190.11	97.00	6.66	208.54	267.08	186.94	136.89	233.88	93.52
06.484	146.63	11196.86	-221.59	98.00	6.70	234.19	292.92	190.93	140.64	240.49	95.70
06.531	146.63	11196.86	-221.59	98.00	6.70	234.19	292.92	190.93	140.64	240.49	95.70
06.593	145.82	11962.58	-264.78	103.00	6.75	234.19	292.92	197.15	146.73	248.81	99.19
06.640	145.82	11962.58	-264.78	103.00	6.75	234.19	292.92	197.15	146.73	248.81	99.19
06.703	145.82	11962.58	-284.16	103.00	6.79	234.19	292.92	201.38	151.03	253.34	101.64
06.750	145.82	11962.58	-284.16	103.00	6.79	234.19	292.92	201.38	151.03	253.34	101.64
06.812	156.00	12787.20	-284.16	111.00	6.79	234.19	292.92	201.38	151.03	253.34	101.64
06.875	156.00	12787.20	-307.16	111.00	6.81	234.19	292.92	208.66	158.71	260.98	106.14
06.921	142.97	13620.57	-307.16	110.00	6.81	234.19	292.92	208.66	158.71	260.98	106.14
06.984	160.07	15382.05	-328.15	115.00	6.84	253.12	317.77	213.10	163.46	265.67	108.97
07.031	160.07	15382.05	-328.15	115.00	6.84	253.12	317.77	213.10	163.46	265.67	108.97

Average TCK Values (Run 1-6)

TIME	DIG_MM	Ave 12.7mm	Std Dev 12.7mm
0.000	1.090	23.469	2.233
0.055	1.128	23.476	2.236
0.115	1.140	23.476	2.236
0.167	1.186	23.482	2.242
0.224	1.194	23.469	2.244
0.276	1.232	23.494	2.268
0.333	1.235	23.507	2.274
0.391	1.235	23.596	2.307
0.445	1.236	23.640	2.331
0.505	1.255	23.665	2.365
0.557	1.264	23.710	2.392
0.617	1.262	23.881	2.547
0.667	1.269	24.108	2.820
0.729	1.271	24.305	2.778
0.781	1.280	24.495	3.008
0.839	1.280	24.495	3.008
0.899	1.282	24.647	3.192
0.951	1.289	25.059	3.173
1.008	1.325	25.596	3.564
1.060	1.339	25.596	3.564
1.120	1.355	26.082	4.038
1.169	1.382	26.562	4.596
1.229	1.399	27.700	4.514
1.292	1.441	28.362	5.129
1.344	1.441	28.362	5.129
1.401	1.537	29.744	6.535
1.453	1.537	30.428	6.097
1.513	1.617	31.107	6.163
1.563	1.683	31.622	6.577
1.622	1.714	32.485	7.538
1.680	1.773	33.492	8.566
1.732	1.818	34.284	9.528
1.792	1.884	35.456	10.670
1.844	1.945	38.002	10.588
1.904	2.004	39.680	9.580
1.953	2.038	41.531	11.226
2.013	2.129	42.688	10.076
2.068	2.190	43.866	11.069
2.125	2.253	44.391	11.704
2.182	2.360	45.659	12.884
2.234	2.410	49.132	13.823
2.294	2.464	52.651	13.513
2.344	2.517	53.174	13.996
2.404	2.586	54.800	10.275
2.461	2.631	56.433	11.811
2.513	2.720	57.116	12.225
2.573	2.764	57.640	12.644
2.625	2.864	61.482	14.580
2.685	2.940	62.005	14.882
2.734	2.988	62.595	15.450
2.794	3.091	64.071	16.410
2.846	3.149	64.815	17.156
2.904	3.214	70.129	11.920
2.964	3.254	70.634	12.506
3.016	3.345	71.828	13.770
3.076	3.400	72.615	14.330
3.125	3.453	73.304	14.797
3.185	3.539	74.166	15.597
3.237	3.599	77.094	16.715
3.297	3.693	77.550	16.952
3.354	3.714	78.284	17.734
3.406	3.825	84.030	12.657
3.466	3.869	85.124	13.777
3.516	3.971	86.539	15.069
3.576	4.047	87.312	15.748
3.628	4.089	88.315	16.658
3.685	4.139	88.315	16.658
3.745	4.167	90.690	17.313
3.797	4.277	92.121	18.258
3.857	4.319	93.108	19.176
3.906	4.409	98.437	14.304
3.966	4.496	99.277	15.114
4.021	4.545	100.192	15.859
4.076	4.594	100.192	15.859
4.133	4.674	101.632	17.235
4.188	4.743	102.125	17.669
4.245	4.765	104.423	18.306
4.297	4.867	105.609	19.140
4.357	4.867	106.073	19.615
4.409	5.007	111.915	15.578
4.469	5.059	112.392	16.096
4.523	5.148	113.728	17.173
4.578	5.186	113.728	17.173
4.635	5.257	114.816	18.246
4.688	5.353	116.224	19.389
4.747	5.403	118.769	20.284
4.800	5.448	119.242	20.701
4.857	5.503	120.468	21.965
4.914	5.621	124.743	17.054
4.969	5.641	125.205	17.569
5.026	5.730	126.133	18.283
5.078	5.753	126.133	18.283
5.138	5.790	126.793	19.078
5.188	5.874	128.096	20.124

Average TCK Values (Run 1-6)

TIME	DIG_MM	Ave 12.7mm	Std Dev 12.7mm	TIME	DIG_MM	Ave 12.7mm	Std Dev 12.7mm
5.247	5.910	130.596	21.067	7.867	7.137	227.595	27.688
5.305	6.015	131.692	21.812	7.922	7.139	234.538	19.609
5.359	6.042	132.945	23.104	7.979	7.142	235.150	20.010
5.417	6.108	137.086	18.069	8.034	7.146	236.318	20.371
5.469	6.155	137.818	18.900	8.094	7.149	236.709	20.649
5.529	6.220	138.321	19.453	8.146	7.153	240.325	23.845
5.578	6.253	138.993	19.760	8.203	7.155	240.898	24.158
5.638	6.291	139.822	20.753	8.258	7.158	241.350	24.477
5.693	6.378	141.064	21.817	8.313	7.164	242.288	24.719
5.750	6.391	143.693	22.763	8.367	7.164	242.288	24.719
5.807	6.481	145.319	23.945	8.422	7.167	247.693	19.411
5.860	6.497	146.156	24.844	8.484	7.172	248.220	19.716
5.917	6.566	151.405	20.354	8.536	7.174	248.658	20.018
5.969	6.582	152.243	21.184	8.594	7.175	248.997	20.243
6.029	6.629	152.798	21.447	8.648	7.180	251.895	22.952
6.083	6.674	153.380	22.094	8.703	7.187	252.214	23.116
6.141	6.699	154.065	22.897	8.758	7.187	252.667	23.048
6.195	6.758	155.996	24.557	8.813	7.193	255.397	19.770
6.250	6.765	159.648	25.965	8.873	7.196	255.684	19.962
6.308	6.811	160.652	26.467	8.927	7.197	258.151	19.832
6.359	6.828	162.509	28.392	8.985	7.198	258.151	19.832
6.422	6.859	169.669	23.751	9.036	7.201	258.538	20.067
6.474	6.897	170.335	24.380	9.094	7.204	259.012	20.352
6.531	6.897	170.335	24.380	9.148	7.206	260.915	22.326
6.586	6.928	171.372	25.536	9.203	7.211	261.409	22.424
6.641	6.952	177.600	27.995	9.263	7.211	261.783	22.606
6.698	6.979	178.303	28.631	9.315	7.215	262.563	22.904
6.750	6.985	180.593	30.295	9.375	7.215	262.563	22.904
6.810	7.010	186.363	28.667	9.427	7.218	264.545	23.028
6.865	7.021	188.490	30.434	9.484	7.220	264.925	23.237
6.922	7.039	192.797	24.641	9.539	7.221	266.472	20.293
6.977	7.044	193.538	25.271	9.594	7.225	266.708	20.441
7.031	7.058	194.728	25.520	9.648	7.227	266.896	20.385
7.088	7.067	195.792	26.552	9.703	7.233	268.775	22.239
7.141	7.083	197.578	27.874	9.766	7.235	268.974	22.323
7.201	7.086	203.606	30.514	9.821	7.233	269.715	22.658
7.253	7.094	205.349	31.636	9.875	7.233	269.715	22.658
7.313	7.095	209.760	30.807	9.930	7.237	272.407	20.330
7.367	7.100	211.016	31.733	9.985	7.239	272.612	20.454
7.422	7.105	217.473	21.322	10.039	7.244	272.967	20.465
7.476	7.107	218.399	21.964	10.094	7.245	273.178	20.600
7.531	7.113	218.941	21.986	10.154	7.245	274.215	22.061
7.591	7.116	219.574	22.527	10.211	7.251	274.682	22.163
7.643	7.123	224.833	26.057	10.266	7.253	274.930	22.267
7.703	7.125	225.535	26.504	10.321	7.253	275.540	22.374
7.755	7.128	226.587	26.873	10.375	7.253	275.540	22.374
7.813	7.137	227.022	27.178	10.430	7.259	278.001	20.166

Average TCK Values (Run 1-6)

TIME	DIG_MM	Ave 12.7mm	Std Dev 12.7mm
10.484	7.259	278.305	20.352
10.547	7.264	278.634	20.337
10.601	7.268	278.814	20.456
10.656	7.269	279.895	21.543
10.714	7.269	280.161	21.709
10.766	7.270	280.322	21.771
10.823	7.273	282.634	19.781
10.878	7.274	282.869	19.924
10.933	7.278	283.236	19.912
10.992	7.280	283.403	20.020
11.047	7.283	283.403	20.020
11.104	7.283	283.880	20.061
11.156	7.284	284.767	21.202
11.214	7.289	284.979	21.104
11.268	7.291	285.418	21.333
11.326	7.293	287.296	19.598
11.380	7.293	287.444	19.693
11.438	7.296	287.586	19.745
11.495	7.299	287.796	19.887
11.547	7.301	288.230	19.839
11.604	7.304	288.602	19.817
11.659	7.304	289.278	20.796
11.714	7.306	289.612	20.863
11.773	7.307	289.792	20.924
11.826	7.309	289.915	20.972
11.883	7.309	290.045	21.060
11.940	7.313	291.912	19.406
11.995	7.316	292.115	19.542
12.050	7.318	292.314	19.436
12.107	7.320	292.437	19.523
12.164	7.321	292.722	19.515
12.219	7.322	293.644	20.550
12.276	7.322	293.644	20.550
12.333	7.325	294.108	20.623
12.386	7.328	294.108	20.623
12.443	7.332	294.930	20.569
12.495	7.332	295.768	19.133
12.555	7.335	296.040	19.124
12.612	7.337	296.194	19.230
12.664	7.338	296.459	19.183
12.724	7.338	297.326	20.187
12.781	7.338	297.326	20.187
12.836	7.343	297.610	20.139
12.891	7.344	298.408	18.908
12.946	7.347	299.210	18.921
13.005	7.347	299.309	18.987
13.055	7.348	299.309	18.987
13.115	7.343	299.556	18.969
13.172	7.342	300.213	19.780
13.226	7.339	300.435	19.850
13.286	7.339	300.435	19.850
13.339	7.337	300.509	19.822
13.396	7.338	301.113	18.813
13.448	7.336	301.619	18.819
13.505	7.332	301.712	18.880
13.568	7.330	301.693	18.876
13.615	7.326	301.619	18.882
13.677	7.326	301.619	18.882
13.729	7.325	301.771	19.312
13.786	7.323	301.771	19.312
13.841	7.322	301.385	19.971
13.896	7.318	301.354	19.950
13.956	7.316	301.027	20.008
14.005	7.314	300.953	19.958
14.068	7.314	300.738	19.928
14.120	7.316	300.422	19.982
14.177	7.316	300.237	19.964
14.232	7.306	299.160	19.341
14.286	7.303	299.160	19.341
14.346	7.300	298.955	19.482
14.396	7.299	297.001	22.645
14.458	7.295	295.778	22.624
14.510	7.289	295.544	22.472
14.568	7.287	295.118	22.445
14.623	7.275	294.549	22.445
14.680	7.274	293.191	20.821
14.737	7.256	292.300	20.755
14.789	7.256	292.300	20.755
14.846	7.232	289.869	20.570
14.899	7.230	285.922	27.404
14.958	7.218	284.910	27.483
15.013	7.193	284.324	27.128
15.071	7.180	283.349	27.211
15.128	7.146	282.929	26.984
15.180	7.146	282.929	26.984
15.237	7.092	278.460	22.696
15.292	7.092	278.460	22.696
15.349	7.057	277.520	22.805
15.406	7.032	277.086	22.537
15.461	6.997	273.668	21.773
15.518	6.932	270.217	27.281
15.571	6.907	269.107	27.225
15.628	6.855	268.205	26.861
15.685	6.855	268.205	26.861

Average TCK Values (Run 1-6)

TIME	DIG_MM	Ave 12.7mm	Std Dev 12.7mm	TIME	DIG_MM	Ave 12.7mm	Std Dev 12.7mm
15.740	6.807	262.764	21.686	18.362	4.971	210.639	16.022
15.794	6.783	262.167	21.214	18.419	4.931	209.631	15.893
15.852	6.728	259.186	25.403	18.471	4.876	208.839	15.723
15.909	6.701	258.793	25.130	18.531	4.823	208.483	15.399
15.964	6.661	255.312	24.350	18.583	4.790	207.832	15.330
16.018	6.603	254.932	24.045	18.643	4.707	205.767	13.647
16.076	6.590	254.004	23.870	18.698	4.707	205.767	13.647
16.128	6.541	250.499	21.163	18.753	4.641	204.822	13.372
16.185	6.532	250.499	21.163	18.813	4.601	204.298	13.015
16.242	6.498	249.283	20.469	18.865	4.564	202.584	14.737
16.297	6.486	248.664	19.839	18.922	4.524	202.584	14.737
16.357	6.415	247.835	19.634	18.974	4.481	200.941	14.399
16.409	6.406	243.840	22.499	19.034	4.431	200.603	14.152
16.466	6.357	243.192	22.254	19.086	4.392	199.694	14.216
16.518	6.312	242.660	21.744	19.143	4.302	197.875	12.493
16.576	6.278	241.646	21.402	19.203	4.283	197.875	12.493
16.633	6.235	239.552	20.041	19.255	4.221	197.171	12.343
16.690	6.223	239.214	19.662	19.313	4.178	195.898	13.889
16.748	6.167	238.545	19.395	19.365	4.108	195.175	13.878
16.800	6.159	236.943	21.471	19.422	4.076	193.845	13.262
16.857	6.125	236.034	21.128	19.474	4.041	193.076	13.357
16.909	6.098	234.073	20.864	19.534	3.991	193.076	13.357
16.966	6.046	233.473	20.615	19.594	3.978	192.257	13.519
17.024	5.999	232.925	20.066	19.643	3.891	190.428	11.705
17.081	5.959	232.173	19.765	19.703	3.854	190.428	11.705
17.135	5.891	229.943	18.375	19.755	3.799	189.852	11.721
17.190	5.891	229.943	18.375	19.813	3.770	188.599	13.290
17.248	5.844	229.355	18.140	19.865	3.710	187.933	13.438
17.300	5.819	229.046	17.800	19.925	3.686	187.933	13.438
17.359	5.773	228.660	17.620	19.984	3.632	187.305	13.560
17.411	5.738	225.994	19.381	20.034	3.556	185.833	12.758
17.469	5.687	225.037	18.984	20.094	3.540	184.048	11.379
17.524	5.652	224.721	18.661	20.146	3.488	183.638	11.236
17.581	5.616	223.909	18.383	20.203	3.488	183.638	11.236
17.638	5.538	223.409	17.894	20.255	3.393	182.991	11.398
17.693	5.519	221.716	16.877	20.313	3.337	181.796	12.878
17.750	5.448	220.936	16.295	20.367	3.282	181.054	13.074
17.805	5.414	220.581	15.959	20.425	3.248	179.824	12.335
17.859	5.367	218.456	15.703	20.484	3.215	179.472	12.575
17.917	5.350	217.630	17.590	20.536	3.135	178.864	12.486
17.971	5.292	216.764	17.328	20.594	3.135	177.821	10.805
18.029	5.239	216.225	16.786	20.648	3.063	177.264	10.935
18.081	5.206	215.849	16.708	20.703	3.042	176.854	10.872
18.141	5.126	213.910	15.314	20.760	2.961	176.311	11.129
18.193	5.126	213.910	15.314	20.815	2.932	175.264	12.597
18.250	5.047	212.370	14.525	20.875	2.873	174.727	12.737
18.308	5.006	211.207	16.097	20.927	2.819	173.511	11.958

Average TCK Values (Run 1-6)

TIME	DIG_MM	Ave 12.7mm	Std Dev 12.7mm
20.984	2.775	172.955	12.203
21.036	2.733	172.724	12.184
21.094	2.733	171.661	10.438
21.148	2.616	170.804	10.524
21.206	2.616	170.804	10.524
21.263	2.549	170.306	10.785
21.318	2.512	169.013	10.043
21.375	2.460	168.643	10.191
21.427	2.404	167.535	11.656
21.484	2.374	166.966	11.851
21.539	2.304	166.481	11.847
21.596	2.304	166.481	11.847
21.656	2.207	164.914	10.352
21.708	2.189	164.914	10.352
21.766	2.113	164.461	10.498
21.823	2.081	163.361	9.777
21.875	2.052	162.896	10.013
21.932	1.986	161.650	11.615
21.984	1.953	161.484	11.587
22.047	1.900	161.134	11.727
22.099	1.865	160.885	11.702
22.156	1.775	159.179	10.115
22.211	1.757	159.179	10.115
22.266	1.723	158.758	10.091
22.326	1.690	158.758	10.091
22.375	1.625	158.268	10.305
22.438	1.550	155.711	11.476
22.492	1.513	155.565	11.441
22.550	1.445	155.208	11.412
22.604	1.407	154.973	11.593
22.659	1.392	153.523	9.776
22.716	1.372	153.523	9.776
22.771	1.278	152.982	9.841
22.831	1.251	151.895	11.569
22.880	1.201	151.533	11.676
22.940	1.146	150.355	10.899
22.992	1.109	150.145	10.819
23.050	1.016	149.529	10.940
23.107	1.016	148.298	9.236
23.161	0.921	147.930	9.320
23.216	0.921	147.930	9.320
23.276	0.871	147.650	9.251
23.331	0.836	147.650	9.251
23.385	0.786	147.231	9.325
23.446	0.706	145.192	10.114
23.500	0.666	145.008	10.014
23.555	0.486	143.557	8.583
23.609	0.429	143.557	8.583
23.667	0.355	143.095	8.602
23.724	0.290	143.095	8.602
23.779	0.061	142.772	8.722
23.836	-0.133	141.636	7.916
23.888	-0.339	141.434	8.064
23.946	-0.464	140.667	9.319
24.000	-0.464	140.667	9.319
24.057	-0.815	140.122	9.277
24.112	-0.879	139.189	8.298
24.169	-1.211	138.778	8.244
24.227	-1.320	138.651	8.229
24.279	-1.480	138.487	8.341
24.336	-1.693	137.455	7.626
24.393	-1.822	137.348	7.700
24.446	-2.017	136.651	8.846
24.503	-2.017	136.651	8.846
24.560	-2.341	135.380	8.104
24.617	-2.399	135.380	8.104
24.669	-2.698	135.026	7.996
24.727	-2.823	135.026	7.996
24.781	-3.008	134.597	7.959
24.836	-3.143	133.977	9.026
24.894	-3.253	133.882	9.077
24.951	-3.565	133.010	8.456
25.005	-3.565	133.010	8.456
25.060	-3.880	132.006	7.871
25.117	-3.944	132.006	7.871
25.169	-4.206	131.653	7.776
25.227	-4.266	131.653	7.776
25.284	-4.450	131.451	7.819
25.341	-4.619	130.749	8.598
25.393	-4.725	130.617	8.663
25.451	-5.102	129.866	8.139
25.508	-5.102	129.784	8.179
25.560	-5.343	129.078	7.678
25.617	-5.418	129.078	7.678
25.675	-5.590	128.814	7.702
25.729	-5.652	128.657	7.676
25.784	-5.912	128.468	7.587
25.841	-6.111	127.407	7.965
25.896	-6.310	127.288	8.014
25.951	-6.466	127.130	7.913
26.008	-6.542	127.130	7.913
26.063	-6.734	126.520	7.715
26.117	-6.796	126.520	7.715
26.175	-7.118	126.181	7.599

Average TCK Values (Run 1-6)

TIME	DIG_MM	Ave 12.7mm	Std Dev 12.7mm
26.232	-7.182	126.181	7.599
26.287	-7.380	125.985	7.447
26.344	-7.566	125.530	8.157
26.399	-7.688	124.958	7.857
26.453	-7.993	124.813	7.874
26.508	-7.993	124.813	7.874
26.565	-8.331	124.185	7.600
26.622	-8.331	124.185	7.600
26.677	-8.600	123.928	7.447
26.734	-8.661	123.928	7.447
26.789	-8.921	123.620	7.369
26.844	-9.000	123.620	7.369
26.899	-9.122	123.180	7.167
26.956	-9.382	122.568	7.722
27.013	-9.382	122.568	7.722
27.065	-9.593	122.386	7.667
27.122	-9.593	122.386	7.667
27.180	-9.745	121.821	7.361
27.234	-9.745	121.821	7.361
27.289	-9.826	121.727	7.405
27.346	-9.826	121.207	7.139
27.401	-9.827	121.207	7.139
27.456	-9.828	120.677	7.688
27.513	-9.828	120.677	7.688
27.571	-9.828	120.457	7.617
27.625	-9.828	120.457	7.617
27.680	-9.828	119.956	7.367
27.737	-9.828	119.956	7.367
27.789	-9.828	119.900	7.394
27.846	-9.828	119.206	7.643
27.904	-9.828	119.131	7.673
27.961	-9.828	118.937	7.623
28.016	-9.828	118.937	7.623
28.071	-9.828	118.479	7.405
28.128	-9.828	118.479	7.405
28.180	-9.828	118.342	7.367

Average Thermocouple Values, OLIPHANT

Time	Z-pos mm	St Dev	12.7 mm
0.000	-0.4671	0.0020	23.9031
0.005	-1.0716	0.0012	24.1107
0.510	-1.6880	0.0034	25.8602
1.015	-2.2332	0.0006	31.2988
1.515	-2.8654	0.0034	40.1433
2.021	-3.4581	0.0021	50.6722
2.515	-4.0824	0.0045	61.4987
3.021	-4.6553	0.0042	72.5768
3.526	-5.2360	0.0032	83.7180
4.031	-5.8879	0.0029	94.4034
4.531	-6.4450	0.0041	104.8729
5.031	-7.0456	0.0041	115.2845
5.531	-7.6421	0.0050	125.3280
6.052	-8.2702	0.0034	135.5241
6.552	-8.3691	0.0031	147.6225
7.057	-8.3691	0.0036	164.5501
7.557	-8.3691	0.0033	183.6649
8.073	-8.3691	0.0032	203.4423
8.563	-8.3691	0.0032	220.2267
9.073	-8.3691	0.0031	233.3541
9.573	-8.3691	0.0032	243.8430
10.073	-8.3691	0.0031	252.5519
10.573	-8.3691	0.0033	259.6666
11.078	-8.3691	0.0032	265.6745
11.583	-8.3691	0.0032	270.9001
12.089	-8.3674	0.0032	275.3098
12.589	-7.9505	0.0030	279.2474
13.094	-7.5328	0.0028	282.3220
13.589	-7.0812	0.0026	280.6632
14.094	-6.6776	0.0063	272.4659
14.594	-6.2627	0.0084	260.5817
15.094	-5.8196	0.0058	246.8624
15.599	-5.3963	0.0059	233.4030
16.120	-4.9194	0.0054	221.2122
16.625	-4.4932	0.0054	210.7916
17.130	-4.0981	0.0030	201.8401
17.630	-3.6832	0.0021	193.9105
18.130	-3.2260	0.0039	187.0149
18.630	-2.8253	0.0022	180.7915
19.130	-2.3427	0.0030	174.8176
19.635	-1.9278	0.0025	169.1575
20.135	-1.5186	0.0035	164.0013
20.646	-1.1235	0.0020	158.9091
21.161	-0.6973	0.0026	154.0908
21.661	-0.2655	0.0044	149.5879
22.161	0.1719	0.0028	145.1504
22.661	0.5430	0.0028	141.0043
23.172	1.9507	0.0026	137.2104
23.672	3.5509	3.4577	123.6863
24.172	4.9832	3.1491	121.7301
24.672	6.4550	2.7164	119.7880
25.182	7.9169	2.4295	118.0748
25.688	9.3393	2.0513	116.5006
26.188	10.8012	1.7920	114.9653
26.688	12.2730	1.6100	113.6049
27.188	13.2203	1.3946	112.2092
27.693	13.2203	1.3393	110.9992
27.974	13.2203	1.1945	110.4764

APPENDIX D

Simulation Data

The results from the three static anvil/dynamic tool temperature models as well as the open table format simulation are included here.

ANVIL25			ANVIL50			ANVIL75		
TIME	HEIGHT	TEMP	TIME	HEIGHT	TEMP	TIME	HEIGHT	TEMP
0.000	0.000	20.000	0.000	0.000	20.000	0.000	0.000	20.000
0.126	0.149	21.170	0.126	0.149	21.100	0.126	0.149	22.110
0.251	0.298	22.310	0.251	0.298	22.300	0.251	0.298	24.540
0.376	0.446	23.670	0.376	0.446	24.360	0.376	0.446	27.980
0.502	0.595	24.830	0.502	0.595	26.880	0.502	0.595	31.410
0.627	0.744	26.850	0.627	0.744	29.360	0.627	0.744	34.080
0.752	0.893	28.020	0.752	0.893	32.170	0.752	0.893	36.380
0.878	1.041	28.820	0.878	1.041	33.860	0.878	1.041	38.810
1.003	1.190	29.470	1.003	1.190	35.250	1.003	1.190	41.040
1.128	1.339	30.350	1.128	1.339	36.550	1.128	1.339	43.060
1.253	1.487	30.900	1.253	1.487	38.030	1.253	1.487	44.940
1.379	1.636	31.400	1.379	1.636	39.150	1.379	1.636	46.840
1.504	1.785	31.680	1.504	1.785	40.180	1.504	1.785	48.610
1.630	1.934	31.940	1.629	1.933	41.200	1.629	1.933	50.200
1.756	2.084	32.310	1.755	2.083	42.120	1.756	2.084	51.840
1.881	2.232	32.760	1.881	2.232	43.200	1.881	2.232	53.270
2.006	2.381	32.990	2.006	2.381	44.060	2.006	2.381	54.760
2.132	2.530	33.770	2.132	2.530	44.920	2.132	2.530	56.150
2.257	2.678	33.740	2.257	2.678	45.700	2.257	2.678	57.490
2.382	2.827	34.700	2.382	2.827	46.940	2.382	2.827	58.770
2.508	2.976	35.330	2.508	2.976	47.590	2.508	2.976	60.140
2.633	3.125	35.430	2.633	3.125	48.770	2.633	3.125	61.320
2.758	3.273	35.870	2.758	3.273	49.800	2.758	3.273	62.540
2.884	3.422	36.240	2.884	3.422	50.340	2.884	3.422	63.910
3.009	3.571	36.360	3.009	3.571	51.640	3.009	3.571	65.160
3.134	3.719	37.530	3.134	3.719	52.490	3.134	3.719	66.630
3.260	3.869	38.000	3.260	3.869	53.580	3.260	3.869	67.870
3.385	4.017	39.570	3.385	4.017	54.910	3.385	4.017	69.690
3.510	4.165	40.710	3.510	4.165	56.190	3.510	4.165	71.400
3.636	4.315	41.770	3.636	4.315	57.010	3.636	4.315	72.790
3.761	4.463	42.850	3.761	4.463	58.840	3.761	4.463	74.590
3.886	4.612	44.290	3.886	4.612	59.840	3.886	4.612	76.420
4.012	4.761	46.410	4.012	4.761	61.280	4.012	4.761	78.020
4.137	4.909	47.250	4.137	4.909	62.830	4.137	4.909	79.780

ANVIL25			ANVIL50			ANVIL75		
TIME	HEIGHT	TEMP	TIME	HEIGHT	TEMP	TIME	HEIGHT	TEMP
4.262	5.058	49.120	4.262	5.058	64.390	4.262	5.058	82.620
4.388	5.207	51.500	4.388	5.207	66.490	4.388	5.207	85.460
4.513	5.356	55.440	4.513	5.356	69.870	4.513	5.356	89.670
4.638	5.504	58.540	4.638	5.504	73.580	4.638	5.504	93.020
4.764	5.653	64.760	4.764	5.653	80.010	4.764	5.653	98.980
4.889	5.802	72.840	4.889	5.802	86.580	4.889	5.802	104.800
5.014	5.950	79.880	5.014	5.950	94.510	5.014	5.950	112.700
5.140	6.100	102.700	5.140	6.100	112.600	5.140	6.100	131.800
5.265	6.248	130.900	5.265	6.248	141.300	5.265	6.248	160.000
5.516	6.546	170.000	5.516	6.546	186.500	5.516	6.546	199.100
5.641	6.694	190.000	5.641	6.694	200.000	5.641	6.694	214.400
5.766	6.843	198.400	5.766	6.843	206.700	5.766	6.843	219.100

OPENTABLE

TIME	HEIGHT	TEMP
0.000	0.000	20.000
0.126	0.149	20.500
0.251	0.298	22.100
0.376	0.446	25.640
0.502	0.595	29.430
0.627	0.744	34.793
0.752	0.893	37.805
0.878	1.041	43.759
1.003	1.190	47.714
1.128	1.339	50.600
1.253	1.487	54.046
1.379	1.636	58.789
1.504	1.785	62.210
1.630	1.934	64.162
1.756	2.084	69.230
1.881	2.232	72.447
2.006	2.381	75.950
2.132	2.530	79.220
2.257	2.678	80.307
2.508	2.976	90.318
2.633	3.125	94.178
2.758	3.273	98.151
2.884	3.422	98.330
3.009	3.571	103.529
3.134	3.719	105.643
3.260	3.869	107.980
3.386	4.018	111.722
3.511	4.167	113.142
3.636	4.315	114.331
3.762	4.464	118.683
3.887	4.613	122.741
4.012	4.761	123.326
4.138	4.911	124.683
4.263	5.059	126.997
4.388	5.207	133.457
4.514	5.357	137.094
4.625	5.488	144.244
4.750	5.637	147.621
4.875	5.785	152.330
5.000	5.934	157.390
5.125	6.082	162.970
5.250	6.230	168.330
5.375	6.379	172.980
5.500	6.527	184.490
5.625	6.675	190.940
5.750	6.824	200.340

OLIPHANT SIMULATION

TIME	HEIGHT	TEMP
0.000	0.000	20.000
0.282	0.335	25.830
0.564	0.669	40.990
0.846	1.003	53.060
1.127	1.337	74.210
1.691	2.007	95.740
1.973	2.341	97.390
2.255	2.676	111.000
2.537	3.011	117.600
2.819	3.345	134.000
3.100	3.679	140.200
3.382	4.013	147.800
3.664	4.348	163.700
3.947	4.684	168.500
3.973	4.715	170.280
3.984	4.728	173.110
4.265	5.061	180.100
4.349	5.161	187.000
4.630	5.494	196.300
4.912	5.829	244.900
4.973	5.901	249.800
5.146	6.107	254.600
5.193	6.163	272.800
5.352	6.351	289.300
5.420	6.432	288.200
5.440	6.456	292.700